DISSERTATION: ENERGETIC THEORY AND HADLEY CELLS AT A SEASONAL SCALE: HOW WILL ITCZ RESPOND TO A WARMING CLIMATE

by

Xiaoyu Bai

A dissertation submitted to the faculty of
The University of North Carolina at Charlotte
in partial fulfillment of the requirements
for the degree of Doctor of Philosophy in
Infrastructure & Environmental Systems

Charlotte

2022

Approved by:

____
Dr. Jacob Scheff

____
Dr. James Amburgey

____
Dr. Casey Davenport

____
Dr. Matthew Eastin

____
Dr. Brian Magi

ABSTRACT

XIAOYU BAI. Dissertation: Energetic Theory and Hadley cells at a seasonal scale: how will ITCZ respond to a warming climate. (Under the direction of DR. JACOB SCHEFF)

The Intertropical Convergence Zone (ITCZ), a belt of convective systems around the equator with showers and thunderstorms, is an important feature not only to the tropical societies whose water budget depends on it, but also to the atmospheric science field to understand how will the Earth respond to a warming climate. Previous studies found that annual and zonal mean ITCZ position is related to interhemispheric atmospheric heat transport (AHT_{total}). The radiative imbalance at the top of the atmosphere (TOA) transported across the equator to the cooler hemisphere explains the ITCZ position and its shift. Using idealized model simulations with a "slab" ocean, researchers found that an increase in the interhemispheric TOA radiation contrast causes an increase in cross-equatorial energy flux by the Hadley circulation and a shift of the ITCZ towards the warmer hemisphere. The theory that relates AHT_{total} and ITCZ position is called energetic theory.

In this dissertation, we analyze Tropical rain belts with an Annual cycle and a Continent-Model Intercomparison Project (TRACMIP) model simulations to test the energetic theory. TRACMIP is a project of idealized models that fill the gap between idealized aquaplanet models and fully-coupled models. TRACMIP models are thermodynamically coupled to a slab ocean. TRACMIP has idealized tropical continent setups with both present-day and quadruple CO2 (4xCO_2) concentration experiments, which can help us understand ITCZ shift and potential precipitation changes over land under a warming scenario. Our findings suggested that TRACMIP simulations do not support energetic theory's expectations under a warming climate.

All of our models simulated a northward shift of ITCZ and mass transport under a warming scenario. Our models disagreed on the changes of the energy transported

by Hadley cells and the total energy transported by the atmosphere. In general, the link between mass transport changes and energy transported by the Hadley cells changes broke down the most during Northern Hemisphere tropical wet season. The link between changes of the energy transported by the Hadley cells and total energy transported by the atmosphere broke down the most during Northern Hemisphere tropical dry season. Breakdown of one or both of these links caused the overall link between ITCZ shifts and total energy transport changes to break down.

We encourage more studies to be done on energetic theory and climate change. We look forward to combining energetic theory with monsoon theories to develop a self-contained tropical climate model.

ACKNOWLEDGEMENTS

I would like to thank Dr. James Amburgey for his support. I would like to extend my deepest gratitude to Dr. Casey Davenport and Dr. Matthew Eastin for their support and suggestions. I would like to pay my special regards to Dr. Brian Magi for his guidance and for sharing his experiences. I am extremely grateful to Dr. Jacob Scheff for his invaluable advice, suggestions, guidance, and support. This work was supported by National Science Foundation Award AGS-1565522 from Aug 2018 to Jul 2020, and Proposal Development Summer Fellowship from the Graduate School at UNC Charlotte from May 2020 to Aug 2020.

TABLE OF CONTENTS

LIST OF TABLES

LIST OF FIGURES

LIST OF ABBREVIATIONS

AHT_{EQ} Atmospheric Heat Transport at Equator

AHT_{Hadley} Atmospheric Heat Transported by Hadley Cells

AHT_{total} Atmospheric Heat Transport

AMIP Atmospheric Model Intercomparison Project

CAM3 Community Atmosphere Model version 3

CAM4 Community Atmosphere Model version 4

CMIP3 Coupled Model Intercomparison Project Phase 3

CMIP5 Coupled Model Intercomparison Project Phase 5

CNRM_AM5 Centre National de Recherches Météorologiques Atmospheric Model version 5

ECHAM61 Atmospheric General Circulation model of European Center (EC) for Medium Range Weather Forecasts model developed in Hamburg (HAM) version 6.1

ECHAM63 Atmospheric General Circulation model of European Center (EC) for Medium Range Weather Forecasts model developed in Hamburg (HAM) version 6.3

EFE Energy Flux Equator

GFDL-AM2.1 Geophysical Fluid Dynamics Laboratory Atmospheric Model version 2.1

ITCZ Intertropical Convergence Zone

LH Latent Heat Flux

LMDZ5A Laboratoire de Météorologie Dynamique Atmospheric General Circulation model (Z standing for the model zoom capacity)

LW Longwave Radiation Flux

MetUM_CTL Met Office Unified Model with Controlled Settings

MetUM_ENT Met Office Unified Model with more Entrainment and Detrainment Settings

MIROC5 Model for Interdisciplinary Research on Climate version 5

MMC Mean Meridional Circulation

MPAS Model for Prediction Across Scales

MSE Moist Static Energy

OHT Ocean Heat Transport

OLR Outgoing Longwave Radiation

SENS Sensible Heat Flux

SHF Surface Heat Flux to the Atmosphere

SST Sea Surface Temperature

SURF Surface

SWABS Shortwave Radiation Absorbed in the Atmosphere

TET Total Energy Transport

TOA Top of the Atmosphere

TRACMIP Tropical Rain belts with an Annual cycle and a Continent Model Intercomparison Project

CHAPTER 1: INTRODUCTION

1.1 ITCZ and energetic theory

The Intertropical Convergence Zone (ITCZ), one of the best identified tropical atmospheric features, is a belt of low pressure systems around the equator, which contributes 32% of globally integrated annual rainfall and 100% of tropical rainfall (Waliser and Jiang 2014; Kang et al. 2018). The ITCZ locates where the tropical surface trade winds, carrying abundant sensible heat and moisture from surface evaporation, meet and rise up to form a zone of deep convection, cloudiness, and precipitation (Waliser and Jiang 2014). The ITCZ is critical to atmospheric energy balance because it releases latent heat during convective processes and its enhanced cloudiness affects the planetary albedo (Waliser and Jiang 2014). Considering the heat, moisture, momentum, and radiation fluxes can change significantly among the ITCZ and the areas to the north and south of the ITCZ, the position, width, structure, and migration of the ITCZ affects not only the Earth's climate on a global scale, but also the ocean-atmosphere and land-atmosphere interactions on a local scale (Waliser and Jiang 2014). At some places, like Kanton Island which is near the edge of the ITCZ, the annual rainfall can change from 3 mm day^{-1} to 10 mm day^{-1} due to a subtle ITCZ shift (Kang et al. 2018). Therefore, to understand and predict the changes of ITCZ under global warming is very important not only to climatologists but also to tropical societies.

Since the ITCZ is a narrow belt of convective systems, we usually analyze it meridionally. In a meridional view, ITCZ locates at the rising branch of the Hadley cells. Hadley cells are the atmospheric meridional overturning circulations in the tropics, which play a major role in meridional energy and mass transport (Held 2001). The equatorial region receives more insolation than the polar areas. The atmosphere and ocean balance the radiative energy imbalance by transporting energy, mass, and momentum to the polar areas (Trenberth and Solomon 1994; Held 2001). Within the atmosphere, Hadley cells appear in pairs, with one in the Northern Hemisphere and one in the Southern Hemisphere. They serve as engines transporting energy, momentum, and mass out of the equator. When air in the tropics is heated up and rises to the upper atmosphere, the air will move poleward both to the North and South. In the sub-tropics, the air will sink and move back to the equator, which finishes the full circle of Hadley cell. This surface, equator moving air flow forms the trade winds when considering the Earth's rotation.

The climatological zonal-mean ITCZ locates north of the equator (Dima and Wallace 2003; Huffman et al. 2009). Frierson and other authors were able to explain why more rain falls north of the equator using idealized climate models. It is mainly due to the hemispheric asymmetry of the atmospheric energy budget (Frierson and Hwang 2012; Hwang and Frierson 2013; Hwang et al. 2013). This hemispheric asymmetry of the atmospheric energy budget is caused by the ocean overturning circulation in the Atlantic, which transports energy from the Southern Hemisphere to the Northern Hemisphere (Frierson et al. 2013). Overall, the Northern Hemisphere atmosphere receives more energy that the Hadley cells need to balance out. The upper branch of the Hadley cell transports net energy and the lower branch of the Hadley cell transports net moisture (Frierson and Hwang 2012). So the net energy transported by the Hadley cells are always in the same direction of the upper branches of the Hadley cells (Kang et al. 2008, 2018; Kang 2020). To transport more energy out of the Northern Hemisphere, the southern Hadley cell becomes stronger to transport energy out of the tropics and to transport moisture into the tropics. The excess moisture transported by a stronger Southern Hadley cell causes the tropical rain belt to move to the north (see schematic Fig. 1.1, credit: Frierson et al. (2013)).

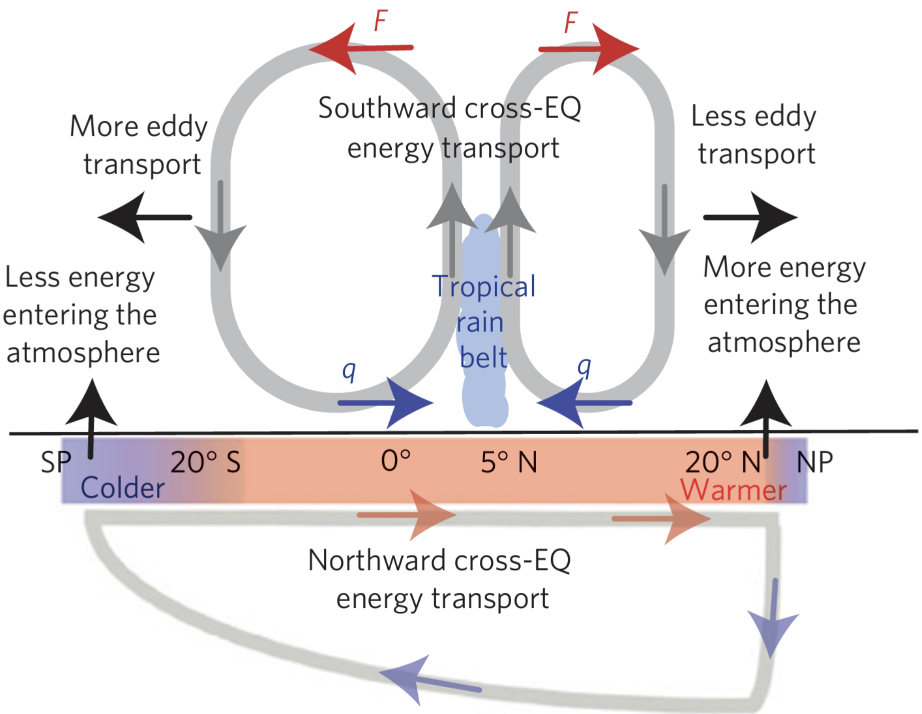

Figure 1.1: Schematic of the ocean heat transport forcing the ITCZ to locate north of the equator (from Frierson et al. (2013)).

Seasonally, the ITCZ also shifts towards a warmer hemisphere (Dima and Wallace 2003; Schneider et al. 2014; Donohoe et al. 2013; Waliser and Jiang 2014; Adam et al. 2016; Kang et al. 2018). Over the central Atlantic and Pacific oceans, ITCZ shifts between 9°N in the boreal summer and 2°N in the boreal winter. Over the Indian Ocean, ITCZ migrates dramatically between approximately 20°N and 8°S (Schneider et al. 2014). The approach that describes where ITCZ is located and why ITCZ is shifting quantitatively is called energetic theory. As we mentioned above briefly, both observations and model simulations show that the ITCZ shifts meridionally when the atmospheric energy balance shifts (Chiang and Bitz 2005; Broccoli et al. 2006; Kang et al. 2008, 2009; Yoshimori and Broccoli 2009; Frierson and Hwang 2012; Kang and Held 2012; Donohoe et al. 2013; Friedman et al. 2013; Fučkar et al. 2013; Hwang and Frierson 2013; Marshall et al. 2014; Kang et al. 2013; Schneider et al. 2014). Some researchers also try to use tropical atmospheric dynamics to explain where ITCZ is located and why ITCZ shifts (Lindzen and Hou 1988; Plumb and Hou 1992). However, this method requires the distribution of boundary-layer moist static energy to be known in advance and therefore never became a distinct framework to the energetic theory (Byrne et al. 2018).

When taking a zonal mean of precipitation and energy transported by the atmosphere, ITCZ is often found near the peak of the precipitation curve, where the energy flux is zero or near zero. The energy flux would be zero near ITCZ because it is where Northern and Southern Hemisphere Hadley cells meet, since Hadley cells transport energy in opposite directions (e.g., Fig. 1.2, credit: Kang et al. (2018)). The latitude where atmospheric meridional energy flux is zero or changes its sign in other words, is called the energy flux equator (EFE) (Kang et al. 2008). Ideally, EFE meridional shift magnitude will be similar to ITCZ migration because the total atmospheric energy transport F_A is a function of Hadley cell mass transport by its upper branch (V) and total gross moist stability (Δm, GMS). That is $F_A = V\Delta m$. The total GMS, which is the ratio of energy transport by the Hadley cell per unit mass (Neelin and Held 1987; Raymond et al. 2009), is an indicator of how efficient the Hadley cells are transporting energy. It can also be considered as an approximation of the moist static energy (MSE) difference between upper and lower branches of the Hadley cells.

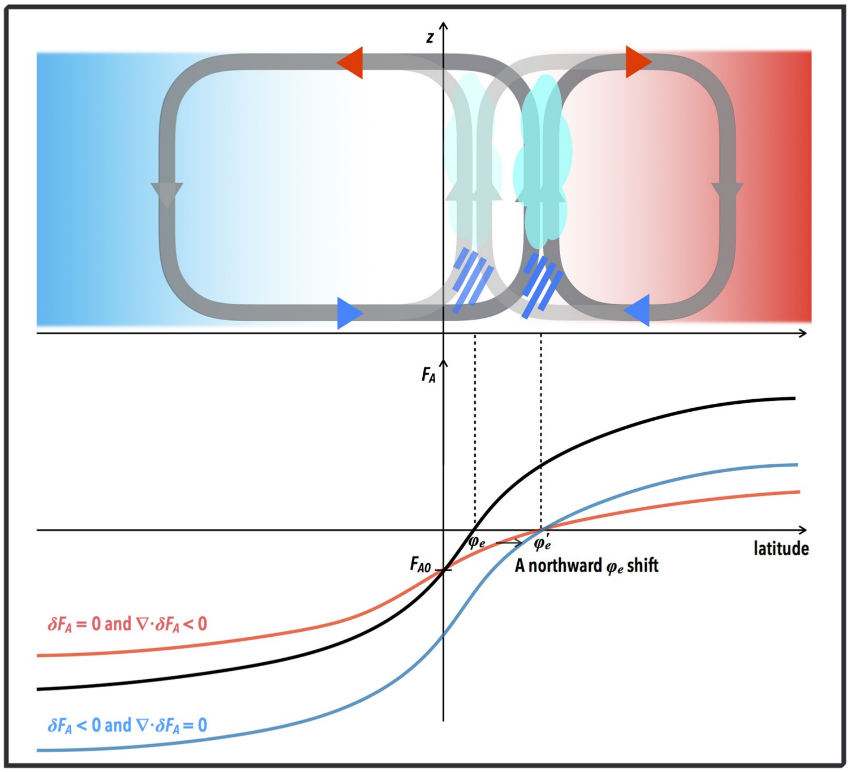

Figure 1.2: Schematic of the relationship between Hadley cells, atmosphere heat transport and energy flux equator (from Kang et al. (2018)).

Practically, EFE change is not a good indicator of ITCZ migration because it does not always coincide with the ITCZ (Chiang and Friedman 2012; Donohoe et al. 2013; Seo et al. 2017; Wei and Bordoni 2018; Kang et al. 2018). Seo et al. (2017) examined the ITCZ responses to a doubling CO_2 and found that when a nearly uniform radiative forcing is presented, the total GMS may change significantly but the Hadley cells may stay still. The idea that a doubling CO_2 can shift ITCZ is because the current climate is hemispherically asymmetric. The CO_2 radiative forcing would shift ITCZ northward by amplifying the hemispheric temperature asymmetry due to positive water vapor feedback (Merlis et al. 2013b). The increase in CO_2 concentration would shift ITCZ southward because a warmer Northern Hemisphere will lose more energy due to more outgoing longwave radiation (OLR) in the warmer hemisphere (Frierson and Hwang 2012). The responses of cloud remain uncertain (Seo et al. 2017).

Also, the ITCZ position is not only sensitive to the changes of hemispherical energy transport caused by a different radiative forcing. ITCZ shift is also sensitive to net energy input to the equatorial atmosphere (atmospheric net radiative energy input minus ocean energy uptake within equatorial region, Bischoff and Schneider (2014)). However, as long as one factor is controlled, the relationship between ITCZ shift and the other factor can be tested.

Paleoclimate data and model simulations also support the energetic theory. Wang et al. (2001) found that the East Asian monsoon recorded by Hulu Cave has a close relationship with Greenland temperature recorded by ice cores. They found that the East Asian monsoon is weaker when Greenland is colder. Chiang et al. (2003) tried to explain why proxy records from Cariaco Basin in the southern Caribbean Sea, showed various changes of ITCZ position by using Community Climate Model version 3 (CCM3) general circulation model with Last Glacial Maximum conditions (more high-latitude land ice, sea ice, especially in the Northern Hemisphere, and different ocean heat transport comparing to present-climate). They found a clear southward shift of the ITCZ. Chiang and Bitz (2005) further investigated on this phenomenon and found that a relatively small sea ice increase in the Northern Hemisphere can cause a large southward shift of the ITCZ. Chiang and other authors were able to prove that extratropics can influence the tropics. These findings updated our typical understanding that tropics drive the tropical-extratropical interactions (Horel and Wallace 1981; Hoskins and Karoly 1981).

1.2 Climate models

Climate models are computational simulations for learning about the climate system, and the learning takes place in the construction and the manipulation of the model (McGuffie and Henderson-Sellers 2014, pg. 24). The dynamical, thermodynamical, physical, chemical, and even biological process interactions make the studies of climate phenomena interesting, complicated, and challenging. Climate modelers, on the one hand, try to simulate by capturing as much of the dynamics as they can in the comprehensive climate models. On the other hand, they simplify and capture the essence of a phenomenon in idealized models to understand the phenomenon (Held 2005). Climate modelers have been trying to build a model hierarchy (Fig. 1.3, credit: Jeevanjee et al. (2017)) with various levels of complexity and comprehensiveness to study the climate system (Jeevanjee et al. 2017). For example, some models can be slab ocean with ideal land and with spectral radiation like the models we use in this dissertation. Some models can be dynamical ocean with real land like CMIP models.

$$\overset{\textbf{Fluid}}{\begin{pmatrix}\text{compressible}\\ \text{hydrostatic}\\ \text{QG}\\ \text{static}\end{pmatrix}} \times \overset{\textbf{Rotation}}{\begin{pmatrix}\text{Coriolis}\\ \beta-\text{plane}\\ f-\text{plane}\\ \text{none}\end{pmatrix}} \times \overset{\textbf{Ocean}}{\begin{pmatrix}\text{dynamical}\\ \text{column}\\ \text{slab}\\ \text{non-uniform } T_s\\ \text{uniform } T_s\end{pmatrix}} \times \overset{\textbf{Surface}}{\begin{pmatrix}\text{land}+\text{ice}\\ \text{real land}\\ \text{ideal land}\\ \text{aqua}\end{pmatrix}} \times \overset{\textbf{Convection}}{\begin{pmatrix}\text{explicit moist}\\ \text{super}-\text{param.}\\ \text{parameterized}\\ \text{large}-\text{scale}\\ \text{dry}\end{pmatrix}} \times \overset{\textbf{Radiation}}{\begin{pmatrix}\text{spectral}\\ \text{gray}\\ \text{Newtonian}\\ \text{fixed}\end{pmatrix}}.$$

Figure 1.3: A general list of climate model frameworks. More components like atmospheric chemistry and microphysics can be added if needed (from Jeevanjee et al. (2017)).

Studies that relate ITCZ and hemispheric asymmetry of the atmospheric energy budget prefer using idealized models (for example, Chiang and Bitz (2005); Broccoli et al. (2006); Kang et al. (2008, 2009); Frierson and Hwang (2012); Donohoe et al. (2013)). As pointed out by Broccoli et al. (2006), ITCZ shift in response to extratropical forcing is most robust when using atmosphere-slab ocean idealized models because the oceanic circulation changes can disrupt the relationship substantially (Broccoli et al. 2006; Kang et al. 2018; Biasutti and Voigt 2020; Kang 2020). Slab ocean is a motionless ocean of fixed depth. The fluid motion of atmosphere and ocean are very different on the timescale. It is unnecessary to calculate the long-term adjustment of the ocean when the atmosphere is the main focus (Schneider and Dickinson 1974). In the earlier days, when Manabe, Bryan and other authors attempted to jointly model atmosphere, ocean and cryosphere, the average temperature of the upper 50 m of the ocean is assumed to be associated with ocean mixed layer (i.e. Bryan and Cox (1968); Manabe and Bryan (1969)). The temperature of this layer is then applied as the surface temperature boundary condition to the atmosphere model.

Slab ocean models are still widely used nowadays. Slab ocean can avoid taking on the complexity of full ocean models to help mechanistic studies to focus on few features (Codron 2012). Slab ocean is often used in idealized geometry models such as aqua-planet because it is easier to conserve the energy of the model surface (Codron 2012). Slab ocean can eliminate limitations caused by using prescribed sea surface temperature (SST) as the lower boundary, such as the frequently unbalanced heat budget at the surface (Lee et al. 2008). Slab ocean allows modelers to study the sensitivity of the climate to external perturbations (Lee et al. 2008), and indeed, we use slab ocean in this study. Moreover, slab ocean configuration does not simulate double ITCZ that is often seen in Atmospheric Model Intercomparison Project (AMIP) which has prescribed SST as the lower boundary (Lee et al. 2008).

In slab ocean models, the ocean can still be dynamic by adding a “Q-flux”. “Q-flux”, a flow of energy between ocean and atmosphere per unit of area per unit of time, was designed to reduce the systematic errors to keep the model simulation closer to reality (Manabe et al. 1991; Murphy 1995; Roberts et al. 1997). For example, Roberts et al. (1997) used “Q-flux” along with other flux adjustments to prevent climate drifts. Climate drifts were originally designed in coupled models, when integrated for a longer time period, the basic model state was not suitable for studying perturbations anymore.

However, nowadays “Q-flux” is used to represent a heat source to mimic ocean heat transport, to do experiments, and to test theories. For example, Frierson et al. (2013) used “Q-flux” to represent two surface heat flux scenarios. One is observed surface heat flux, which includes the effect of the present-day climate cross-equatorial ocean heat transport that causes a 1-2 K warmer Northern Hemisphere. The other is a symmetrized surface heat flux. The simulations of these two scenarios proved that the heat asymmetry causes the tropical precipitation peak in the warmer hemisphere. Rencurrel and Rose (2018) used eight different "Q-flux" sets to represent convergence and divergence of ocean heat transport in different regions ranging from subtropics to polar area to experiment how the Hadley Cell responds to different ocean heat transport (OHT). They found that when the OHT convergence patterns are near the equator, the Hadley Cells are momentum-conserving. When the OHT convergence patterns are near midlatitudes, the streamfunction of Hadley cells has anomalies that tilt the Hadley cells in the outer branches, which changes GMS effectively.

1.3 Applying climate models to better understand tropical precipitation

Donohoe et al. (2013) adopted cross-equatorial energy flux instead of EFE to study annual ITCZ shifts and seasonal ITCZ location. Cross-equatorial energy flux, termed as atmospheric heat transport across the equator (AHT_{EQ}) by their paper, shares a similar idea with EFE. They found that, when EFE and ITCZ lie further north, southward energy transport over the equator is stronger. It is because, when the energy imbalance between Northern and Southern Hemisphere is larger, more energy needs to be transported across the equator by the Hadley cell. More precisely, the magnitude of the AHT_{EQ} is proportional to the location of the ITCZ relative to the equator (Donohoe et al. 2013). In addition, if the total energy absorbed by the atmosphere increases, the ITCZ position will shift toward the pole region further (Schneider et al. 2014). Donohoe et al. (2013) performed an aqua-planet experiment with various depth of 2.4, 6, 12, 24 and 50 m slab ocean using Geophysical Fluid Dynamics Laboratory Atmospheric Model version 2.1 (GFDL-AM2.1). The results show that the ITCZ and AHT_{EQ} are strongly anticorrelated with a multimodel average correlation coefficient of -0.95 over the seasonal cycle. Therefore, one can expect that, especially for slab ocean simulations, a northward ITCZ position has a strong relationship with southward AHT_{EQ}. Their paper also tested, under global warming, how the ITCZ will shift and the AHT_{EQ} will change at an annual mean scale. The results showed that the annual mean ITCZ shifts and AHT_{EQ} changes in response to global warming are significantly negatively correlated among different model outputs, with an average correlation coefficient of -0.81.

To more deeply investigate the energetic theory, Tropical Rain belts with an Annual cycle and a Continent Model Intercomparison Project (TRACMIP) was created (Voigt et al. 2016). TRACMIP, as an idealized climate modeling project, is designed to reproduce essential features of present-day and expected future climate changes. TRACMIP can capture the ITCZ, Hadley cells, and eddy-driven jets. By capturing these essential phenomena, TRACMIP is constructed to help answer the challenging question of "What controls the tropical rain belts" (Voigt et al. 2016). TRACMIP have control runs and quadrupling CO2 (4xCO_2) simulations that study the ITCZ responses to future radiative forcings (Voigt et al. 2016).

TRACMIP also applied a "Q-flux" to its slab ocean (see section 1.2). "Q-flux" in TRACMIP is prescribed as the observed zonal mean and annual mean effect of ocean currents (Fig. 1.4, from Biasutti and Voigt (2020). "Q-flux" in TRACMIP helps avoid zonal asymmetry, which causes stationary eddies (Biasutti and Voigt 2020). Stationary eddies dominate the cross-equatorial total energy transport, which will affect the robustness of the relationship between the ITCZ and total energy transport (Marshall et al. 2014). "Q-flux" in TRACMIP allows transient eddies to influence Hadley cells (Schneider 2006). Dynamically, momentum fluxes associated with transient eddies affect Hadley cells and ITCZ significantly (Geen et al. 2020). This idealization of oceanic heat transport can also provide a meridional asymmetry in all simulations to: 1) make the Northern Hemisphere warmer than the Southern Hemisphere as in the real world; 2) avoid double ITCZ problem in climate models; and 3) position ITCZ north of the equator as in reality (Lee et al. 2008; Frierson et al. 2013; Voigt et al. 2016; Biasutti and Voigt 2020).

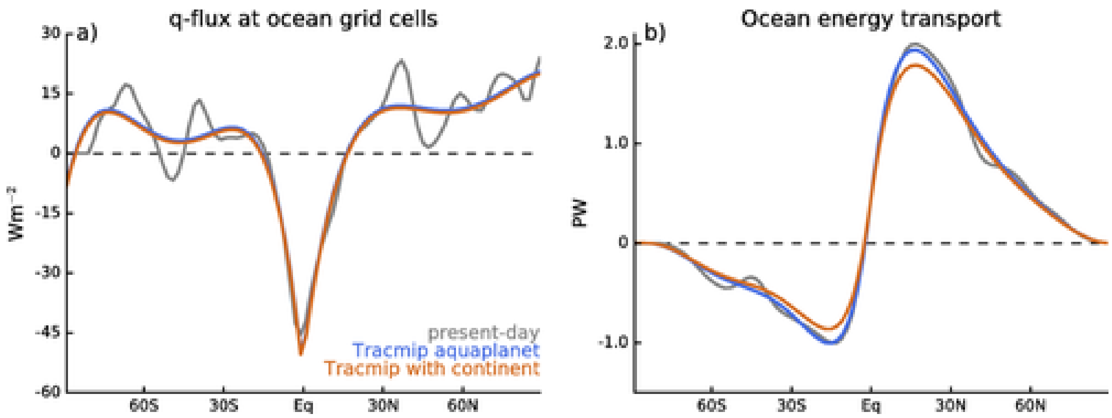

Figure 1.4: TRACMIP "Q-flux" and ocean energy transport settings (from Voigt et al. (2016)).

To serve the purpose of studying the tropical rain belts, TRACMIP organized five idealized experiments, with two aquaplanet and three idealized tropical continent setups (Fig. 1.5). These experiments were simulated by one simplified and 13 comprehensive atmospheric models thermodynamically coupled to a slab ocean and driven by seasonal varying insolation (Voigt et al. 2016). In our study, we used the tropical continent setups' simulations. The "idealized tropical continent" is a rectangular patch of the slab ocean with reduced evaporation and increased albedo and zero "Q-flux". This flat "jello" like region locates from 30°S to 30°N, 0°E to 45°E, which can be considered as analogous to the African continent.

Experiment	Land	CO_2 (ppmv)	Eccentricity ϵ	Years	Initial Condition
AquaControl	No	348	0	15 + 30	Arbitrary initial state, 15 years of spin-up
LandControl	Yes	348	0	40	Year 45 of AquaControl
Aqua4xCO2	No	1392	0	40	Year 45 of AquaControl
Land4xCO2	Yes	1392	0	40	Year 40 of LandControl
LandOrbit	Yes	348	0.02	40	Year 40 of LandControl

[a] The control configuration is an aquaplanet coupled to a slab ocean. Insolation varies with diurnal and annual cycles. CO_2 is varied, and a tropical jello-continent and different orbital parameters are used to study tropical rainfall in present-day-like conditions and in conditions mimicking the mid-Holocene and global warming.

Figure 1.5: TRACMIP experiment settings to explore different scenarios (from Voigt et al. (2016)).

This idealized continent setting filled the gap between aqua-planet and fully coupled models in studying the similarities and differences between ITCZ and monsoon. Bordoni and Schneider (2008) found that, even for aqua-planet models, monsoon can occur as long as the surface has a sufficient low thermal inertia when the ITCZ migrates rapidly into the warmer hemisphere. When the ITCZ shifts further to the north, Hadley cells are no longer eddy driven features but approaching conservation of angular momentum, which is a monsoon like condition. Once it turns into a monsoon regime, the circulation is no longer constrained by the zonal momentum budget but is constrained by the energy budget, which means the circulation will respond to thermal forcing strongly (Geen et al. 2020). Geen et al. (2019) investigated on how “further north” the Hadley cells are no longer eddy-driven using aqua-planet models. They found that 7° is the latitude where ITCZ migrates poleward fastest, which means it’s the most unstable latitude and suggesting it’s the poleward limit of an ITCZ. For the effects of continent on monsoon circulations, Bordoni (2020) did experiment using zonally symmetric continents in the Northern Hemisphere with different southern boundaries. She found that when the continents extended to the tropics (from 20°N to the equator), monsoon circulations extended to the subtropics.

The meridional symmetric continents in TRACMIP can help us further investigate the transition between ITCZ and monsoon, especially African monsoon. The initial purpose of this study was to break the energetic theory into seasonal and regional scales like Boos and Korty (2016), who calculated both zonal and meridional total energy flux and demonstrated how ENSO associated total energy transport anomalies affected local ITCZ shift. We planned to apply this seasonal and regional energetic theory to study the onset of the monsoon developed on the idealized continent under both present-day and 4xCO_2 conditions to take the advantage of the predictability of energetic theory. This combination of the energy-based theories and momentum-based (monsoon) theories can generate a self-constrained model for the tropical climate (Biasutti et al. 2018). However, as analysis moved on, explaining why the zonal-mean seasonal energetic theory breaks down for TRACMIP simulations became the main purpose of this study.

Like the other simplified models, the limitation of TRACMIP is that the model output cannot be validated against observations. However, if the experiments are well-designed, this limitation can be compensated by the clarity gained in comparing the model formulations (Lee et al. 2008). Considering models that have higher realism did not decrease the spread of model member outputs, instead, the complexity introduced new uncertainties (Bony et al. 2013), TRACMIP model outputs are still valuable for examining the mechanisms of ITCZ shifts, for giving the researchers insights of potential ITCZ responses to a warming climate, and for understanding the differences between models.

CHAPTER 2: DATA

In our study, all analyses are carried out using model simulations. TRACMIP simulations provide standard Coupled Model Intercomparison Project output variables (detailed variables are listed in Table 2.1). The models we will analyze are shown in Table 2.2. The models have 40 years of simulation and the spin-up simulations are not included in the 40-year simulation (Voigt et al. (2016)). In this dissertation, all 40-year simulations were used to do the analysis. 10 out of 13 models are chosen because the other three models do not provide the full variables that we need. We will use numbers 0 to 9 to represent the models in our figures in section 4.

Table 2.1: Variables used in this analysis.

Variable Description	Variable Name	Units
Air Pressure at Sea Level	psl	Pa
Air Temperature	ta	K
Geopotential Height	zg	m
Precipitation	pr	kg m^{-2} s^{-1}
Specific Humidity	hus	1 (kg kg^{-1})
Surface Downwelling Longwave Flux in Air	rlds	W m^{-2}
Surface Downwelling Shortwave Flux in Air	rsds	W m^{-2}
Surface Upward Latent Heat Flux	hfls	W m^{-2}
Surface Upward Sensible Heat Flux	hfss	W m^{-2}
Surface Upwelling Longwave Flux in Air	rlus	W m^{-2}
Surface Upwelling Shortwave Flux in Air	rsus	W m^{-2}
Top of the Atmosphere (TOA) Incoming Shortwave Flux	rsdt	W m^{-2}
TOA Outgoing Longwave Flux	rlut	W m^{-2}
TOA Outgoing Shortwave Flux	rsut	W m^{-2}
Eastward Wind	ua	m s^{-1}
Northward Wind	va	m s^{-1}

Table 2.2: Climate models used in this analysis.

Model#	Model Name	Resolution	Remarks
1	CAM3	T42 (2.8°); 26 levels	Atmosphere component of CCSM3 (https://www.cesm.ucar.edu/models/ccsm3.0/)
2	CAM4	1.9° lat × 2.5° lon, finite volume (nominally 2.0°); 26 levels	Atmosphere component of CCSM4 (https://www.cesm.ucar.edu/models/ccsm4.0/)
3	CNRM_AM5	T127 (0.9° lat × 0.9° lon); 31 levels	Atmosphere component of CNRM_CM5 (https://portal.enes.org/models/earthsystem-models/cnrm-cerfacs-1/cnrm-cm5)
4	ECHAM61	T63 (1.9° lat × 1.9° lon); 47 levels	Atmosphere component of MPI_ESM (https://mpimet.mpg.de/en/science/models/mpi-esm)
5	ECHAM63	T63 (1.9° lat × 1.9° lon); 47 levels	Update of ECHAM61
6	LMDZ5A	1.9° lat × 3.8° lon; 39 levels	Atmosphere component of IPSL_CM5A_LR (https://cmc.ipsl.fr/international-projects/cmip5/)

7	MetUM_CTL	N96 (1.9° lat × 1.3° lon); 85 levels	Standard configuration of GA6.0 (https://www.metoffice.gov.uk/research/foundation/global-modelling)
8	MetUM_ENT	N96 (1.9° lat × 1.3° lon); 85 levels	+ 50% convective entrainment and detrainment compared to MetUM_CTL
9	MIROC5	T85 (1.4° lat × 1.4° lon); 40 levels	Model for Interdisciplinary Research on Climate Version Five (https://glisaclimate.org/node/2539)
10	MPAS	240 km; 30 levels	Model for Prediction Across Scales (http://mpas-dev.github.io/)

In our study, all comparisons are calculated using 4xCO_2 scenarios minus present-climate-like (control runs, CTL hereafter) conditions. We chose the idealized continent rather than the aqua-planet experiment because we aimed for regional and monsoon analysis when we initialized this study. The idealized land will not strongly affect the zonal-mean energetic theory and ITCZ shift analyzed in this study. Biasutti and Voigt (2020) used aqua-planet simulations and found similar results.

CHAPTER 3: METHODS

3.1 ITCZ shift

We use two methods to quantify the ITCZ shift under a warming scenario in this study. The first one is to use centroid changes of the zonal-mean precipitation curve to represent the ITCZ shift. The latitude of ITCZ is quantified by the centroid of zonal-mean precipitation, developed from Harrop et al. (2018):

$$\phi_{\mathrm{ITCZ}} = \frac{\int_{\phi_1}^{\phi_2} \phi \, [P] \, d\phi}{\int_{\phi_1}^{\phi_2} [P] \, d\phi} \tag{3.1}$$

with ϕ_1 as 30°S and ϕ_2 as 30°N, $[P]$ as the zonal-averaged precipitation.

We also tried to use maximum zonal-mean 30° N to 30° S precipitation latitude and the average of top 30% maximum zonal-mean precipitation latitudes to quantify the ITCZ position. We found that the centroid method is the most reliable one. That is because the maximum method can be affected easily by a few very large precipitation latitudes. This centroid method is used to compare TRACMIP simulation to other studies that use reanalysis or Coupled Model Intercomparison Project Phase 3 (CMIP3) simulations.

The second method will be introduced in section 3.5.1.

3.2 Atmospheric Total Energy Transport

We use the method of Donohoe and Battisti (2013) at a zonal-mean, seasonal-mean scale to understand the ITCZ response to climate change. Since we use slab ocean model simulations, the energy budget of the atmosphere at any latitude can be denoted by (schematic see Fig. 3.1)

$$\mathrm{AHT}_{total} = \langle \mathrm{SWABS} \rangle - \langle \mathrm{OLR} \rangle + \langle \mathrm{SHF} \rangle - \langle \mathrm{STOR}_{atmos} \rangle, \tag{3.2}$$

where AHT_{total} is the total northward atmospheric energy transport. The brackets indicate the spatial integration starting from 90°S to a specific latitude. SWABS is the shortwave radiation absorbed in the atmosphere and represents the direct heating from the sun from both the top of the atmosphere (TOA) and the surface (SURF):

$$\mathrm{SWABS} = \mathrm{SW}_{\downarrow \mathrm{TOA}} - \mathrm{SW}_{\uparrow \mathrm{TOA}} + \mathrm{SW}_{\uparrow \mathrm{SURF}} - \mathrm{SW}_{\downarrow \mathrm{SURF}}. \tag{3.3}$$

OLR is the outgoing longwave radiation at TOA. SHF is the surface heat flux to the atmosphere, which is the delayed effect of the sun and ocean heat transport. SHF is a summation of sensible heat flux (SENS), latent heat flux (LH), and longwave flux (LW) from the surface into the atmosphere:

$$\mathrm{SHF} = \mathrm{SENS}_{\uparrow \mathrm{SURF}} + \mathrm{LH}_{\uparrow \mathrm{SURF}} + \mathrm{LW}_{\uparrow \mathrm{SURF}} - \mathrm{LW}_{\downarrow \mathrm{SURF}}. \tag{3.4}$$

The STOR_{atmos} denotes the energy stored by the atmosphere, which is calculated as:

$$\mathrm{STOR}_{\mathrm{atmos}} = \frac{d}{dt} \left[\frac{1}{g} \int_{10hPa}^{1000hPa} (c_p T + Lq)\, dp \right], \tag{3.5}$$

where c_p is the heat capacity at constant pressure, T is the air temperature (in K), L is the latent heat of vaporization of water, q is the specific humidity. Calculating d/dt uses centered differencing at a monthly timescale. The model top layer is 10 hPa instead of 0 hPa in TRACMIP simulations. TRACMIP model output that we selected contains all the variables that we need.

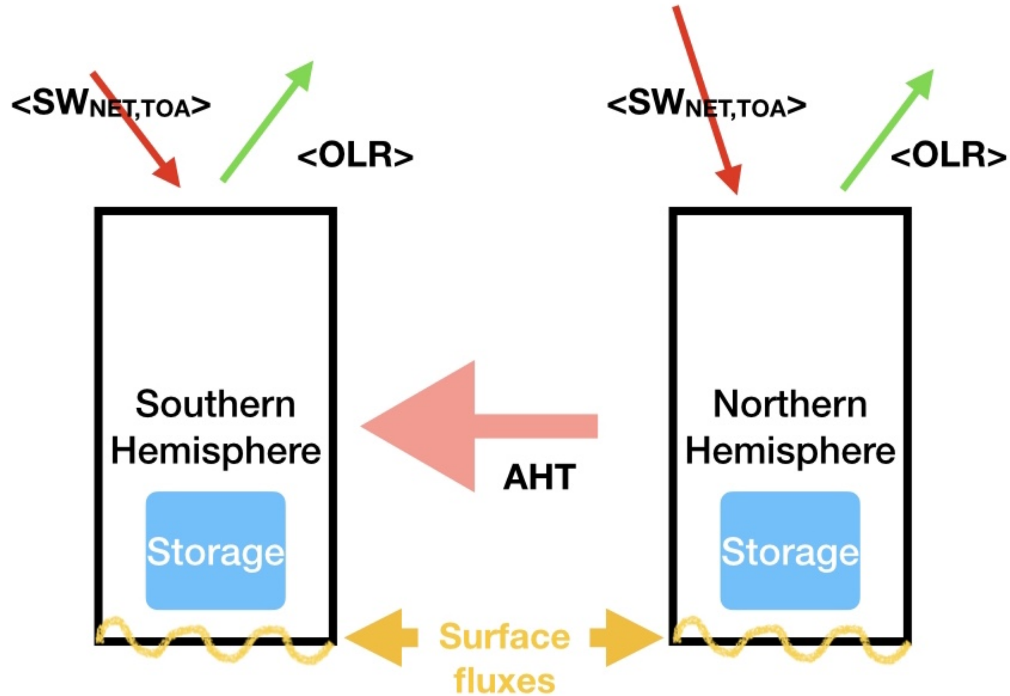

Figure 3.1: Schematic of how atmospheric total energy transport is calculated.

3.3 Mass Transport

The mean meridional circulation (MMC), which is often called the Hadley cell in the tropics, can be described by a mass stream function. By calculating the northward mass flux above 500 hPa in this study, the MMC/Hadley cell streamfunction at 500 hPa is defined as (Hartmann 2016, pg. 165):

$$\Psi_M = \frac{2\pi acos\phi}{g} \int_{10hPa}^{500hPa} [v]dp, \tag{3.6}$$

where brackets indicate zonal mean. As we mentioned before, the top layer of the model simulations is 10 hPa instead of 0 hPa. So we use 10 hPa as the top of the atmosphere. For the mean meridional stream function, the mass transport between any two streamlines equals to the difference in the stream function values (Hartmann

2016, pg. 165). The mass conservation for the zonal mean flow implies the relationship between the mass stream function and the mean meridional vertical velocity at 500 hPa (Hartmann 2016, pg. 165):

$$-[\omega] = \frac{g}{2\pi a^2 cos\phi} \frac{\partial \Psi_M}{\partial \phi}. \tag{3.7}$$

That is, the zonal averaged vertical velocity depends on the rate of the stream function change with latitude (Hartmann 2016, pg. 165).

At an annual timescale, integrating v-wind from 10 hPa to 1000 hPa using equation 3.6 would be zero because the Hadley cells transport mass to the polar regions in the upper branches and transport mass back to the equator in the lower branches. The total column integrated mass transport by the Hadley cell will be canceled between the upper and lower branches. In our study, since we focus on a seasonal timescale, the upper and lower branches do not cancel with each other all the time due to net mass transport between hemispheres. Thus, to obtain the Hadley component of v-wind, we adjust the v-wind to have zero column average by subtracting the vertical averaged v-wind:

$$[v]_{Hadley} = [v] - \frac{1}{1000hPa - 10hPa} \int_{10hPa}^{1000hPa} [v] dp, \tag{3.8}$$

where brackets indicate zonal mean. Then equation 3.6 becomes:

$$\Psi_{M,Hadley} = \frac{2\pi a cos\phi}{g} \int_{10hPa}^{500hPa} [v]_{Hadley} dp. \tag{3.9}$$

We will also calculate the changes of $\Psi_{M,Hadley}$ with latitude (we notate it as $\mathrm{d}\Psi_{M,Hadley}/\mathrm{d}\phi$), since $\mathrm{d}\Psi_{M,Hadley}/\mathrm{d}\phi$ is proportional to the vertical motion.

3.4 Heat Transported by the Hadley Cells

The moist static energy (MSE) is defined as the sum of sensible, latent, and potential energy, which can be denoted by:

$$\mathrm{MSE} = c_p T + Lq + gz, \tag{3.10}$$

where c_p is the heat capacity at constant pressure, T is the temperature (in K), L is the latent heat of vaporization of water, q is the specific humidity, g is gravitational constant, and z is geopotential height.

Using zonal-averaged MSE times zonal-averaged meridional mass transport by Hadley cells, then integrating from 10-1000 hPa gives us the heat transported by Hadley cells:

$$\mathrm{AHT}_{Hadley} = \frac{2\pi a cos(\phi)}{g} \int_{10hPa}^{1000hPa} [\mathrm{MSE}][v_{Hadley}]dp. \tag{3.11}$$

We will also calculate the changes of AHT_{Hadley} with latitude ($\mathrm{dAHT}_{Hadley}/\mathrm{d}\phi$) to compare with $\mathrm{d}\Psi_M/\mathrm{d}\phi$.

As we mentioned in section 1.3, the relationship between the ITCZ shift and AHT_{total} changes simulated by TRACMIP is not as robust as previous studies. We break the link between ITCZ shift and AHT_{total} changes into smaller links (for illustration see Fig. 3.2). We call these small links between two factors as inner links in contrast to the outer link between ITCZ shifts and AHT_{total} changes. Theoretically (Schneider et al. 2014; Kang et al. 2018), when AHT_{total} changes under a warming scenario, AHT_{Hadley} will also change since it is a part of AHT_{total}. When the energy transport by the Hadley cell changes under global warming, the Hadley cell would also change. Hadley cell changes will certainly affect the vertical motion of the tropics, which will affect the position of ITCZ.

In summary, we calculate $\Psi_{M,Hadley}$, $d\Psi_{M,Hadley}/d\phi$, AHT_{Hadley}, and $d\mathrm{AHT}_{Hadley}/d\phi$ in addition to AHT_{total}. We also calculate GMS, which is the ratio between AHT_{Hadley} and $\Psi_{M,Hadley}$. We calculate $d\Psi_{M,Hadley}/d\phi$ to compare to the precipitation curve to check if the vertical motion simulation agrees with the precipitation simulation. To make it comparable to $d\Psi_{M,Hadley}/d\phi$, we calculate $dAHT_{Hadley}/d\phi$ also. In this way, from top and bottom variables on Fig. 3.2, AHT_{total} and ITCZ are connected through energy transport by the Hadley cells and mass transport (Hadley cells). We call these variables as factors and the relationship between two factors as a link.

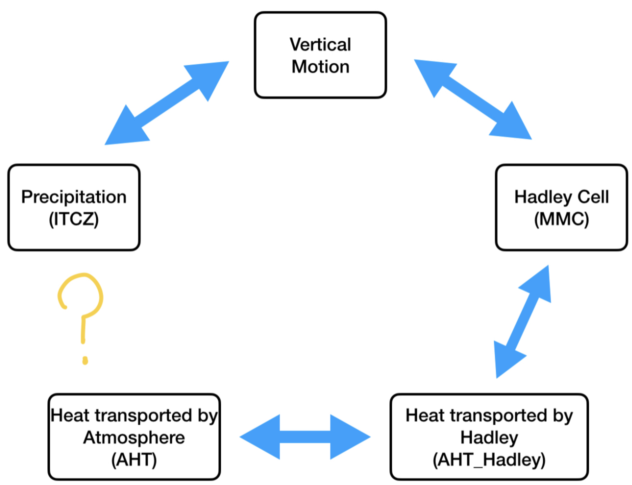

Figure 3.2: Relationship between our analyzed factors. The relationship between two factors is defined as an inner link. The factors themselves and their changes are both connected with each other.

3.5 Quantification of shifts

The total variables we are going to compare add up to 12 when considering both 4xCO_2 and CTL conditions. Shown in Fig. 3.3, the CAM3 September simulation suggested a northward shift of zonal-mean precipitation while AHT_{total} almost remains the same. Mass transport shifted to the north around the latitudes where the precipitation shifted to the north. The mass transport change with latitudes curve showed a very similar pattern to the zonal-mean precipitation curve. That is, the mass transport has a clear connection with precipitation. The energy transported by Hadley cells showed a southward shift south of 15°N and a northward shift north of 15°N. The changes of Hadley transported energy with latitudes suggested a southward shift south of 20°N and a northward shift north of 20°N. Apparently, the Hadley transported energy disagreed with the shift of the ITCZ. This result is consistent with Merlis et al. (2013a); Seo et al. (2017); Wei and Bordoni (2018); Biasutti and Voigt (2020) who found the vertical energy stratification changes play a role in balancing the hemispheric heat distribution.

Although figures like 3.3 can give us a lot of information, it's unsuitable to display all models' behavior on the same plot. Therefore, we propose two quantification methods of detecting the shift of the curves between 4xCO_2 and CTL.

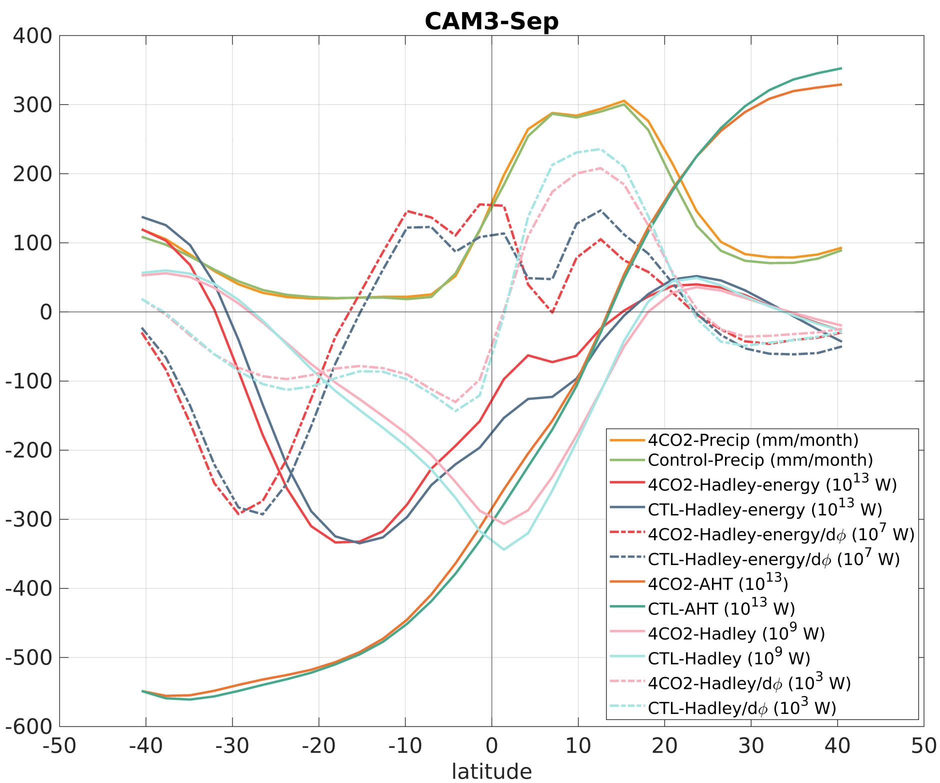

Figure 3.3: Example of all 12 curves displaying on the same plot. The model is CAM3. All warm colors are 4xCO_2 simulations and cool colors represent CTL simulations.

3.5.1 Cross-correlation

Cross-correlation is used to identify the shift between two curves along the x-axis. In general, the cross-correlation method is moving one curve left or right to match with the other curve's peaks and troughs. After the movement, the curves are correlated to each other the most. The movement that satisfies the maximum correlation of the curves will be defined as the shift between the curves. Ideally, the only difference between the curves should be an unknown shift. Our curves often behave close to this requirement. To make the shift detection process more accurate, we will restrict the domain of the curves, and our searching window for the shift.

Our analysis mainly focuses on the latitude belt near the ITCZ. We use the centroid of the precipitation curve to represent where ITCZ is. The traditional way (see equation 3.1) of calculating the centroid by using symmetric area from the equator will make the centroid skew to the opposite hemisphere of the peak precipitation. For example, the precipitation may peak around 15° N. However, the traditional method that will count from 30° S makes the centroid skew to the south. Our method will make the searching window more flexible. We first find the peak latitude of the CTL precipitation curve. Then we use the latitudes 20° north and south from the peak latitude to calculate the centroid of the CTL precipitation curve. This centroid latitude will help us restrict our domain of the curves. Also, this latitude is where CTL ITCZ located.

Using the centroid latitude of the CTL precipitation as a reference, we use the window 20° north and south from it as our domain for all the variables' curves to calculate the cross-correlation between the CTL and 4xCO_2 scenarios. In this way, the curves far from the ITCZ will not affect our analysis. The cross-correlation is computed by:

$$\hat{\mathrm{R}}_{\mathrm{xy}}(\phi) = \begin{cases} \sum_{n=\phi_1}^{\phi_2-\phi-1} x_{n+\phi}\, y_n, & \phi \geq 0 \\ \hat{R}_{yx}(-\phi), & \phi < 0 \end{cases}, \tag{3.12}$$

where x indicates CTL curve and y indicates $4xCO_2$ curve. $\hat{R}_{xy}(\phi)$ is the cross-correlation value at shift ϕ. The ϕ values will be integers because the numerical calculation can only move the curves by grid points.

The $\hat{R}_{xy}(\phi)$ value forms another curve with the shift ϕ. Ideally, the ϕ value corresponding to the largest $\hat{R}_{xy}(\phi)$ value is the shift of the curves. However, the largest $\hat{R}_{xy}(\phi)$ value sometimes occurs at the edges of the cross-correlation curve, which means that the shift is around 20°. This shift value is unreasonable considering our domain is only 40° and none of our spaghetti plots (like Fig. 3.3) has a huge shift like this. The reason for this situation is that the method is trying to match different peaks to achieve the largest cross-correlation. To avoid this type of shifts to be detected, we also restrict our shift searching area as 15° left and right from the 0° shift value. The cross-correlation peaks that fall out of this restriction area will be considered as NaN for the shift values.

The peak remaining after the searching area restriction is not necessarily the largest cross-correlation value, considering the shift values ϕ are integers. For example, in fig. 3.4, the actual largest cross-correlation occurs between 1 grid point and 2 grid point shifts. Therefore, we find the peak $\hat{R}_{xy}(\phi)$ value and one point left, one point right to the peak value. These three points can form two slopes, with one as positive (left to peak) and one as negative (peak to right). If we do interpolation between these two slopes, the zero slope will indicate where the largest cross-correlation value is (along y-axis). The shift value (along x-axis) corresponding to this largest cross-correlation value is defined as the shift of the curve. Then we multiply this shift value by the model grid spacing to get the shift value in degrees of latitudes. The positive values indicate a northward shift and the negative values indicate a southward shift.

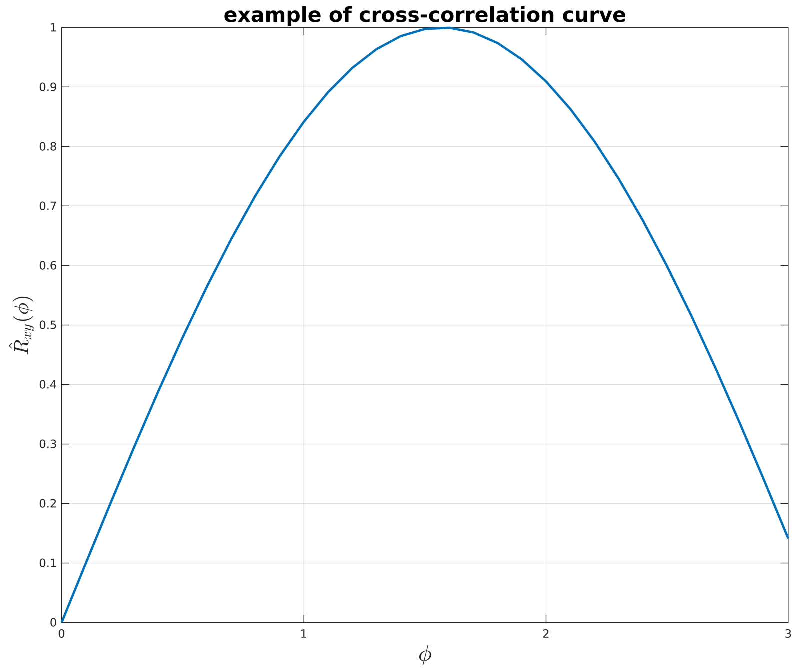

Figure 3.4: Example of cross-correlation curve. The shift values are integers, but the largest cross-correlation value occurs between two integer shifts 1 gridpoint and 2 gridpoints.

Among all the curves, the total energy transport curves do not have peaks and troughs. Therefore, the shift values between them are relatively small. We tried alternative methods to compute the shifts of total energy transport curves and found that the shifts were less correlated with the other shifts. Therefore, we kept the smaller shifts of the total energy transport for our analysis.

After we obtain all the different models' shift values of the curves, we scatter plot them for each month by using one factor's shifts as the x-axis and the other factor's shifts as the y-axis. For example, ITCZ shifts as the x-axis and mass transport changes as the y-axis to scatter plot 10 models' simulated shifts. Then we apply linear regression to show the relationship between the factors. R values and P values of the relationships will also be calculated. We tried robust regression method (robustfit function in Matlab) for the regression and found this method only ignores the outliers on the x-axis. Therefore, we decided to use the classic linear regression method.

CHAPTER 4: RESULTS

4.1 Model Simulation Check

We first checked the model simulation of the 10 selected TRACMIP models for basic planetary precipitation features. The seasonal cycle of the tropical (30° S to 30 °) precipitation centroid showed that the precipitation latitude usually peaks around August, September and October (ASO, Fig. 4.1). This peak is around one month later than the real world, which was also noticed by Voigt et al. (2016) when introducing TRACMIP. The spatial distribution of the ASO precipitation simulation represented the essential patterns (Fig. 4.2). All models showed that the precipitation is heavier near the equator where ITCZ locates. Mid-latitude storm tracks can also be noticed at annual (Fig. 4.4) and seasonal scale (Fig. 4.5). June, July, August (JJA) precipitation simulation has a stronger monsoon pattern (Fig. 4.3). This monsoon pattern that was not shown in the precipitation centroid seasonal cycle may come from the zonal averaging. To zoom to a regional view, some models (CAM3, CAM4, CNRM_AM5, and MIROC5, Fig. 4.6) have clear monsoon low pressure systems and tropical westerlies. The other models all have clear westerlies. Models simulations are similar to each other in the other months, too. The MIROC5 model surface winds have missing values after we changed our data server. Here we provide an older version of MIROC5' JJA surface configuration in appendix A.1. In addition, an older version of regional wind simulation that includes MIROC5 can be found in appendix A.

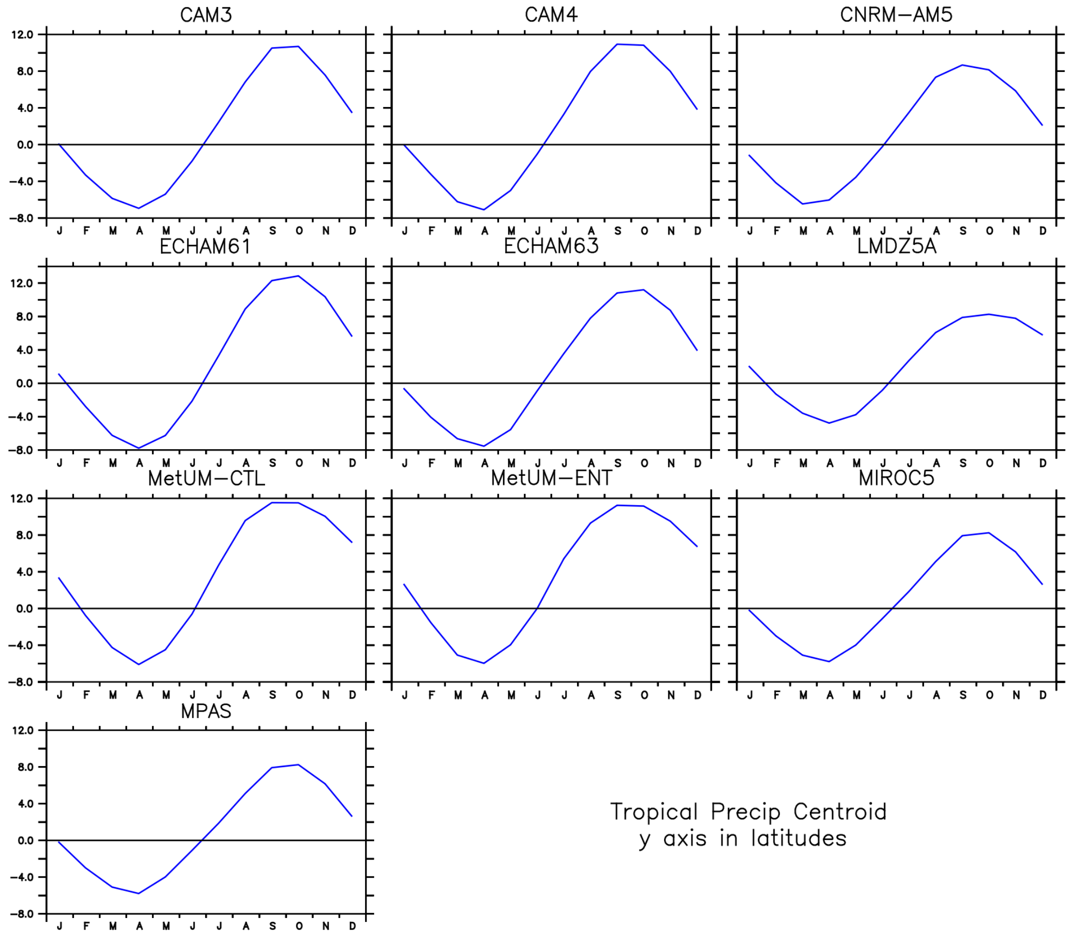

Figure 4.1: Seasonal cycle of tropical (30° S to 30 ° N) precipitation centroid simulated by each model. The y-axis represents latitude in degrees.

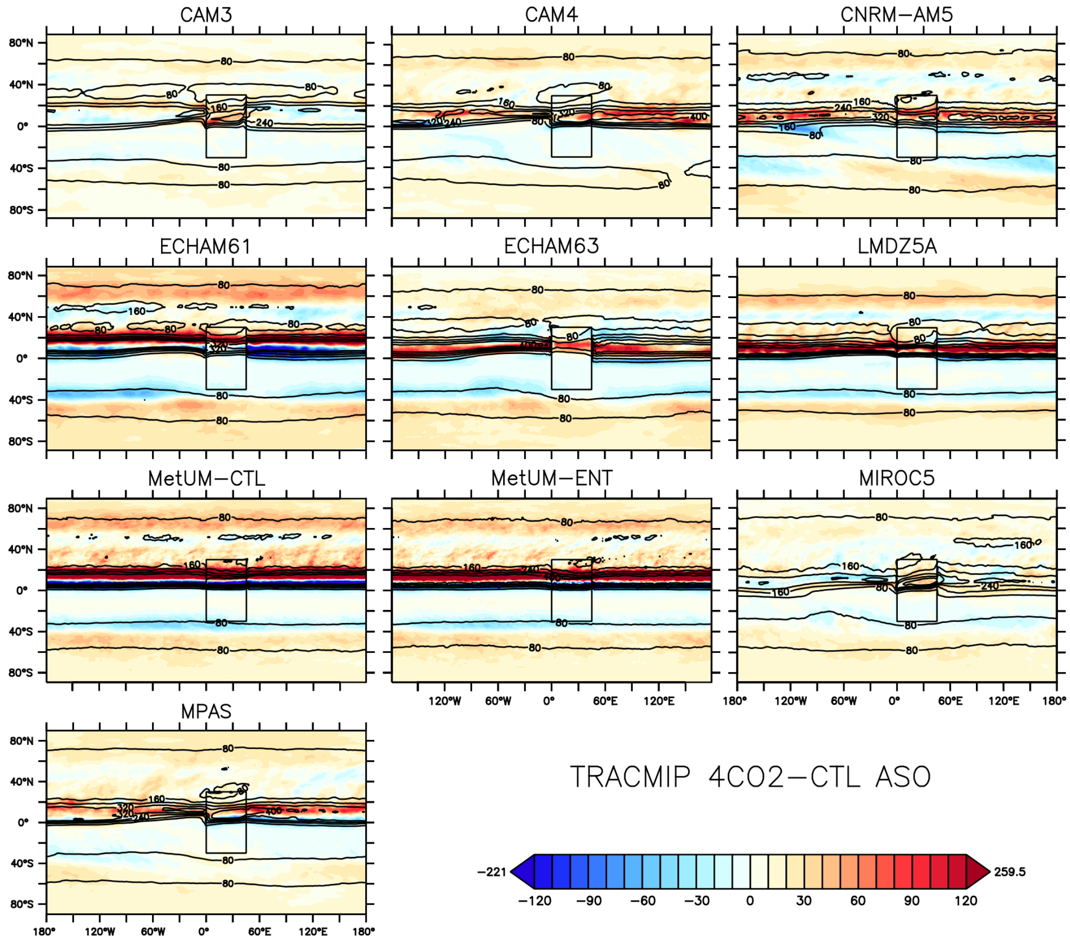

Figure 4.2: August, September, and October (ASO) precipitation simulations (mm/month). Contours are for CTL, and shadings are the difference between 4xCO_2 and CTL experiments. The rectangle represents where the idealized continent is.

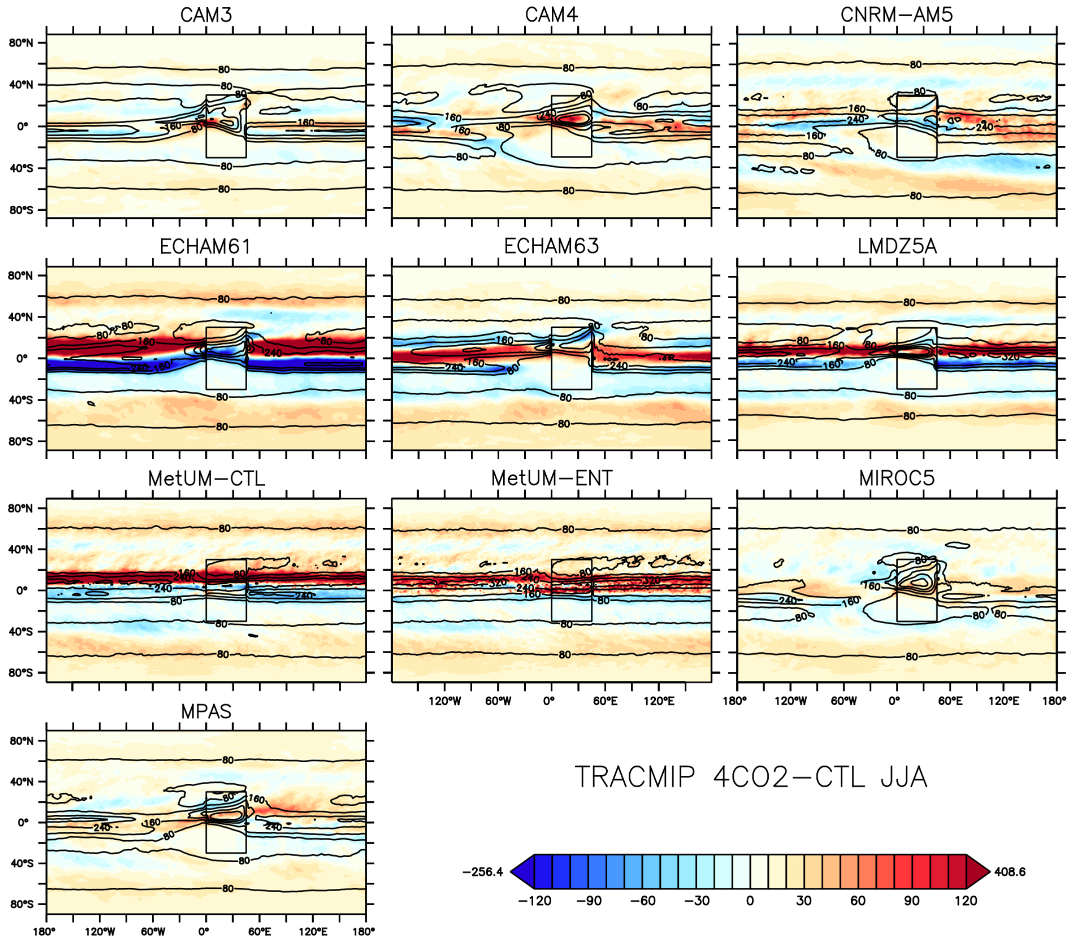

Figure 4.3: As Fig. 4.2 but for June, July, August (JJA).

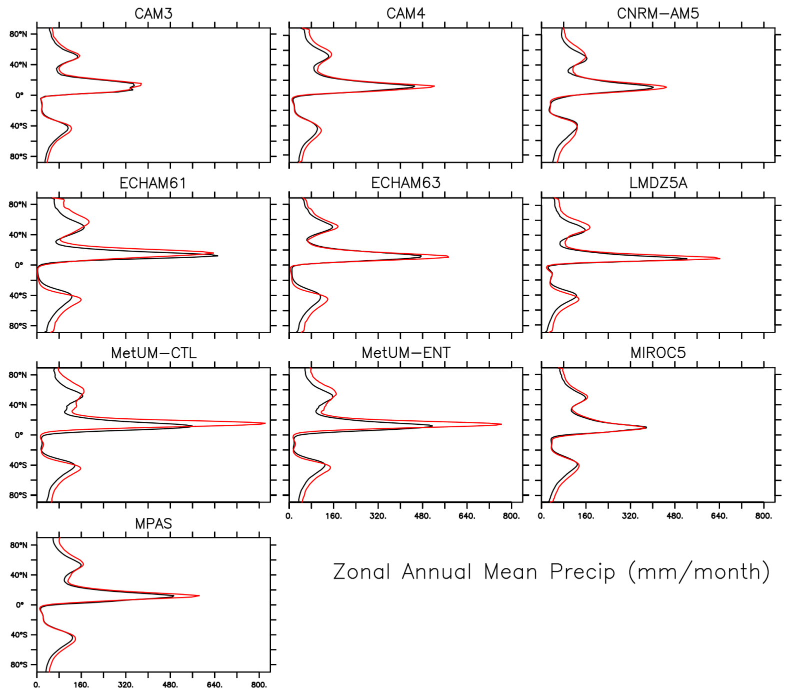

Figure 4.4: Annual-mean, zonal-mean precipitation simulations (mm/month). Red color indicates 4xCO_2 experiment and black color indicates CTL experiment.

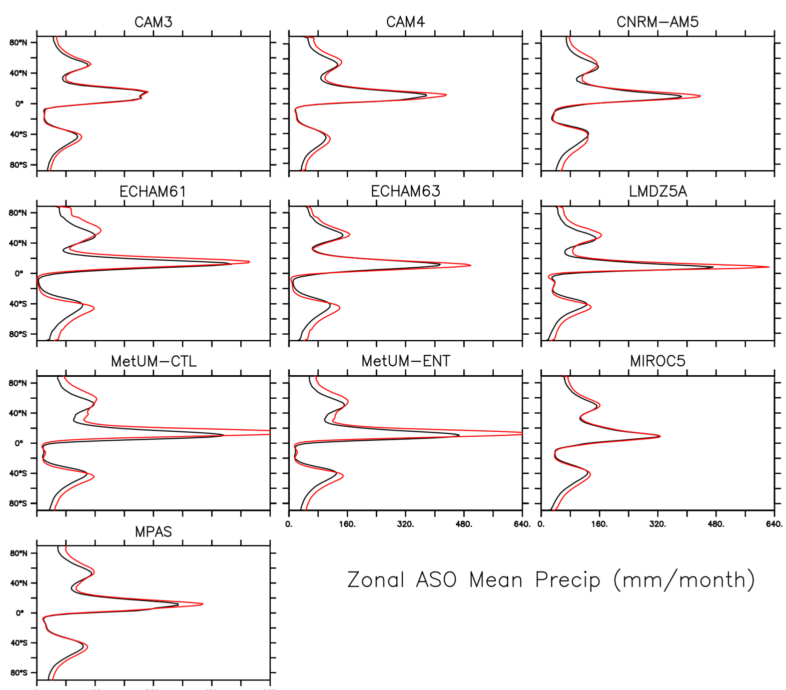

Figure 4.5: ASO-mean, zonal-mean precipitation simulations (mm/month). Red color indicates 4xCO_2 experiment and black color indicates CTL experiment.

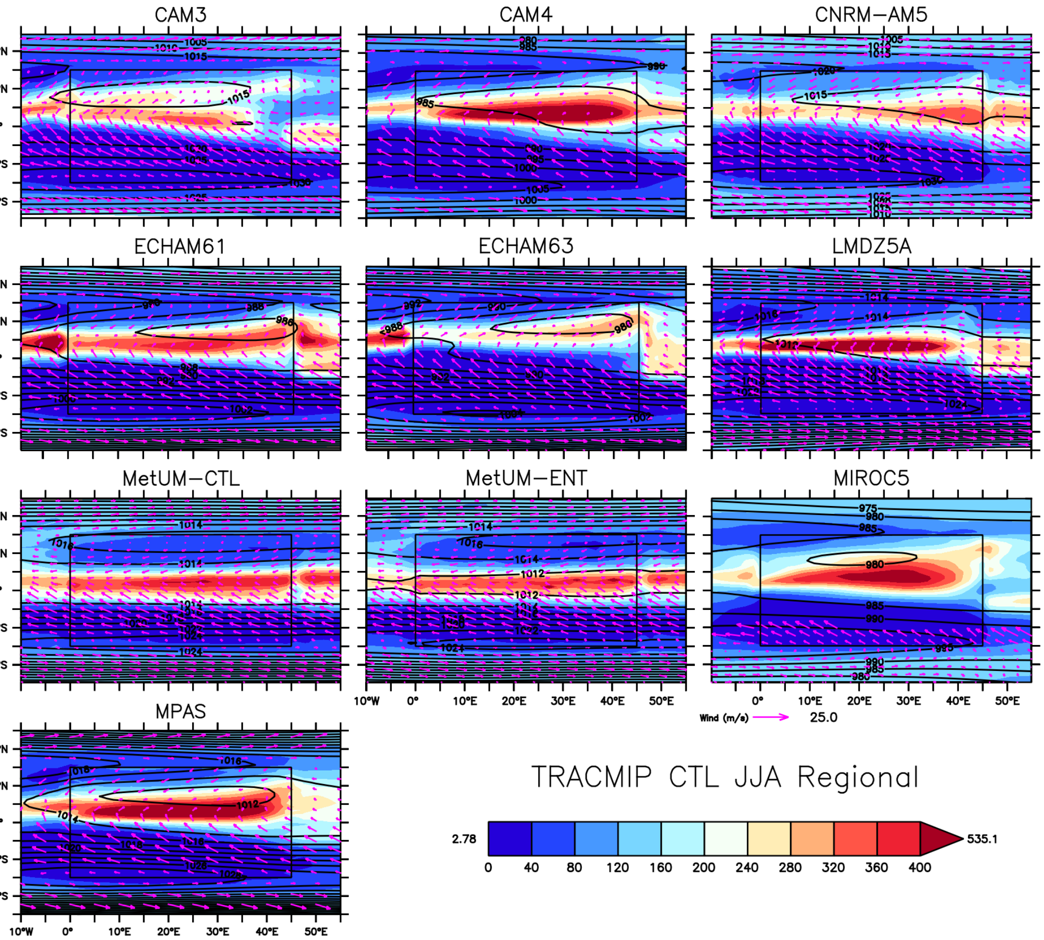

Figure 4.6: Regional JJA precipitation (mm/month, shading), pressure (hPa, contour) and wind (m/s, vector) simulations. The box indicates where the idealized continent is. The MIROC5 wind simulation has missing values after we changed our simulations' storage server. A more complete MIROC5 wind simulation can be found in appendix A.

We then examined the energy budget terms we introduced in section 3.2, simulated by TRACMIP models (Fig. 4.7). The integral area is from 90° S to the equator to represent the AHT_{EQ}. The shortwave absorption $\langle$SWABS$\rangle$ is the largest energy budget term. $\langle$SHF$\rangle$ and $\langle$OLR$\rangle$ are generally anti-phased. Compared to what Donohoe et al. (2013) calculated in their paper using CMIP3 simulations, TRACMIP's $\langle$OLR$\rangle$ peaks around two months in advance, $\langle$STOR$\rangle$ peaks one month later, and $\langle$SHF$\rangle$ peaks one month later. Convection is expected to lag the CMIP simulations or real world conditions around one or two months due to the relative deep slab ocean used in the TRACMIP simulations (Voigt et al. 2016). The ⟨OLR⟩ peaks earlier than the CMIP simulations, may be due to a later peak in ITCZ clouds. A late cloud peak would reduce the ⟨OLR⟩ in the later season, making the ⟨OLR⟩ look like it peaks in the earlier season. This earlier ⟨OLR⟩ peak will not affect our calculation of ITCZ shifts and energy budget factor changes, since the only difference between the 4xCO_2 and CTL is the radiative forcing.

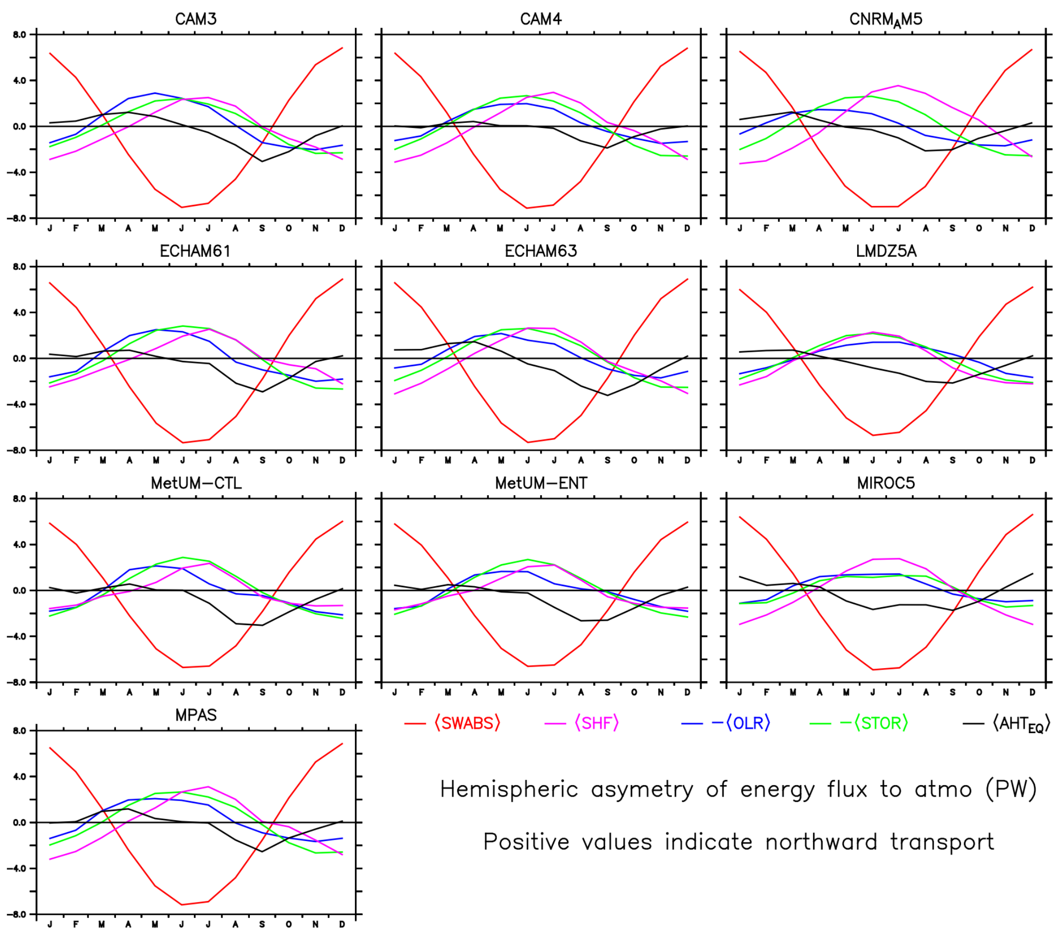

Figure 4.7: Seasonal cycle of energy budget terms. OLR and STOR terms are multiplied by -1 to match their sign in the equation to calculate AHT$_{EQ}$.

4.2 Relationship Breakdown between ITCZ Shift and AHT Changes

Since the model simulations are reasonable, we first checked the relationship between ITCZ shift and AHT_{EQ} changes under climate change (4xCO_2 minus CTL) at a seasonal scale. The theory would expect that a negative AHT_{EQ} change corresponding with stronger southward AHT_{total}, and would correspond with a northward shift of ITCZ (Kang et al. 2018; Schneider et al. 2014; Donohoe et al. 2013). That is, a negative correlation coefficient between AHT_{EQ} changes and ITCZ shifts under global warming is expected. The correlation coefficient between our models at each month indicated that nine months' correlation were not significant. Only two months (April, July) had an absolute value over 0.7 (Table 4.1). The highest correlation coefficient value in July is affected by one large ITCZ shift simulated by ECHAM61 (Fig. 4.8. April's relationship is more towards a typical expectation of energetic theory (Fig. 4.9). The precipitation centroid peak month, September, did not show a strong relationship between ITCZ shift and AHT_{EQ} change (Fig. 4.10). The simulation of January, February, October and December even have a positive correlation coefficient (for example, Fig. 4.11). The other months' relationships can be found in appendix B.

Table 4.1: Model-to-model correlation coefficient between AHT_{EQ} change and ITCZ shift simulated at each month. Bold correlation coefficient values indicate the p-value is under 0.05.

Month	Correlation Coefficient	Ranking (from high correlation to low)
January	0.49	6
February	0.47	7
March	-0.43	9
April	**−0.74**	2
May	-0.53	5
June	-0.38	11
July	**−0.91**	1
August	-0.53	4
September	-0.42	10
October	0.23	12
November	**−0.67**	3
December	0.43	8

Table 4.2: Models numbered from 0 to 9 in the figures to make the figure layout easier to read.

Model Name	Numbered in Figures
CAM3	0
CAM4	1
CNRM_AM5	2
ECHAM61	3
ECHAM63	4
LMDZ5A	5
MetUM_CTL	6
MetUM_ENT	7
MIROC5	8
MPAS	9

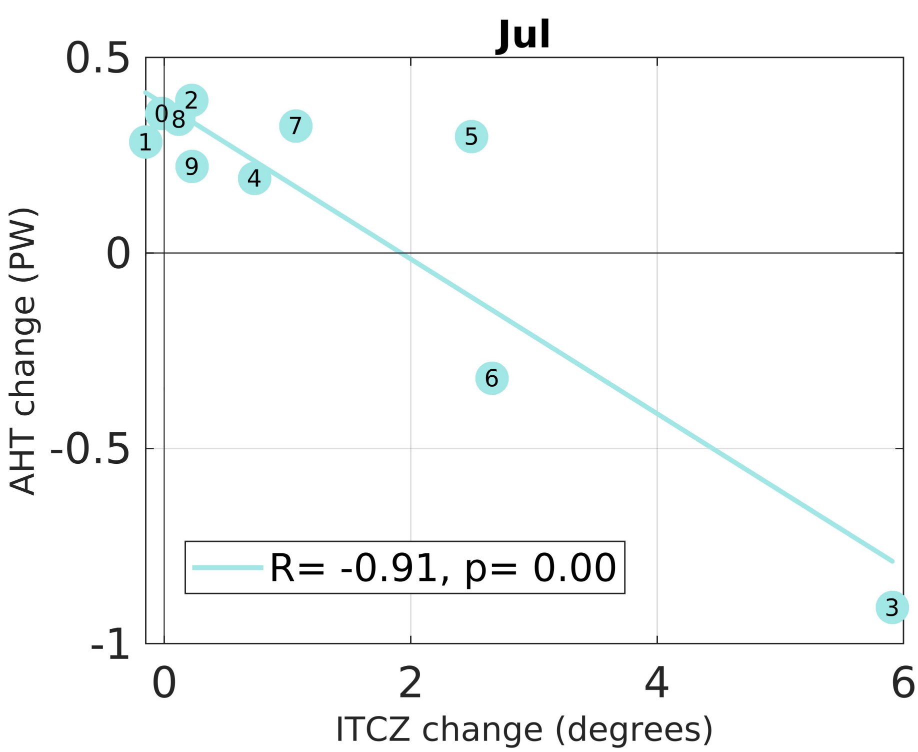

Figure 4.8: July ITCZ shift and AHT_{EQ} change under $4xCO_2$ warming scenario ($4xCO_2$ minus CTL) scatter plot. Each number is a different model, see Table 4.2.

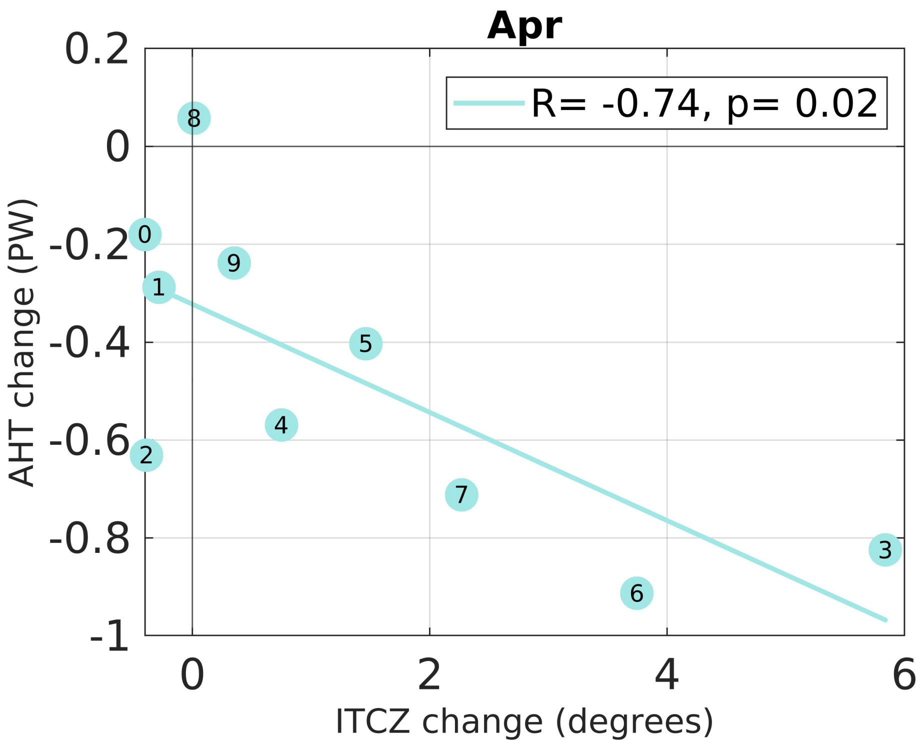

Figure 4.9: As Fig. 4.8 but for April.

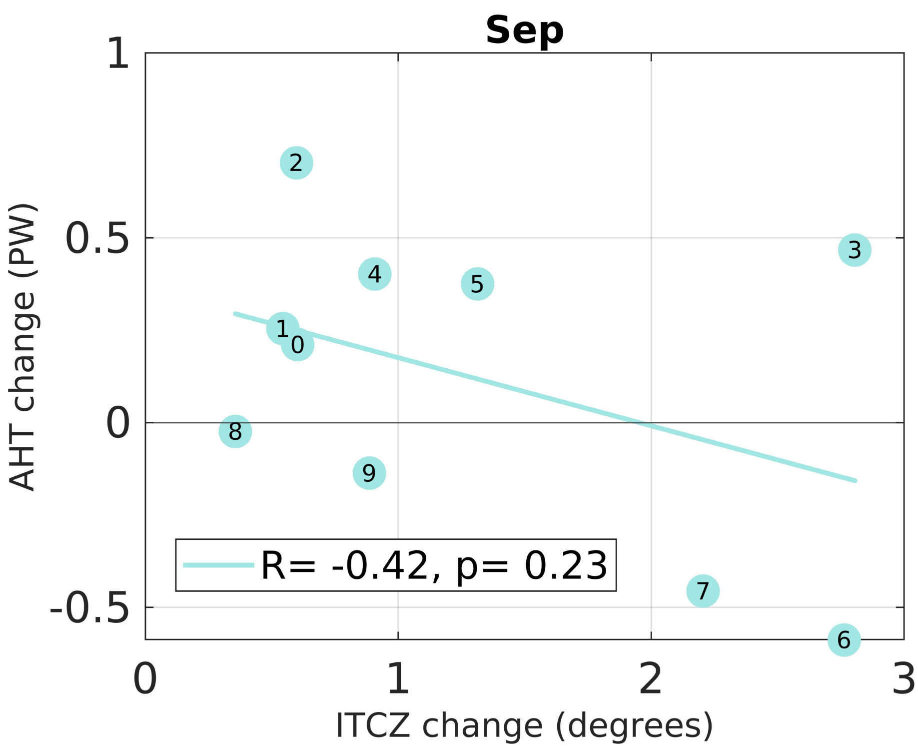

Figure 4.10: As Fig. 4.8 but for September.

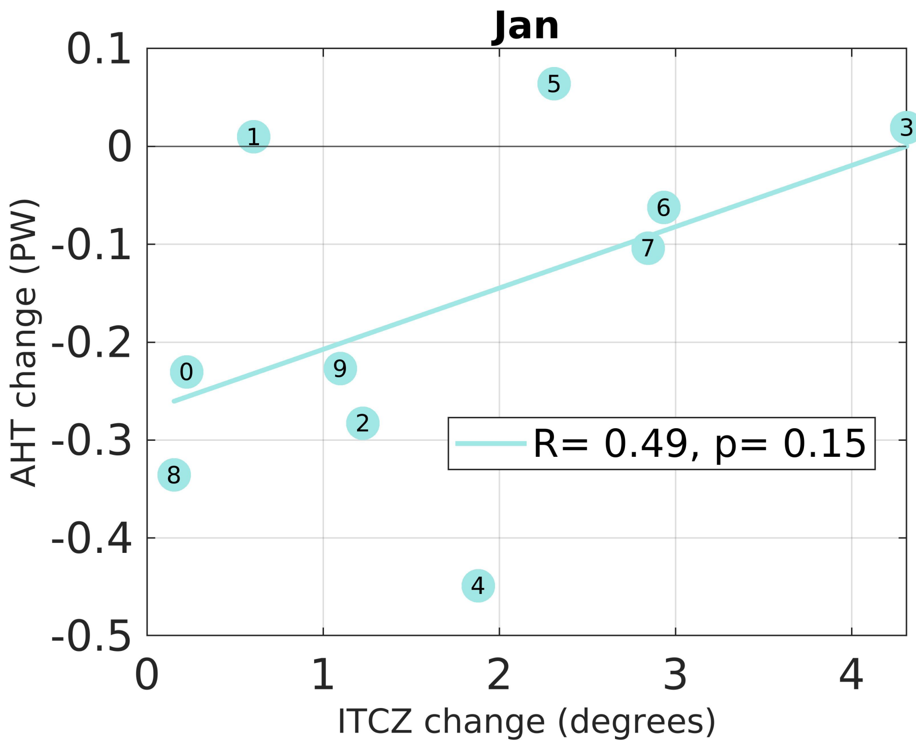

Figure 4.11: As Fig. 4.8 but for January.

We then calculated the annual relationship under a climate change condition to compare to the results calculated by Donohoe et al. (2013). The robust relationship was not supported by our analysis (Fig. 4.12). Models do not agree with each other on how AHT_{EQ} will change under a warming scenario. All 10 models simulated a northward shift of ITCZ and only six models simulated a negative AHT_{EQ} change which would be expected by the energetic theory.

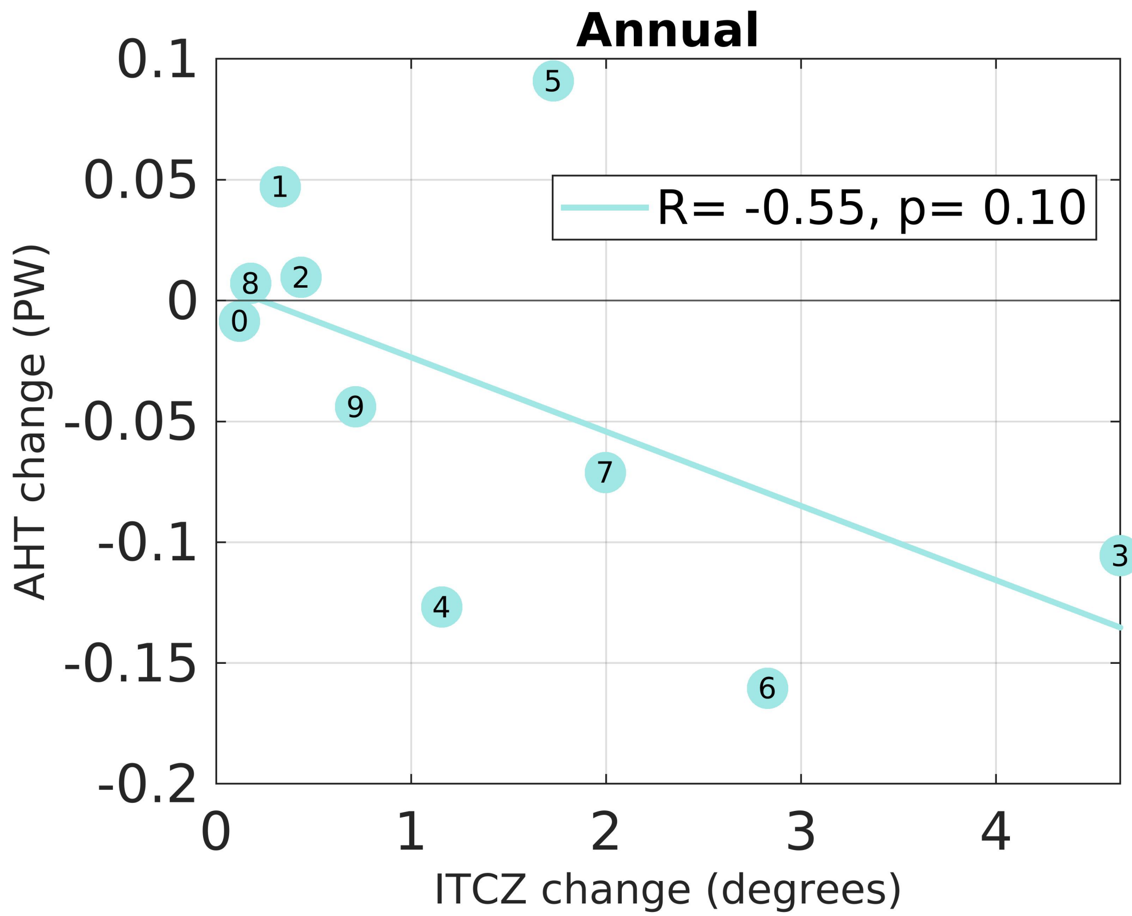

Figure 4.12: Annual ITCZ shift and AHT_{EQ} change under a warming scenario scatter plot.

The annual correlation coefficient value under climate change we calculated is in general much lower than the value calculated in Donohoe et al. (2013). In addition, Donohoe et al. (2013) did not have any positive correlation coefficient values. In the beginning, we thought this lower correlation coefficient was caused by the warming scenario because Donohoe et al. (2013) only examined the relationship between ITCZ position and AHT_{EQ} instead of the relationship between their changes under a warming scenario at a seasonal scale. Therefore, we also calculated the seasonal cycle relationship between ITCZ position and AHT_{EQ} under both CTL and $4xCO_2$ conditions for each model. Interestingly, most of the models simulated a relatively good relationship under the CTL scenario but not under the $4xCO_2$ condition. This can explain why the relationship between ITCZ shift and AHT_{EQ} changes under a warming scenario is less robust.

Only three models (CAM3, ECHAM63, and MPAS) simulated a relatively good seasonal relationship between ITCZ position and AHT_{EQ} under both CTL and 4xCO_2 scenarios (for example, Fig. 4.13). Most of the models (CAM4, CNRM_AM5, ECHAM61, MetUM_CTL, MetUM_ENT) simulated a relatively good relationship under CTL condition but not so good relationship under 4xCO_2 circumstance (for example, Fig. 4.14). Some models like LMDZ5A and MIROC5 do not support the energetic theory's expectation (For example, Fig. 4.15) under both scenarios. More figures can be found in appendix C. Except for MIROC5, all nine models simulated a less robust relationship between ITCZ position and AHT_{EQ} under a warming scenario. Although MIROC5 simulated a better relationship under 4xCO_2 condition, neither of the correlation coefficient were significant. A summary of the correlation coefficient of the ITCZ position and AHT_{EQ} over the seasonal cycle can be found in Table 4.3. From here on, we limit our analysis to discussion of inter-model relationships between ITCZ shifts and AHT changes under a warming scenario.

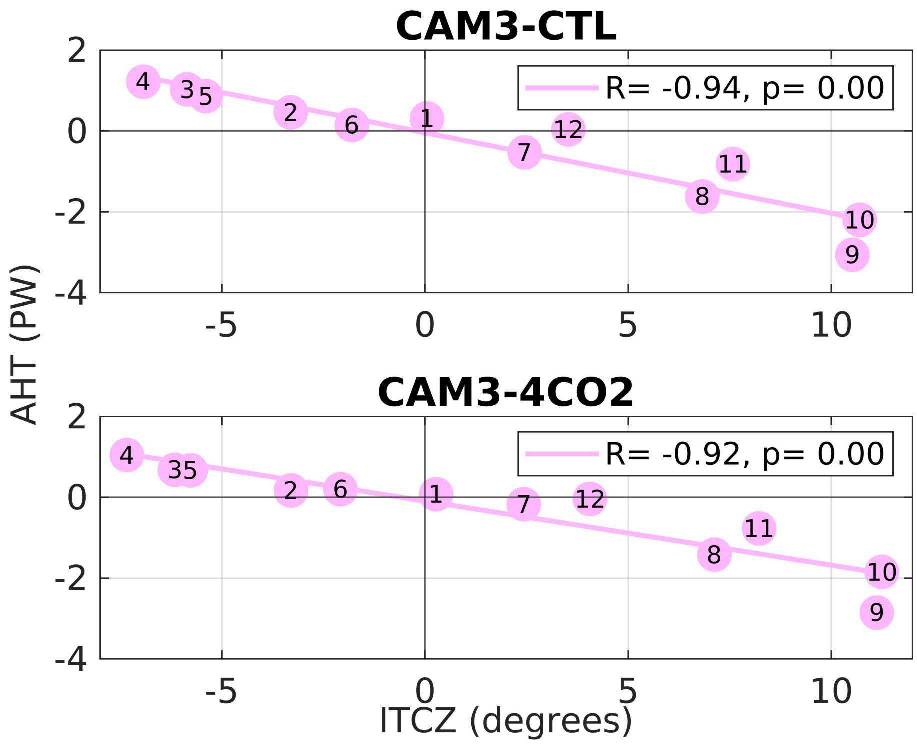

Figure 4.13: CAM3 simulated relationship between ITCZ position and AHT_{EQ} under both CTL and $4xCO_2$ scenarios. Numbers indicate months.

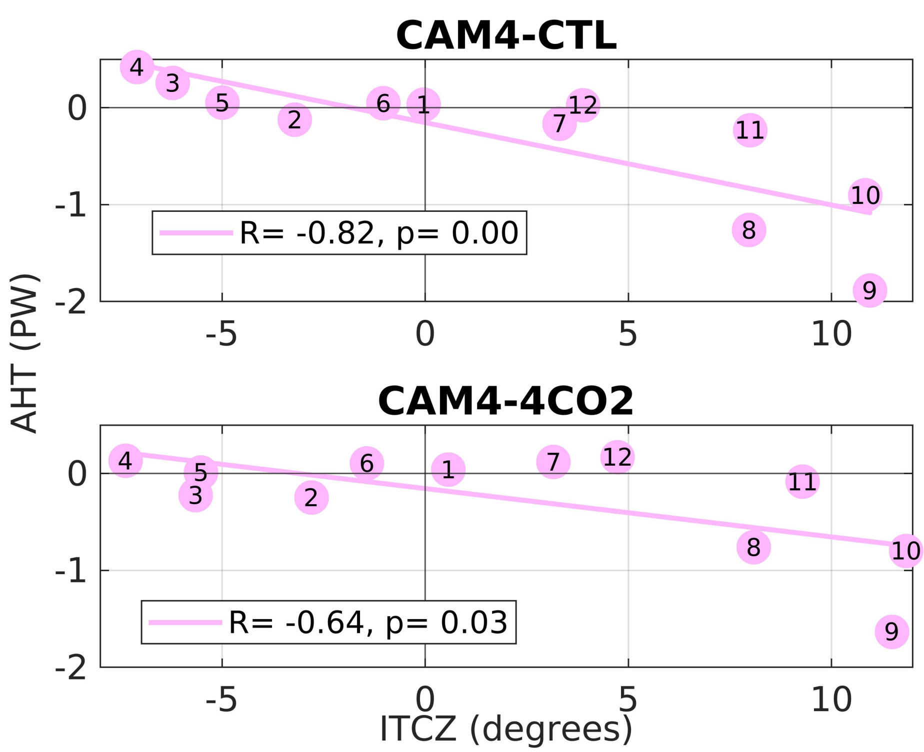

Figure 4.14: As Fig. 4.13 but for CAM4.

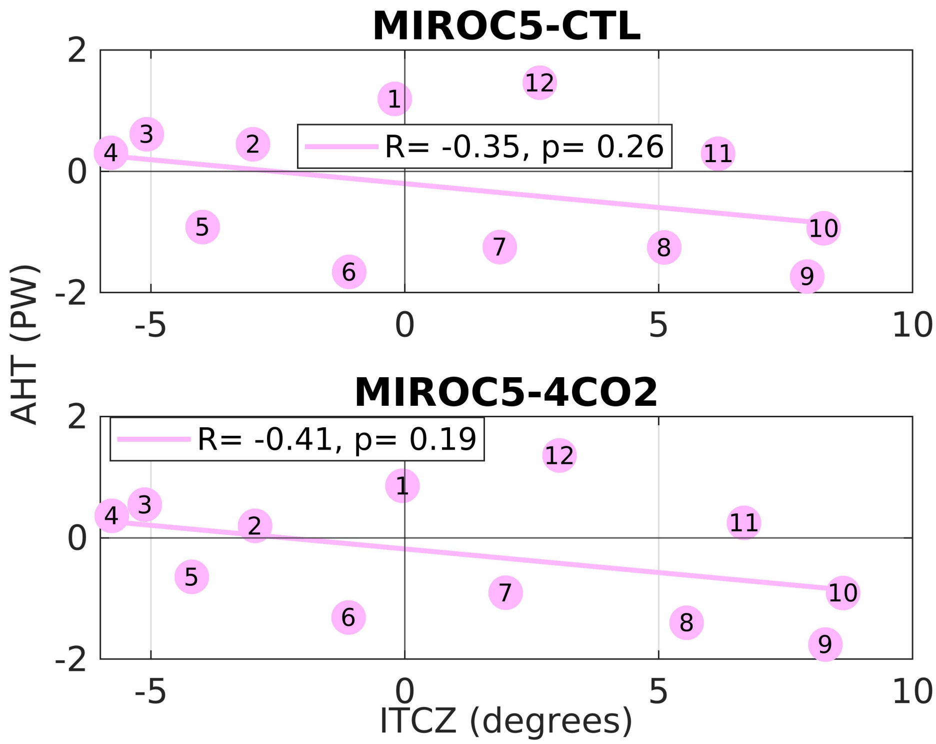

Figure 4.15: As Fig. 4.13 but for MIROC5.

Table 4.3: Month-to-month correlation coefficient between AHT_{EQ} and ITCZ position simulated by each model. Bold correlation coefficient values indicate the p-value is under 0.05.

Model	CTL Correlation Coefficient	$4xCO_2$ Correlation Coefficient
CAM3	**−0.94**	**−0.92**
CAM4	**−0.82**	**−0.64**
CNRM_AM5	**−0.88**	**−0.62**
ECHAM61	**−0.79**	-0.50
ECHAM63	**−0.91**	**−0.89**
LMDZ5A	**−0.64**	-0.34
MetUM_CTL	**−0.77**	-0.57
MetUM_ENT	**−0.73**	-0.51
MIROC5	-0.35	-0.41
MPAS	**−0.90**	**−0.93**

We also suspected that this less robust relationship may be due to that we only focused on the equator. Although AHT_{EQ} represents the interhemispheric energy transport well, it may not represent the whole AHT changes. Therefore, we calculate AHT_{total} at each latitude under both CTL and $4xCO2_2$ conditions. So the AHT_{total} became a curve like the zonal-mean precipitation curve. AHT_{total}'s value when crossing the equator, is AHT_{EQ}.

The results still showed that the relationship between ITCZ shift and AHT_{total} change was not as clear as expected. Using the precipitation peak month September as an example, CAM3, ECHAM63, MIROC5, and MPAS simulated no ITCZ shift and no AHT_{total} changes (for example, Fig. 4.16). CAM4 simulated no ITCZ shift but a southward shift of AHT_{total} (Fig. 4.17). CNRM_AM5 and LMDZ5A simulated a northward ITCZ shift but a southward shift of the AHT_{total} (Fig. 4.18). ECHAM61, MetUM_CTL and MetUM_ENT simulated a northward shift of the ITCZ but no shift of the AHT_{total} (for example, Fig. 4.19). The rest of the figures can be found from appendix D.

Certainly, models do not agree with each other on how ITCZ shifts and AHT_{total} changes under a warming scenario. The only thing that the models agree on is that the EFE and ITCZ position match with each other well. Like Fig. 4.17, the latitudes where the precipitation curves peak are where the AHT_{total} curves change their sign. This analysis also demonstrates that EFE method would not give us a better relationship between ITCZ shift and AHT_{total} changes. For example, ECHAM61 simulated almost no AHT_{total} change but a large precipitation shift around the equator (Fig. 4.19) which means the EFE change would be around zero while the ITCZ shift is relatively large.

In summary, the energetic theory's expectation was not supported by the TRACMIP simulation annually or monthly. To find out why the energetic theory was not supported by TRACMIP simulations, we want to analyze the inner links (Fig. 3.2), such as energy transported by the Hadley cells and mass transport by the atmosphere, to examine where the connection breaks down. In addition, to avoid the uncertainty caused by using just one latitude (EFE and equator) to represent the changes of the interhemispheric energy, we consider the changes of the curves in the whole tropical area. In this case, the correlation coefficient between ITCZ shift and AHT_{total} curve shift will be positive, since the extra radiative forcing will move them both to the warmer Hemisphere. Since the 4xCO_2 AHT_{total} curve will shift to the north, its value on the equator will be more negative. If we use 4xCO_2 AHT_{EQ} minus CTL AHT_{EQ}, the difference will be negative. Therefore, the former correlation coefficient between ITCZ shift and AHT_{EQ} change is negative.

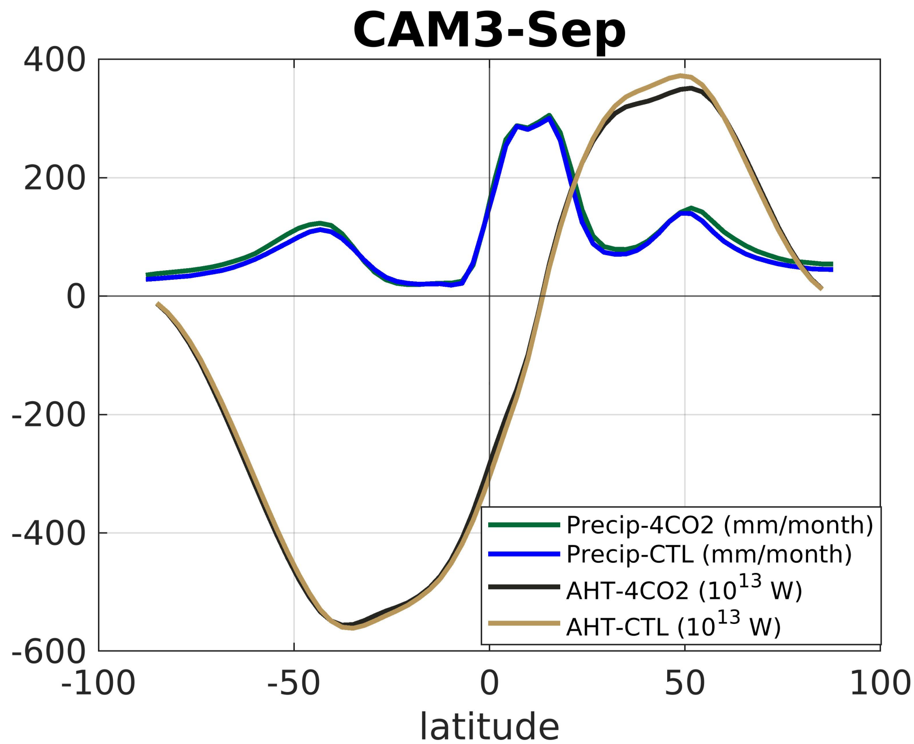

Figure 4.16: CAM3 September precipitation and AHT_{total} simulation at each latitude for both CTL and $4xCO_2$ scenarios.

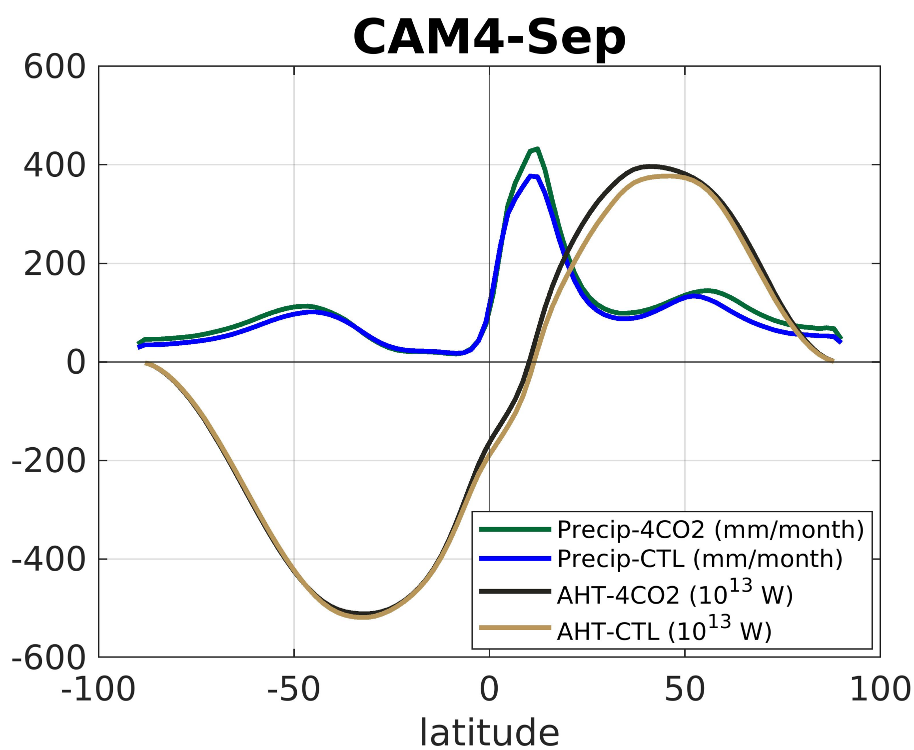

Figure 4.17: As Fig. 4.16 but for CAM4.

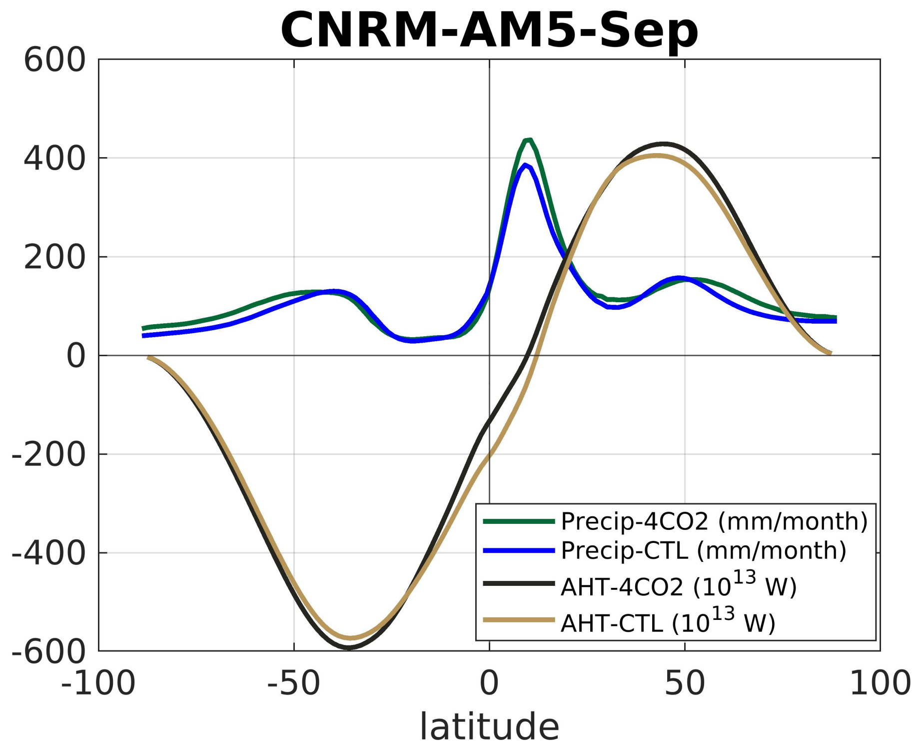

Figure 4.18: As Fig. 4.16 but for CNRM_AM5.

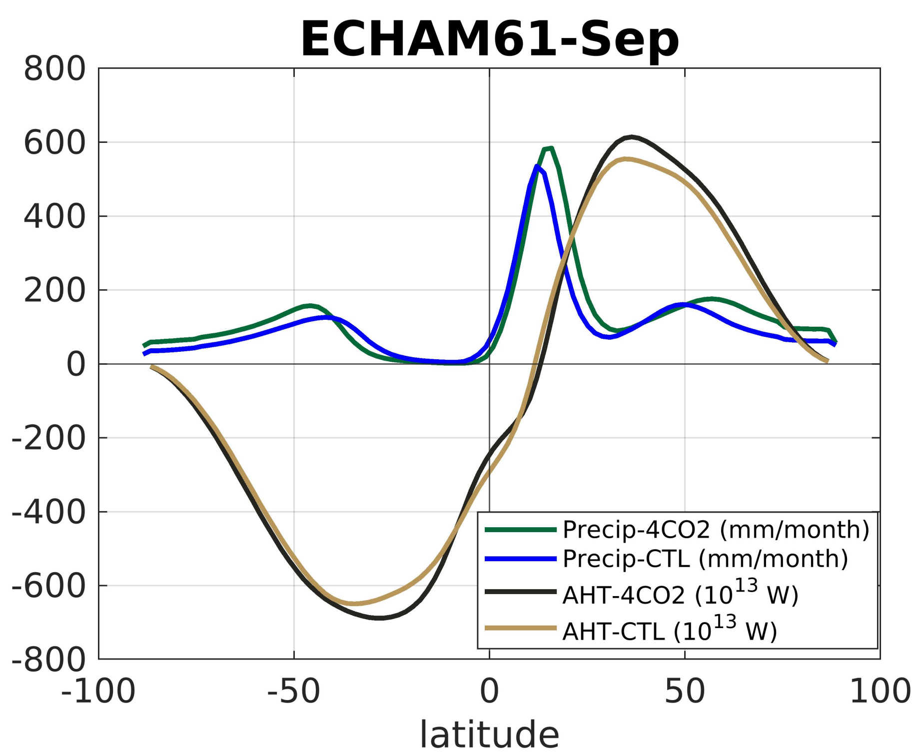

Figure 4.19: As Fig. 4.16 but for ECHAM61.

4.3 Which Inner Link Breaks Down

After we introduce the inner links, we have 12 curves in one plot, as we mentioned in section 3.5. Not all curves have a clear indication where the 4xCO_2 curve shifts, like our example figure 3.3 has. For example, in CNRM_AM5's November's simulation, it is not easy to define the shifts of the AHT_{Hadley} curves (solid red and blue curves, fig. 4.20). The patterns of the two curves are different. Considering our shift quantification methods will focus on 20° north and south from the CTL precipitation centroid, we can focus from 10° S (-10 on the figure) to 30° N. The 4xCO_2 curve has a clear peak around 5° N and trough around 18° N. The CTL curve does not have as obvious peak and trough as the 4xCO_2 curve. We can roughly say the peak is around 5° S and the trough is around 11° N. If the method tried to match the two troughs together, we may expect a large shift value around 7°. It's the same case for the ECHAM61 September curves (Fig. 4.21) which affects the inner links' relationship significantly that we will discuss later in this section. However, we will not exclude these shifts, since we cannot prove that they are unreasonable values. If they are affecting our results significantly, we will provide both analysis with and without these large values. We plotted these inner links figures for each model at each month. We provide the September (precipitation centroid maximum month) ones in appendix E.

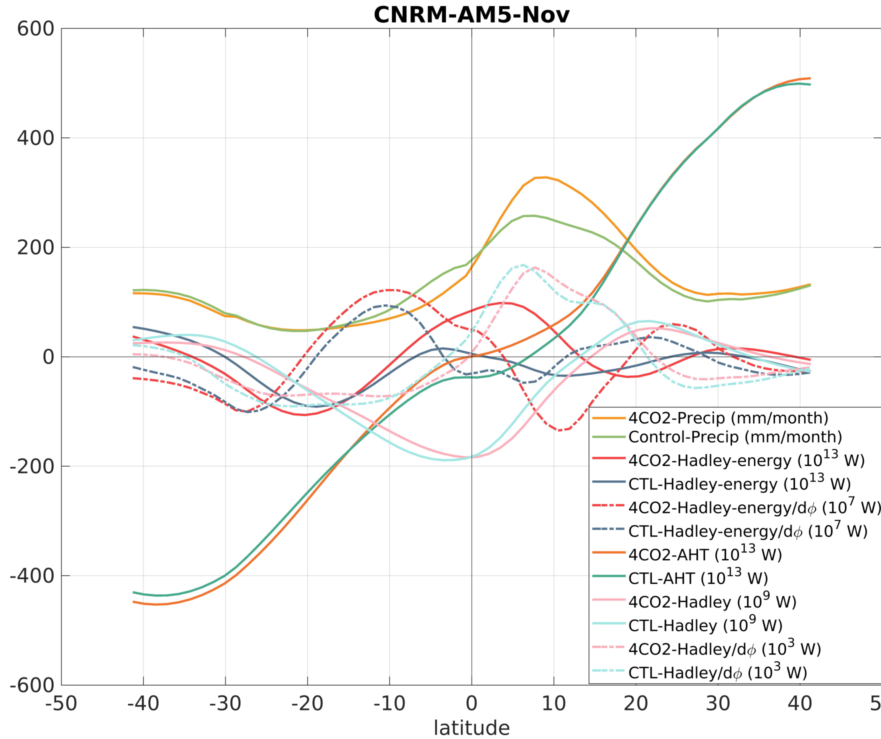

Figure 4.20: November CNRM_AM5 simulated inner links in the tropical area. All warm colors are 4xCO_2 simulations and cool colors represent CTL simulations.

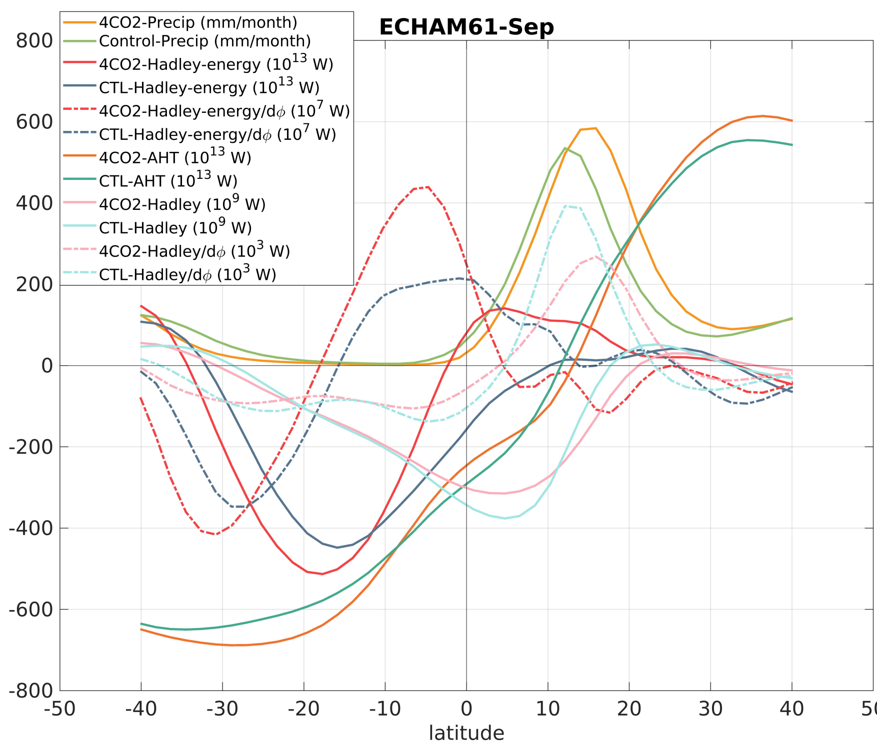

Figure 4.21: September ECHAM61 simulated inner links in the tropical area. All warm colors are 4xCO_2 simulations and cool colors represent CTL simulations.

There are two sets of inner links: 1. ITCZ shift to mass transport ($\Psi_{M,Hadley}$) changes, mass transport changes to AHT_{Hadley} changes, and AHT_{Hadley} changes to AHT_{total} changes. 2. ITCZ shift and the remaining factors/dϕ. We were considering the possibility that the relationship between ITCZ (ITCZ shift) and mass transport (mass transport changes) was not very good. Precipitation is more equivalent to d(mass transport)/dϕ. Since the relationship came as relatively good, we consider the d/dϕ related links as a supplementary in appendix G.

A summary of the main inner links' model-to-model correlation coefficient and corresponding p-value can be found from Fig. 4.22 and Fig. 4.23. Comparing to the AHT_{EQ} and precipitation centroid method, instead of having nine separated months when the relationship breaks down (Table 4.1), our method showed that, in general, from November to May (can be considered as Northern Hemisphere tropical dry season) the relationship between AHT_{total} changes and ITCZ shifts breaks down. From June to October (can be considered as Northern Hemisphere tropical wet season), the relationship is relatively good. August and October's correlation coefficient values are lower than 0.7 but still larger than the dry season months, and October's p value is around 0.05 (0.0592).

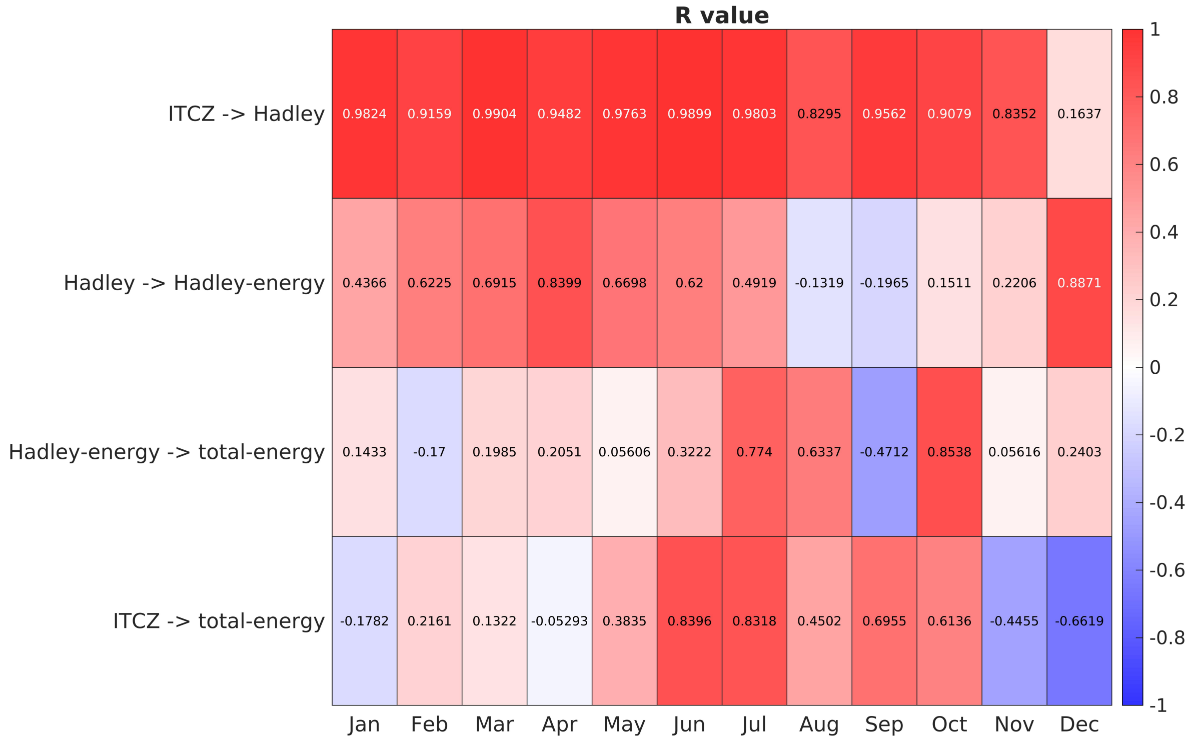

Figure 4.22: Heatmap of the inner links' correlation coefficient between models at each month.

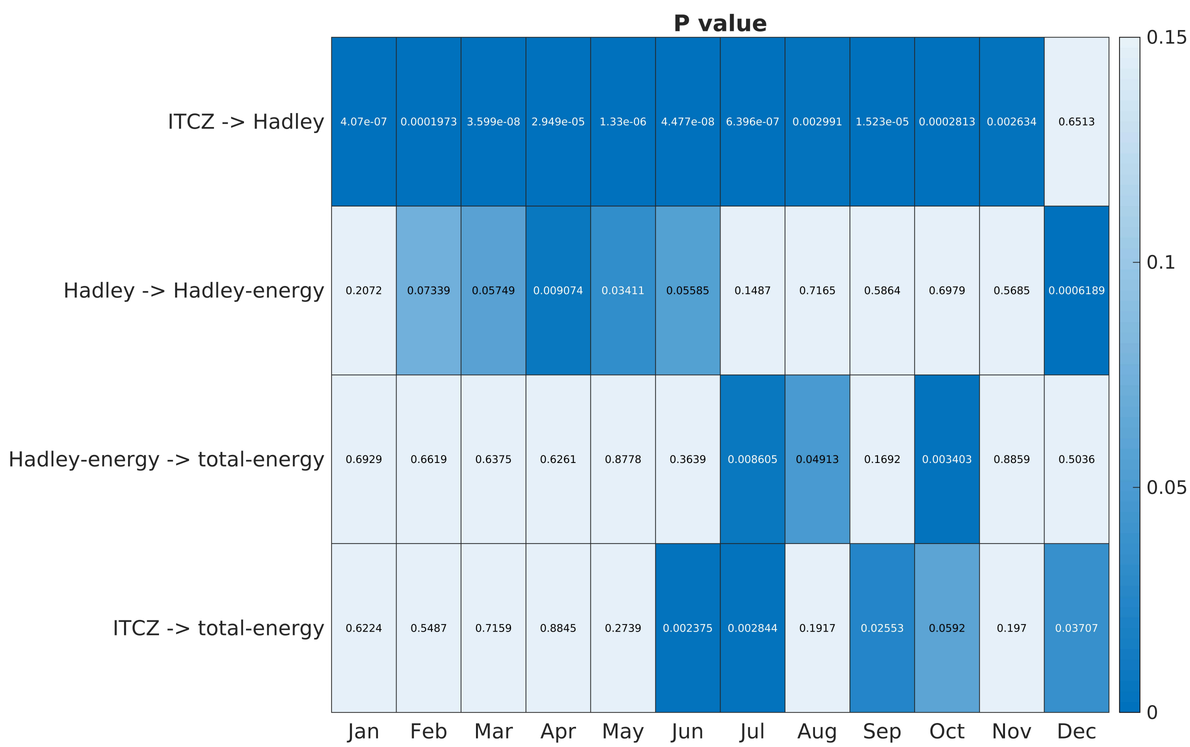

Figure 4.23: Heatmap of the inner links' p values corresponding with the correlation coefficient between models at each month.

December's relationship breaks down the most with an overall negative correlation and with both ITCZ to mass transport and AHT_{Hadley} to AHT_{total} inner links breaking down (Fig. 4.24). December's mass transport to AHT_{Hadley} link is relatively good, which means the GMS is steady this month. Except for December, all the other 11 months suggest a good relationship between ITCZ shift and mass transport changes (for example, January's simulation Fig. 4.25). Their correlation coefficient are over 0.7 and the p values are near 0. We expect this relatively good relationship because the precipitation is tightly relied on the vertical motion. If this link broke down, it may indicate that the models have bad precipitation representations. The correlation coefficient between mass transport changes and AHT_{Hadley} changes starts to decrease from the Northern Hemisphere tropical dry season to the wet season. The relationship between AHT_{Hadley} and AHT_{total} acts almost opposite to the mass transport and AHT_{Hadley} inner link, that the correlation coefficient is higher in the Northern Hemisphere warm season except for September. September has two inner links broke down but still have a relatively good relationship between ITCZ shift and AHT_{total} changes.

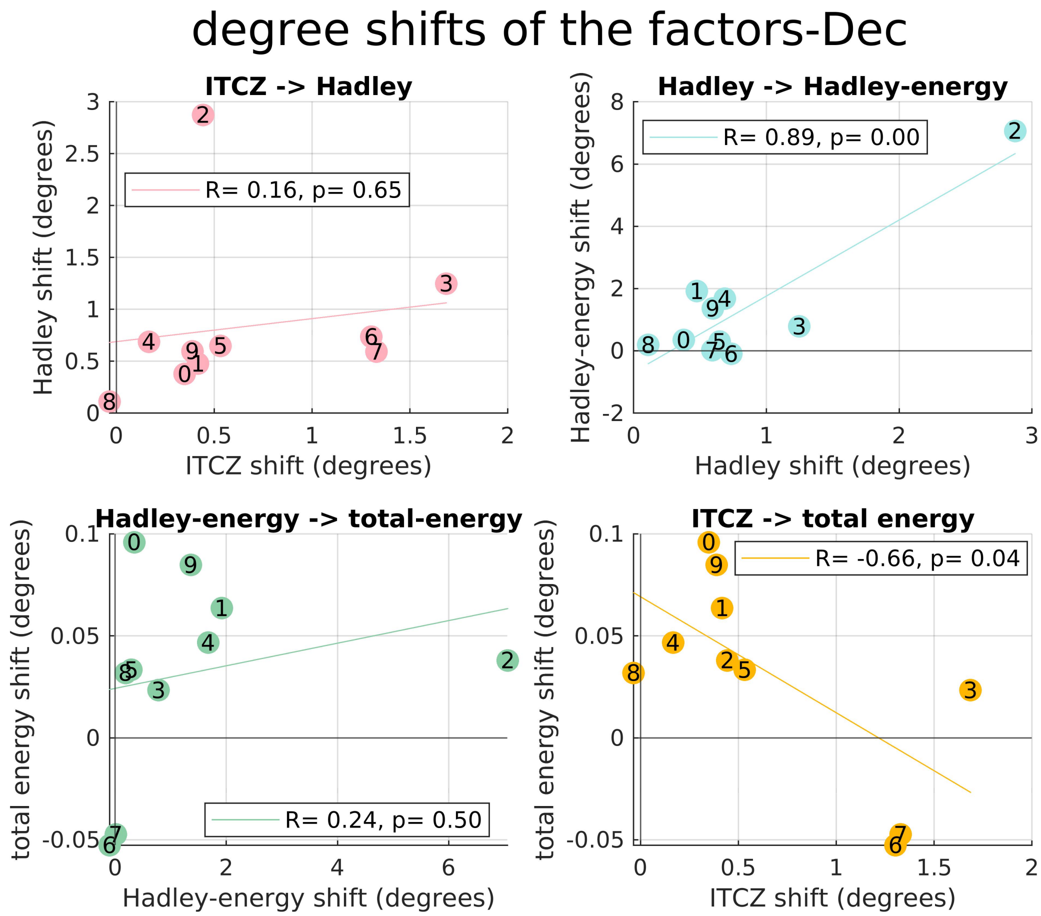

Figure 4.24: December inner links simulated by the models.

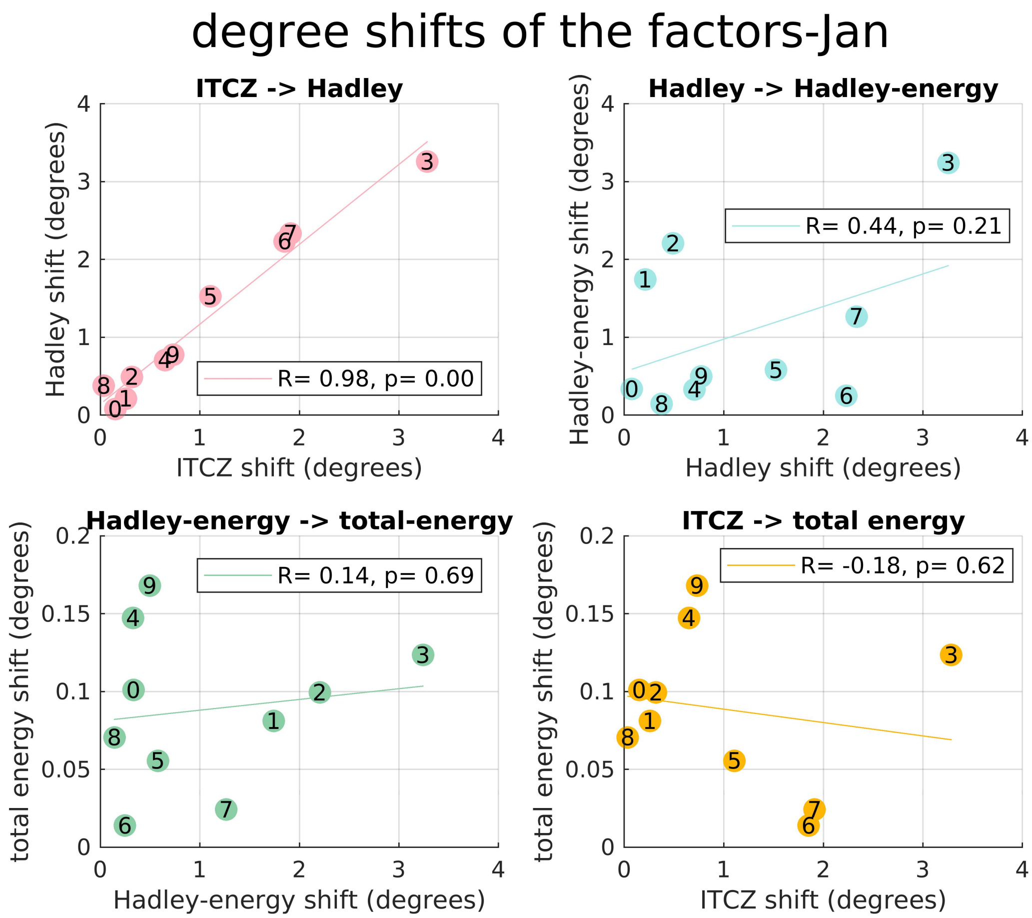

Figure 4.25: January inner links simulated by the models.

If we check the September scatter plot (Fig. 4.30), we will find that ECHAM61 (denoted by 3 in the figure) simulated some large shift values that we were expecting when we were qualitatively analyzing the curves. In addition, ECHAM61 is not the only outlier model. For example, for May's simulation and November's simulation (Fig. 4.26 and Fig. 4.27), the relationships between mass transport changes and AHT$_{Hadley}$ changes, AHT$_{Hadley}$ changes and AHT$_{total}$ changes are disproportionately affected by CNRM_AM5 and ECHAM61 (denoted by 2 and 3 in the figures). We examined the relationship between the factors using eight models without CNRM_AM5 or ECHAM61. The results did not improve significantly (Fig. 4.28 and Fig. 4.29) except for September (Fig. 4.30 comparing to Fig. 4.31). After excluding CNRM_AM5 and ECHAM61, September's simulation showed a similar pattern of other summer months (July, August, and October). We still decided to use all 10 models to examine the model simulated relationships between the factors under a warming scenario and use eight models as a supplement to the main results since these two models do not affect the results significantly.

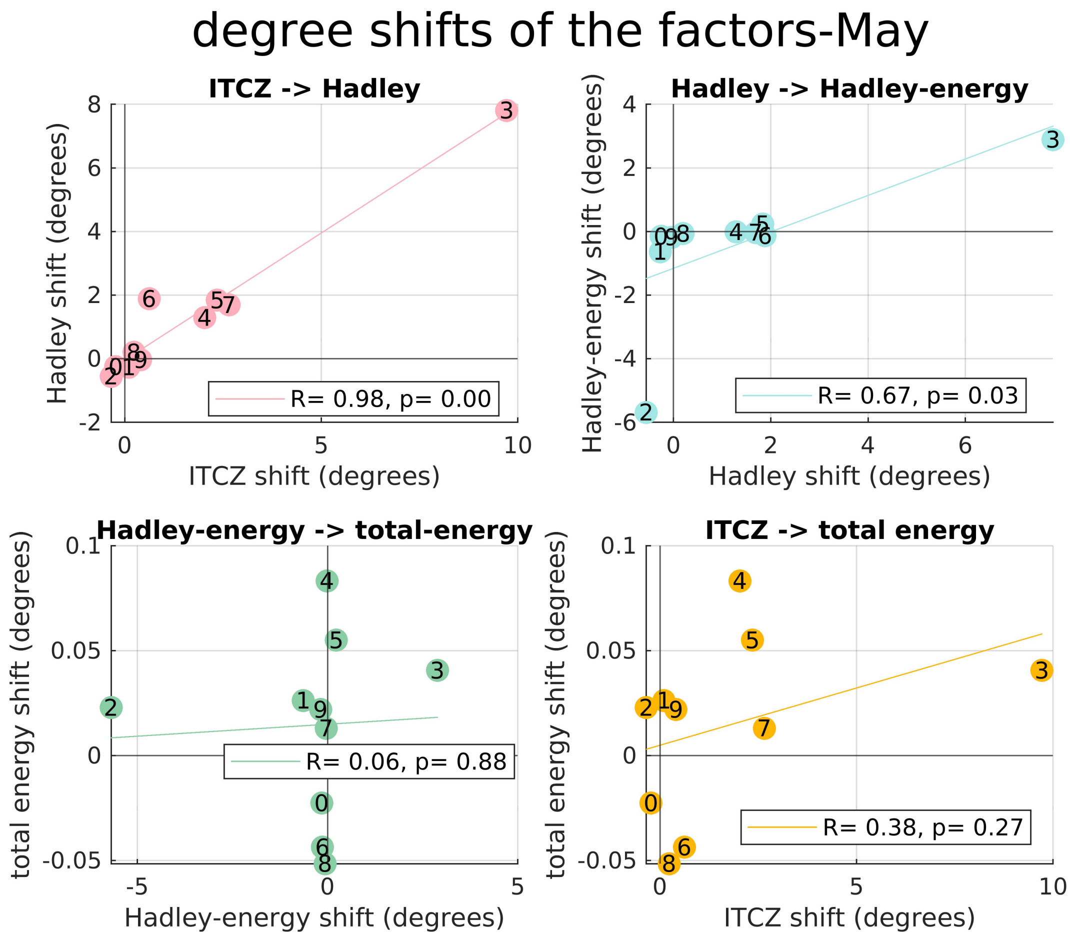

Figure 4.26: May inner links simulated by 10 models.

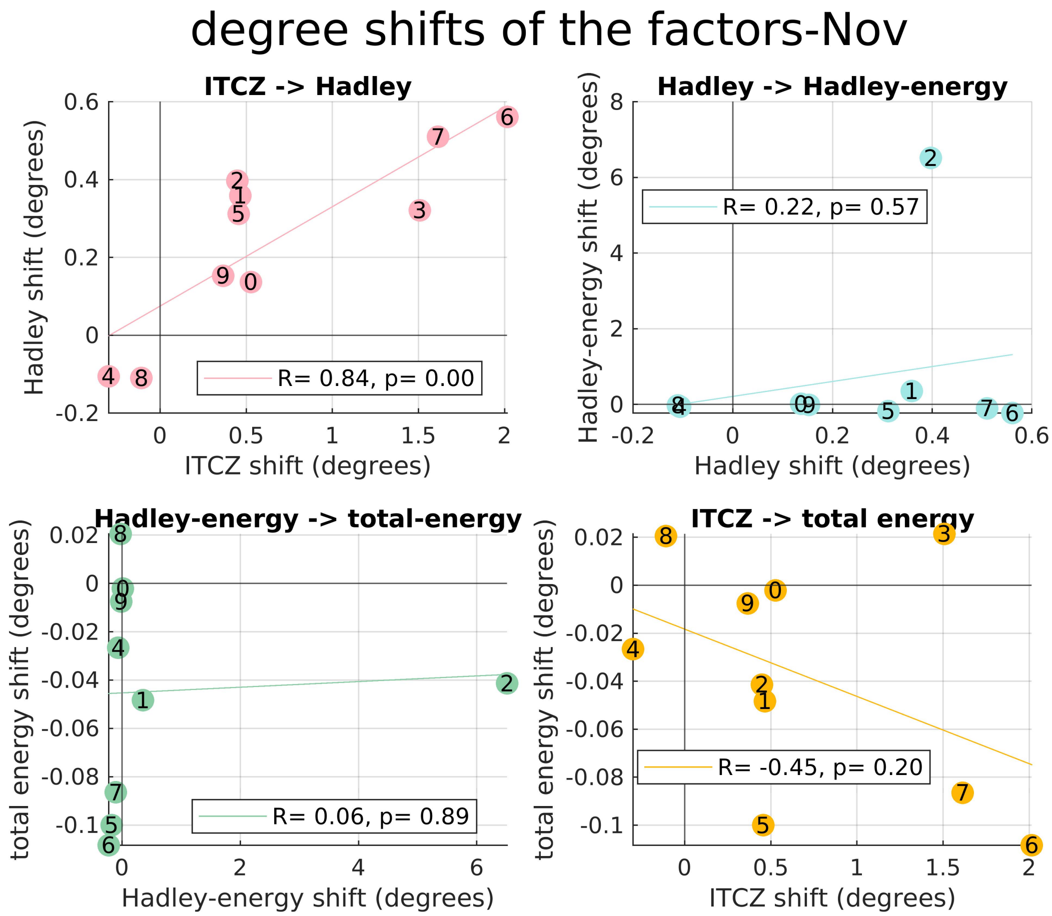

Figure 4.27: November inner links simulated by 10 models.

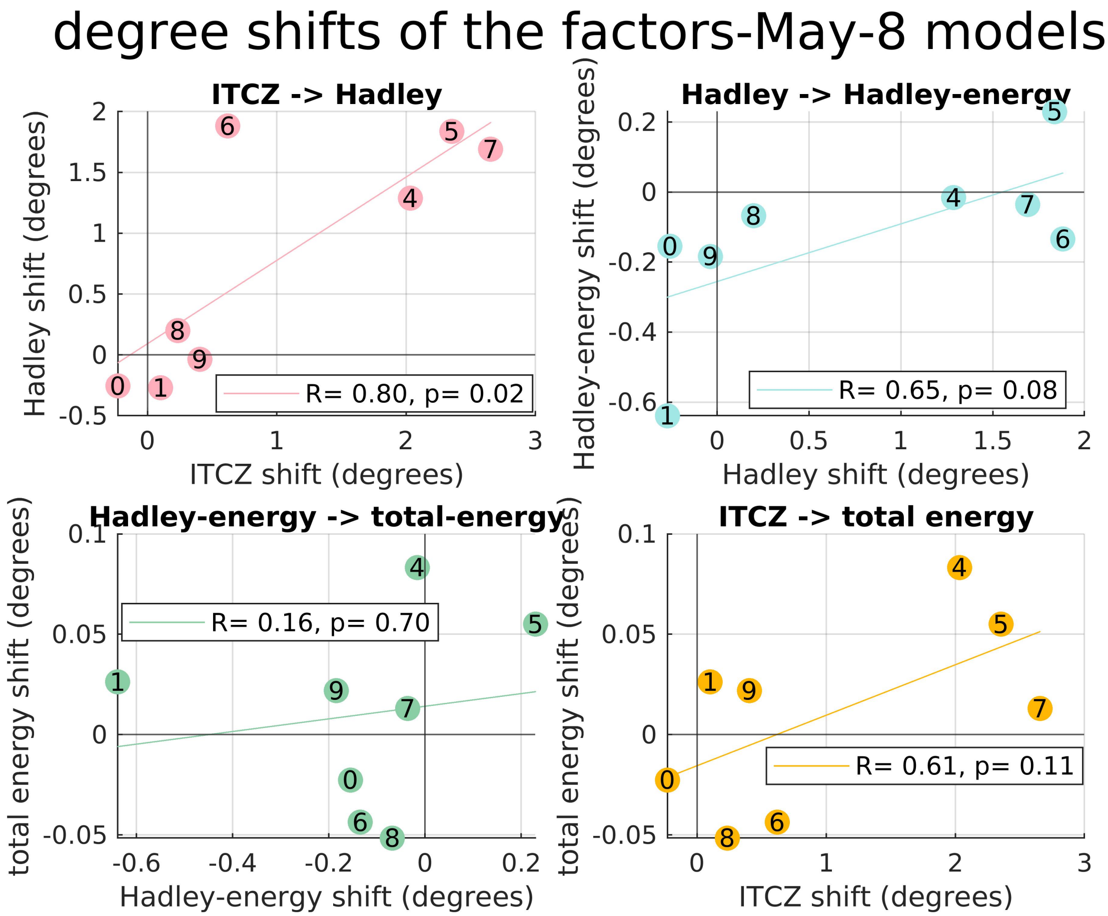

Figure 4.28: May inner links simulated by eight models.

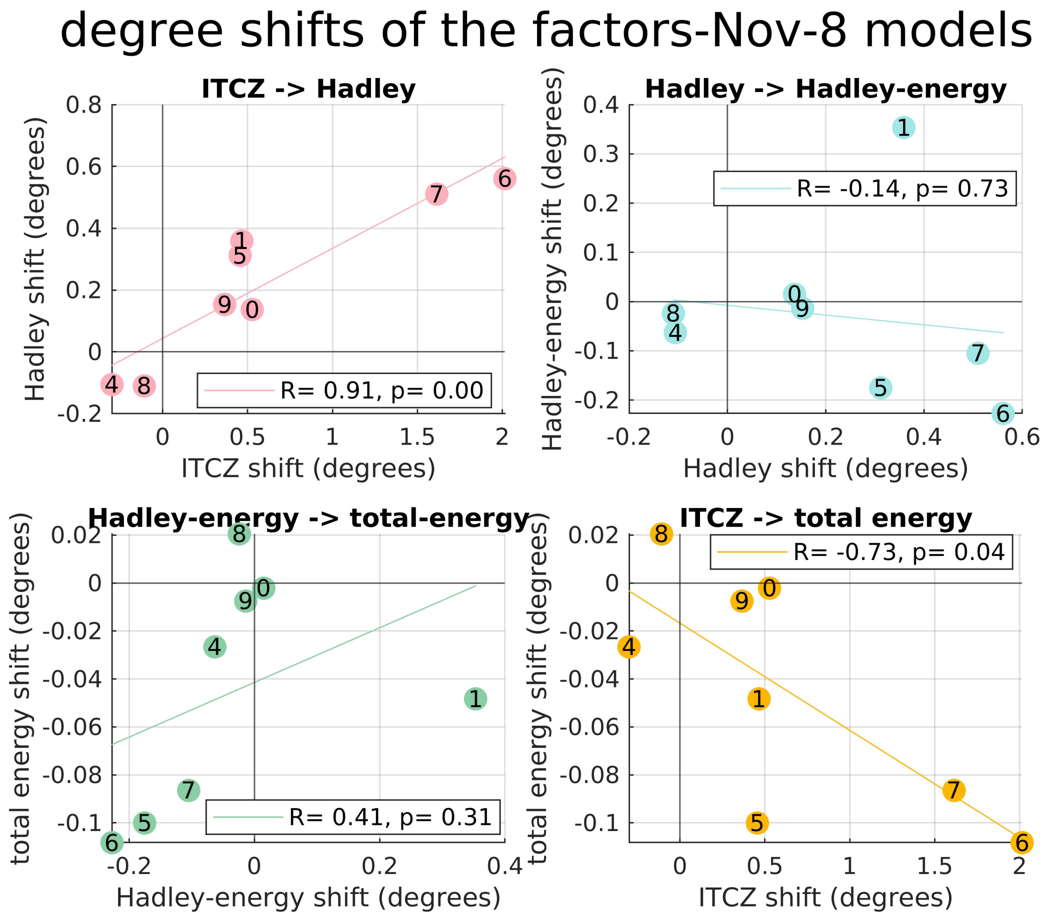

Figure 4.29: November inner links simulated by eight models.

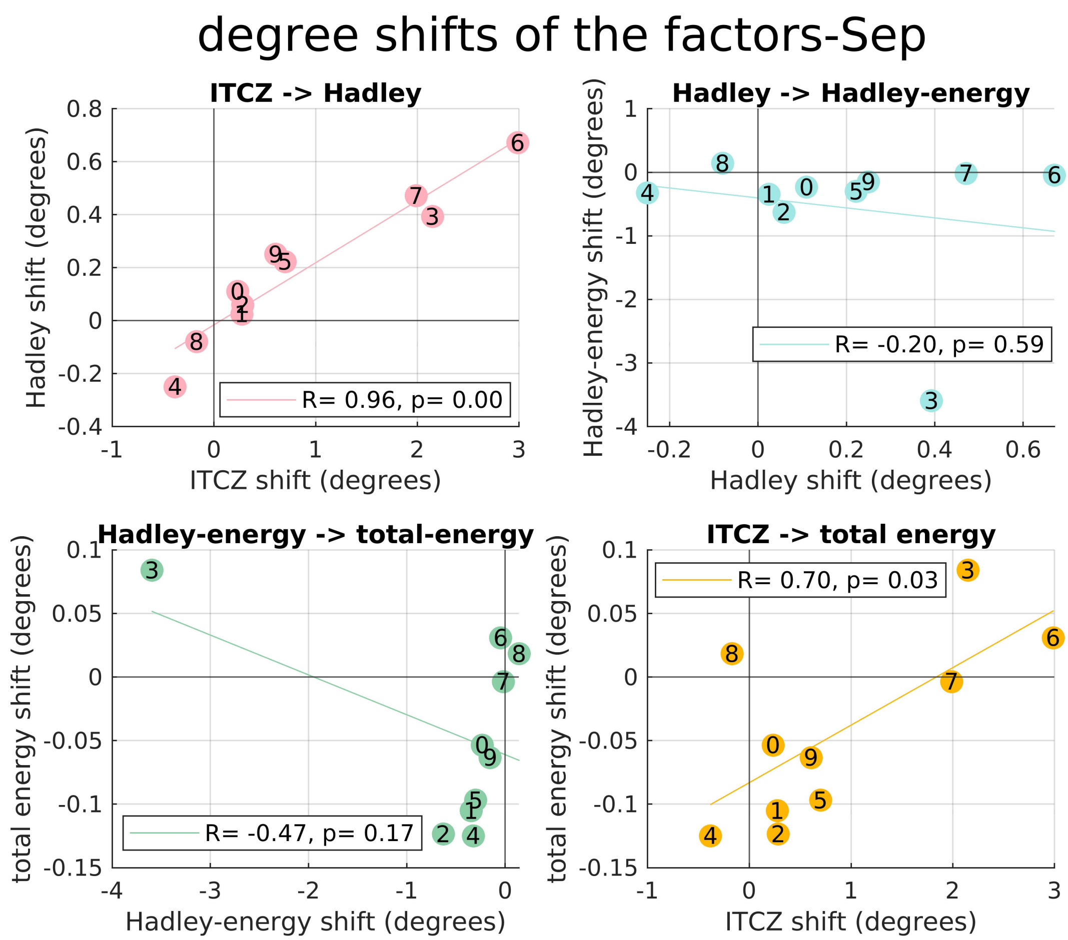

Figure 4.30: September inner links simulated by 10 models.

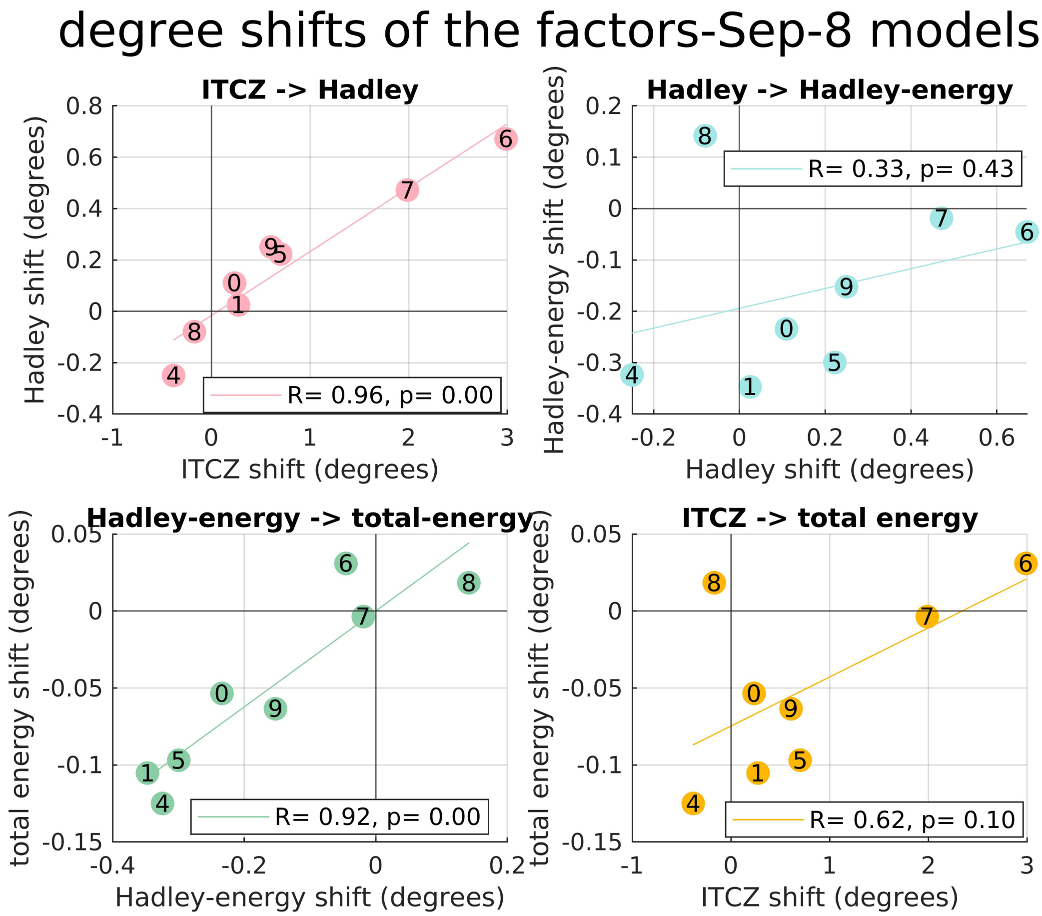

Figure 4.31: September inner links simulated by eight models.

By using all 10 models, we found that December's ITCZ shifts to mass transport changes link broke down the most. When we say break down the most, we are comparing the inner links within the same month. The smallest positive or the largest negative correlation coefficient will be considered as the most broken link. In three months (July, August, and October), the link between Hadley energy transport and total energy transport broke down the most (for example, July's simulation, Fig. 4.33). In eight months (January, February, March, April, May, June, September, and November), the link between mass transport and Hadley energy transport broke down the most (for example, February's simulation, Fig. 4.32). In January and November, the only link that did not break down is ITCZ shifts and mass transport changes (for example, November's simulation, Fig. 4.27). In September, two links break down but the original ITCZ shifts and AHT$_{total}$ changes link is relatively good that we explained in the above paragraph.

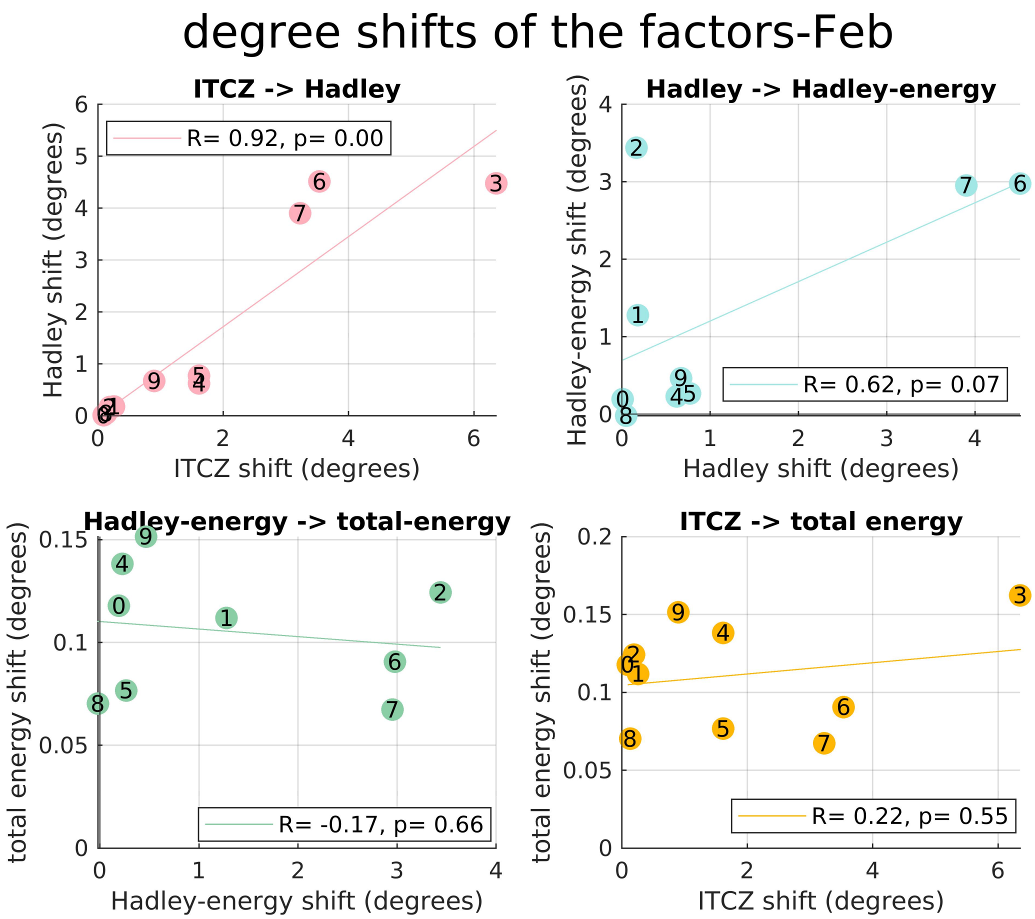

Figure 4.32: February inner links simulated by the models.

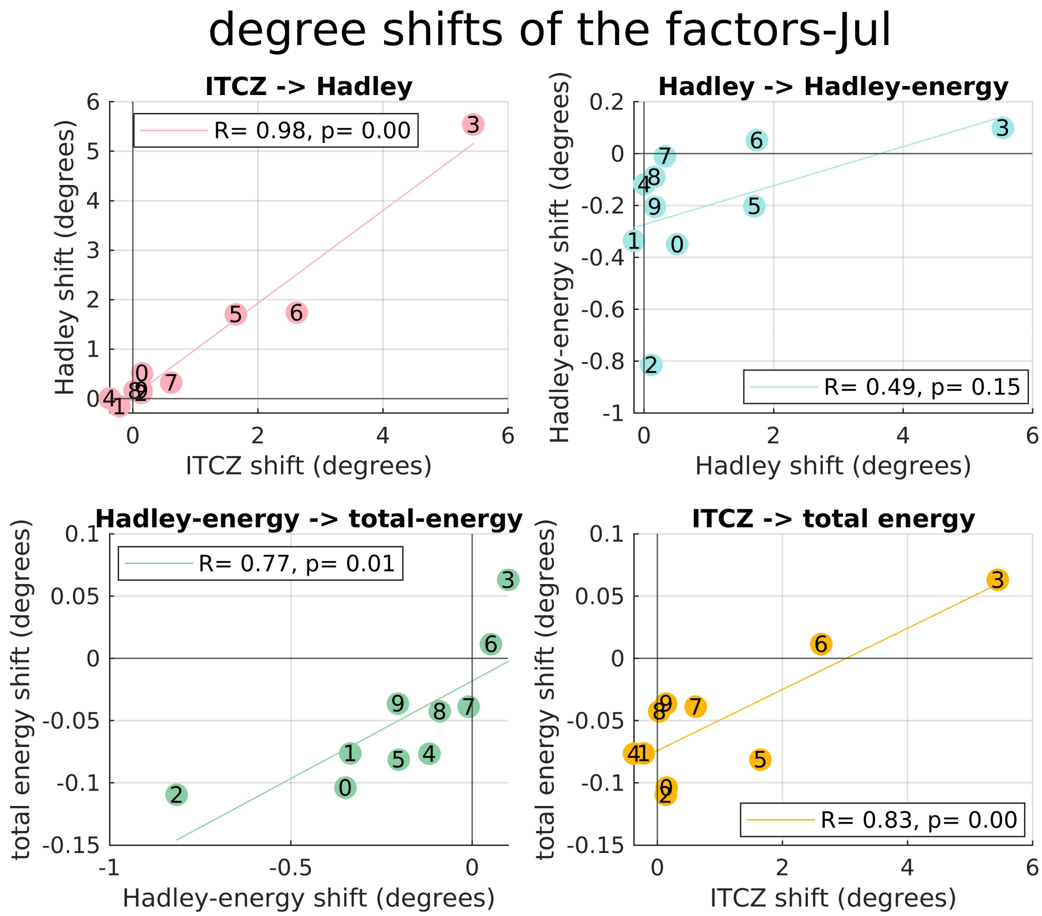

Figure 4.33: July inner links simulated by the models.

When the link between mass transport changes and AHT_{Hadley} changes broke down, the ratio between AHT_{Hadley} and mass transport is not steady anymore. Therefore, the GMS between CTL and $4\mathrm{xCO}_2$ conditions must not be steady. Our analysis of GMS supported this suggestion. Since plotting 10 models' monthly GMS for both CTL and $4\mathrm{xCO}_2$ scenarios would be very noisy, we plot the GMS model by model. We do not demonstrate all 12 months together, either. We chose April (GMS was relatively good, AHT_{Hadley} changes and AHT*total* changes broke down), July (GMS broke down, AHT_{Hadley} changes and AHT*total* changes relationship was relatively good) and November's (both inner links broke down) GMS for each model. If GMS is the only reason that causes the link between ITCZ shift and AHT_{total} changes to break down, we would expect the GMS curves to look similar in April but not in July or November.

CAM3, CAM4 and LMDZ5A supported this expectation. For example, CAM3's April GMS curves under CTL and 4xCO_2 scenarios look very similar to each other, while July and November have many missing values (Fig. 4.34). The missing values in GMS are caused by the near zero mass transport where Hadley cells meet with each other. Our outlier models, CNRM_AM5 and ECHAM61 together with non-outlier models MetUM_CTL and MetUM_ENT, simulate quite different GMS. For example, CNRM_AM5 simulated negative GMS and the GMS curves' troughs' latitude changes between CTL and 4xCO_2. When GMS is negative, mass transport curve and AHT_{Hadley} curve do not shift in the same direction anymore.

We may expect these four models to simulate a relatively large AHT_{total} change with a subtle ITCZ shift. However, from our scatter plots (like Fig. 4.27 bottom right panel), we find that number 2 and 3 models (CNRM_AM5 and ECHAM61) simulated a relatively large ITCZ shifts but not a large AHT_{total} change while number 6 and 7 models (MetUM_CTL and MetUM_ENT) simulated a large ITCZ shifts and a large AHT_{total} change. Some models (ECHAM63, MIROC5 and MPAS) simulated relatively steady GMS for all three months. Like MIROC5, although it has missing values near the ITCZ, the shapes of the GMS curves between CTL and 4xCO_2 are pretty similar to each other (Fig. 4.36). The remaining models' results can be found in appendix H.

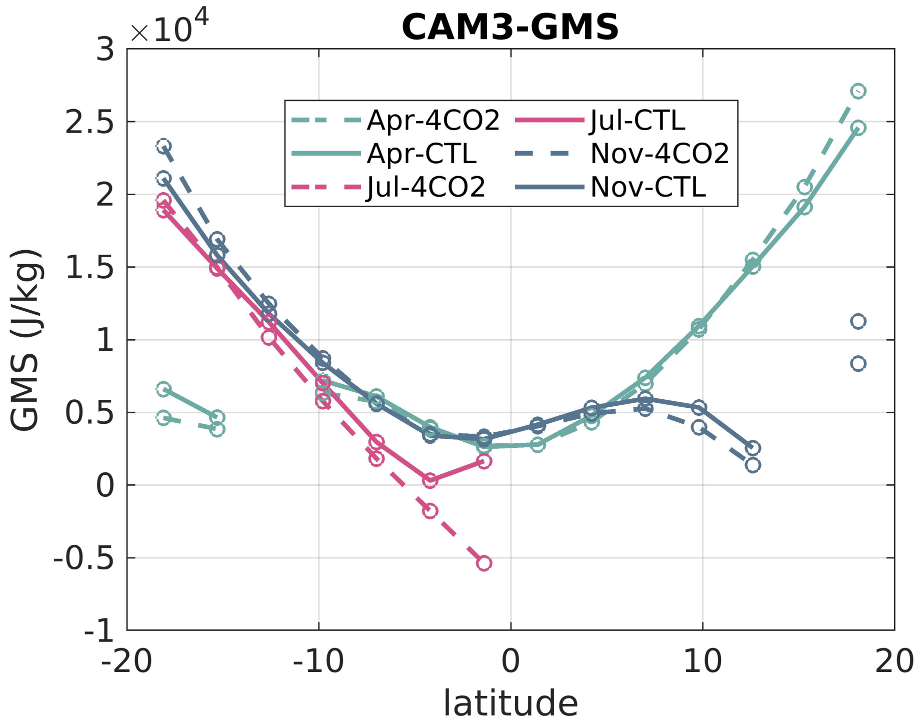

Figure 4.34: CAM3 simulated GMS in April, July and November.

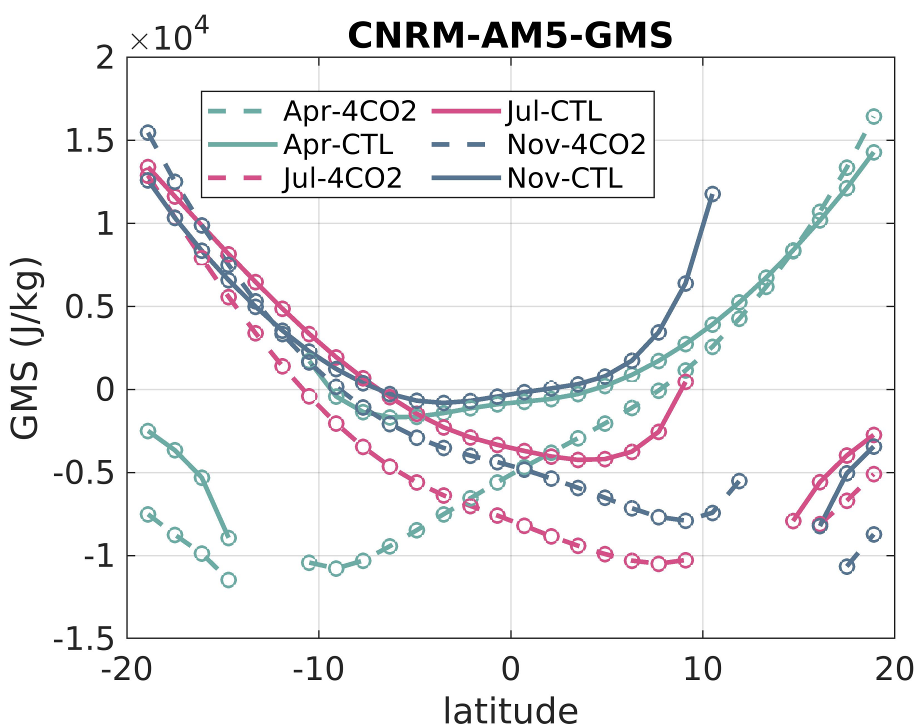

Figure 4.35: CNRM_AM5 simulated GMS in April, July and November.

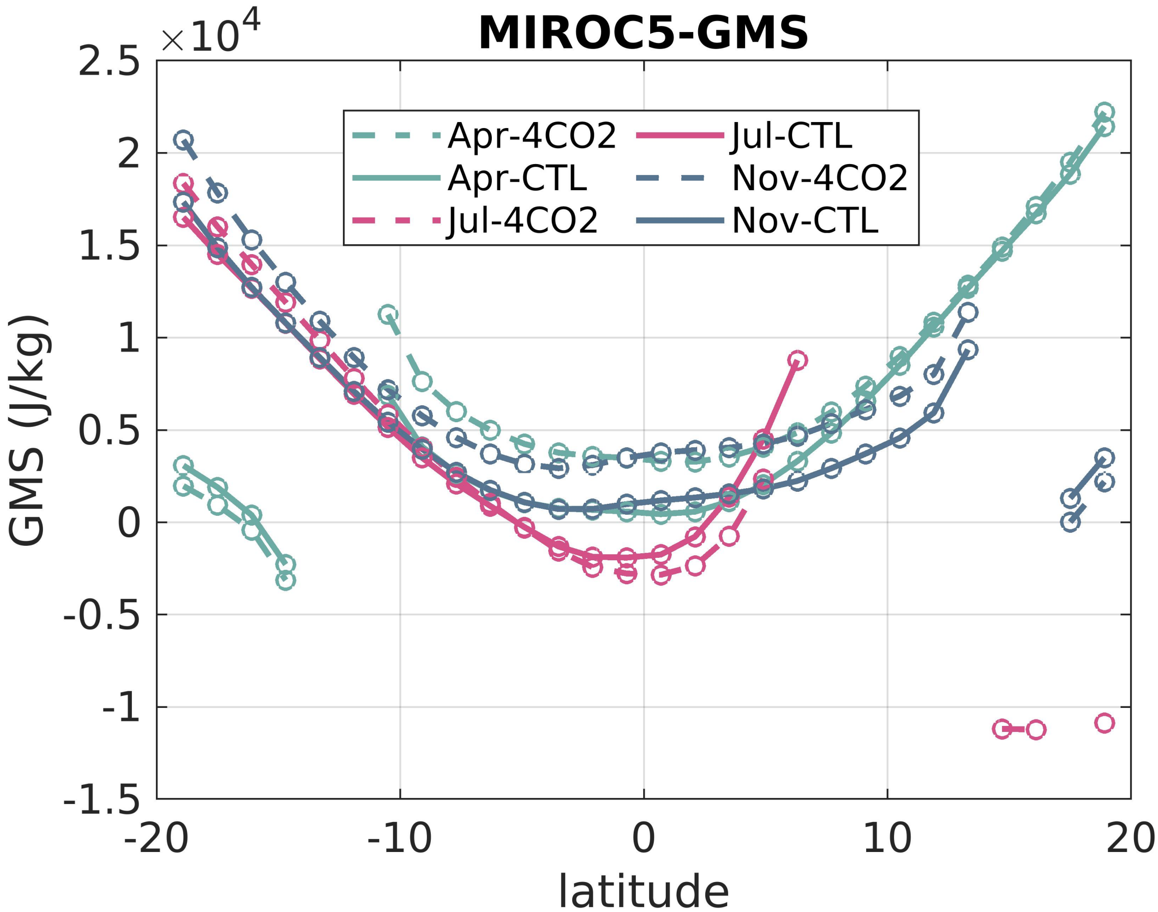

Figure 4.36: MIROC5 simulated GMS in April, July and November.

The GMS analysis may seem quite complicated but the core information that it provides is that GMS is only one factor that can break down the link between ITCZ shift and AHT_{total} changes. However, it is not the reason for the TRACMIP simulated relationship breakdown. We also have three months' (July, August and October) analysis showing that although the link between mass transport and AHT_{Hadley} changes break down, as long as the link between ITCZ shift and mass transport changes, AHT_{Hadley} changes and AHT_{total} changes do not break down, the original link ITCZ shits and AHT_{total} does not break down.

We also provide heatmap of eight models without CNRM_AM5 and ECHAM61 (Fig. 4.37 and Fig. 4.38). The overall inner links' relationship was not changed significantly. The first link is still fairly strong and the second link, mass transport changes to AHT_{Hadley} changes, starts to decrease during Northern Hemisphere tropics wet season. During Northern Hemisphere summer, the link between AHT_{Hadley} changes and AHT_{total} changes is relatively strong. The original link's correlation coefficient between ITCZ shift and AHT_{total} changes values becomes smaller after excluding the two outlier models.

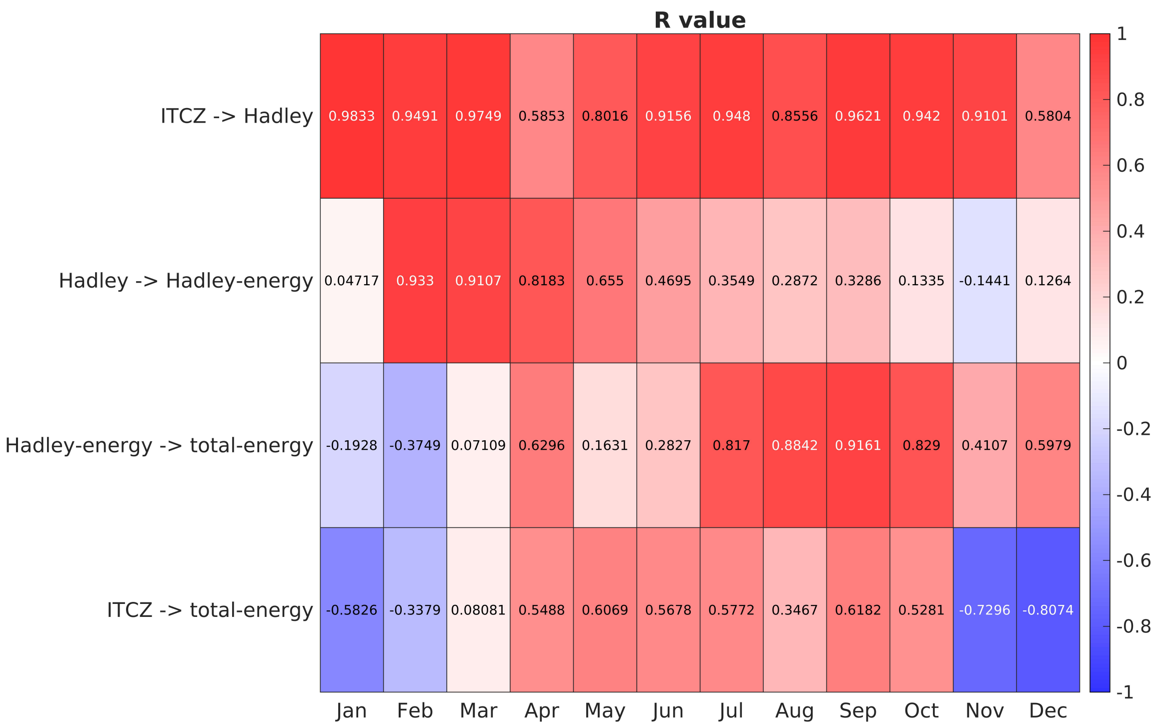

Figure 4.37: Heatmap of the inner links' correlation coefficient between models at each month, excluding the two outlier models CNRM_AM5 and ECHAM61.

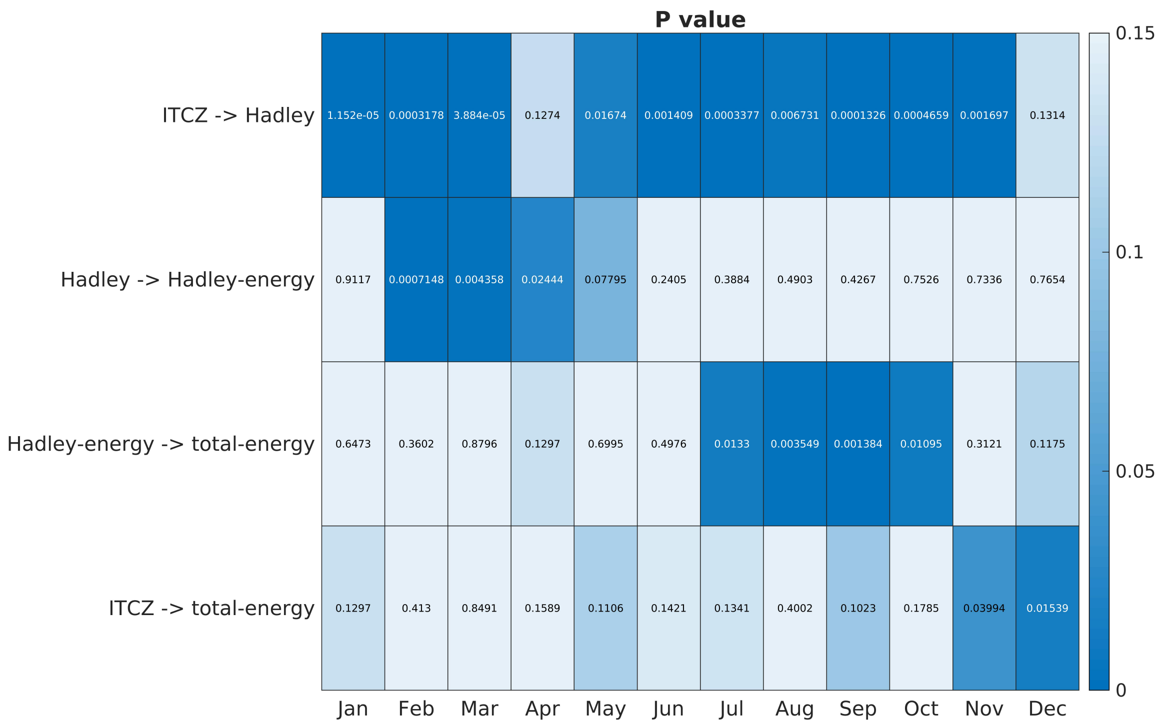

Figure 4.38: Eight models' heatmap of the inner links' p values corresponding with the correlation coefficient between models at each month.

4.4 Seasonal Cycle of Changes Simulated by Each Model

In this section, we show how the inner link factors' seasonal cycle change under a warming scenario simulated by each model. The former section we used every month to show 10 models' behavior. In this section, we use every model to show its seasonal cycle. Although TRACMIP did not support the energetic theory, the simulations can still provide us the information about how will ITCZ and other factors respond towards a warming climate. We will plot the changes of the factors along each month and calculate the correlation coefficient between the factors' changes to show which two changes are more(less) correlated.

CAM3 simulated a general northward shift of the ITCZ throughout the year except for April and May (Fig. 4.39) under a warming scenario. We expect to see a northward shift of ITCZ for most of the models from our annual ITCZ shift and AHT_{EQ} changes scatter plot (Fig. 4.12). Mass transport changes showed a similar northward shift pattern except for March, April and May. Therefore, the correlation coefficient between ITCZ shift and mass transport changes is relatively good (r=0.59) with p-value under 0.05. AHT_{Hadley} changes disagree with mass transport changes but agree well with AHT_{total} changes. Both AHT_{Hadley} and AHT_{total} shift to the south during Northern Hemisphere tropical wet season and shift to the north during Northern Hemisphere tropical dry season. AHT_{total} changes totally disagree with ITCZ changes. In this model, the link between mass transport change and AHT_{Hadley} broke down the most.

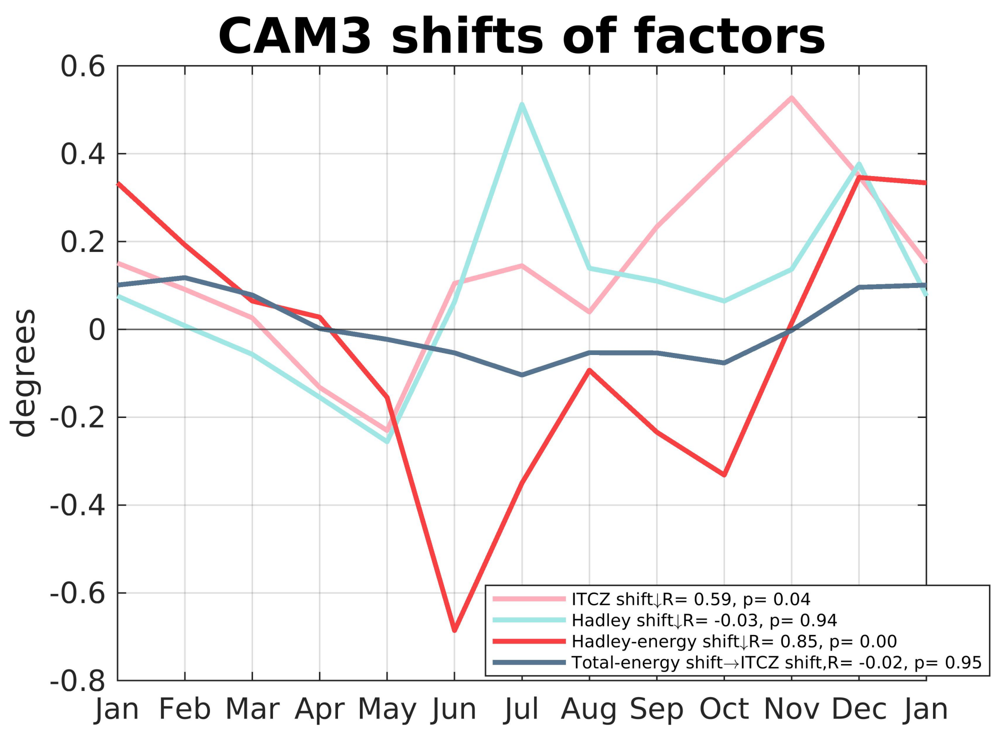

Figure 4.39: CAM3 simulated inner link factors' shifts at each month. In legend, the factor name after the colored line indicates the curve's name. The down arrow indicates the r and p values are calculated between this factor and the factor below to save space.

CAM4 also simulated a general northward shift of the ITCZ throughout the year except for June, July and August (Fig. 4.40). Mass transport changes agree with ITCZ shift well and agree with AHT_{Hadley} relatively well (r=0.66) with p value as 0.02. AHT_{total} changes totally disagree with ITCZ changes again. Both AHT_{Hadley}

and AHT_{total} show a northward shift during Northern Hemisphere tropical dry season and a southward shift during Southern Hemisphere tropical wet season. AHT_{Hadley} changes are one month in advance of AHT_{total} changes. CAM4 simulated shifts are larger than CAM3.

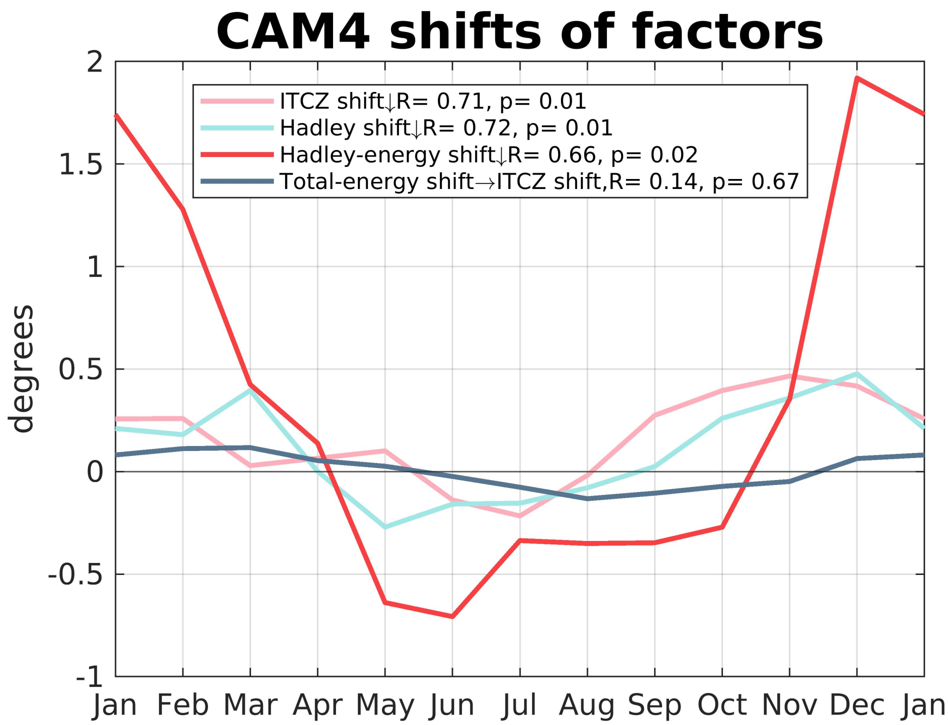

Figure 4.40: CAM4 simulated inner link factors' changes at each month. In legend, the factor name after the colored line indicates the curve's name. The down arrow indicates the r and p values are calculated between this factor and the factor below to save space.

CNRM_AM5, one of our outlier models, simulated a quite different shift pattern as comparing to CAM3 and CAM4 (Fig. 4.41). The shifts simulated by CNRM_AM5 are almost an order of magnitude larger than CAM3's. The shifts of ITCZ, mass transport, and AHT_{total} are very small comparing to AHT_{Hadley} changes. ITCZ and mass transport shift to the north from July to February. AHT_{total} shifts to the north from January to May. AHT_{Hadley} shifts similarly as CAM3 and CAM4, with northward shift during the Northern Hemisphere tropical wet season and southward shift during the Southern Hemisphere tropical dry season. AHT_{Hadley} shifts have the same sign as the mass transport change but with larger values, so the correlation coefficient between them is high. This model also does not simulate a strong correlated relationship between ITCZ shift and AHT$_{total}$ changes.

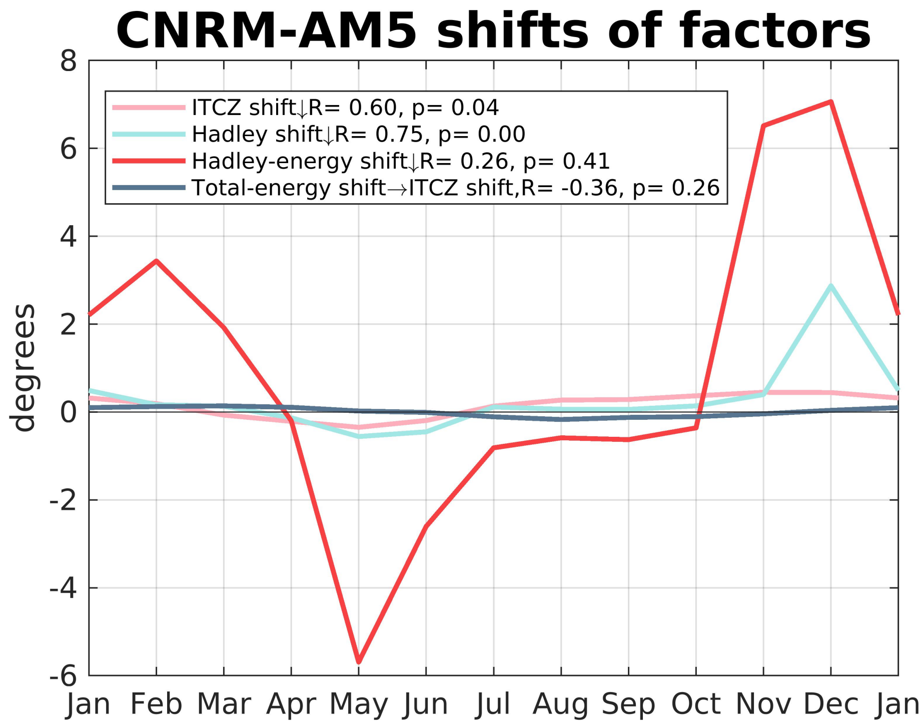

Figure 4.41: CNRM_AM5 simulated inner link factors' changes at each month. In legend, the factor name after the colored line indicates the curve's name. The down arrow indicates the r and p values are calculated between this factor and the factor below to save space.

Another outlier model, ECHAM61, simulated dramatic northward ITCZ and mass transport shifts but not for AHT$_{total}$ changes (Fig. 4.42). AHT$_{total}$ almost shows a no shift pattern throughout the year. AHT$_{Hadley}$ changes have missing values. When using AHT$_{Hadley}$ changes to calculate correlation coefficient values, we exclude both the missing value and the value it corresponds to. For example, if AHT$_{Hadley}$ changes have missing value in April, the other factor's April shift value will also be excluded. This is the first model we discussed so far, that the ITCZ shifts have a relatively bad correlation with mass transport changes. It is the fourth model we discussed so far, that do not support that the ITCZ shift and AHT$_{total}$ is correlated to each other.

The model simulated the largest shift values among 10 models.

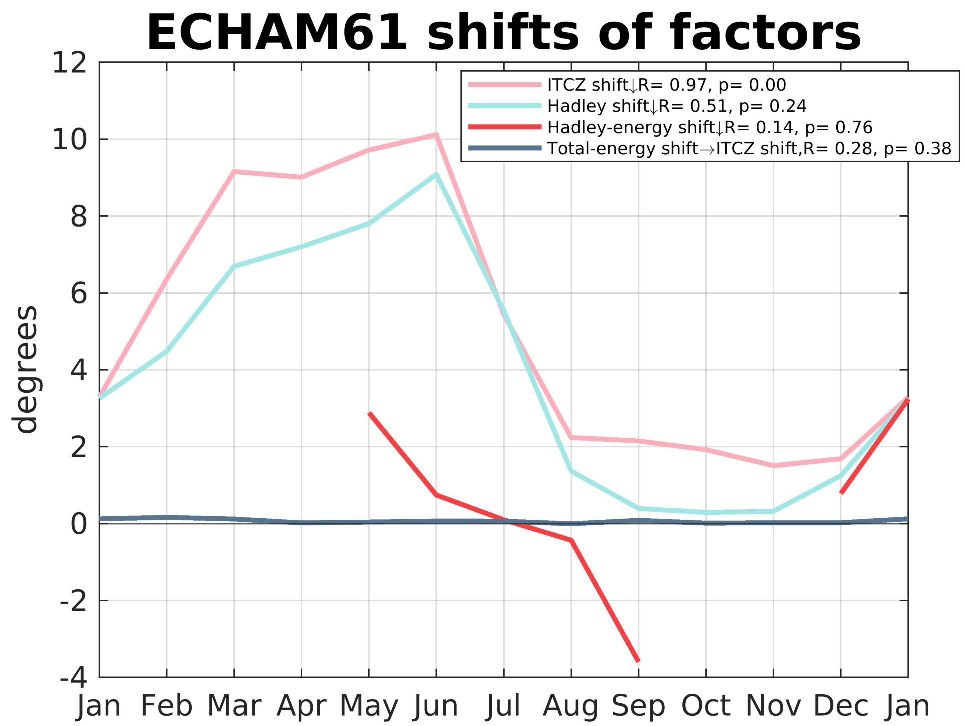

Figure 4.42: ECHAM61 simulated inner link factors' changes at each month. In legend, the factor name after the colored line indicates the curve's name. The down arrow indicates the r and p values are calculated between this factor and the factor below to save space.

ECHAM63, unlike CAM3 and CAM4 which simulated a general northward shift of ITCZ and mass transport, simulated a northward shift during the Northern Hemisphere dry season and a southward shift during the Northern Hemisphere wet season (Fig. 4.43). ECHAM63 simulated shift degrees are similar to CAM4's. AHT_{total} changes in a similar pattern and lead to a well correlated ITCZ shift and AHT_{total} changes. This is the first model we discussed so far that support the relationship between ITCZ shifts and AHT_{total} changes. However, the correlation between ITCZ shift and mass transport changes, and between mass transport changes and AHT_{Hadley} changes are not very high.

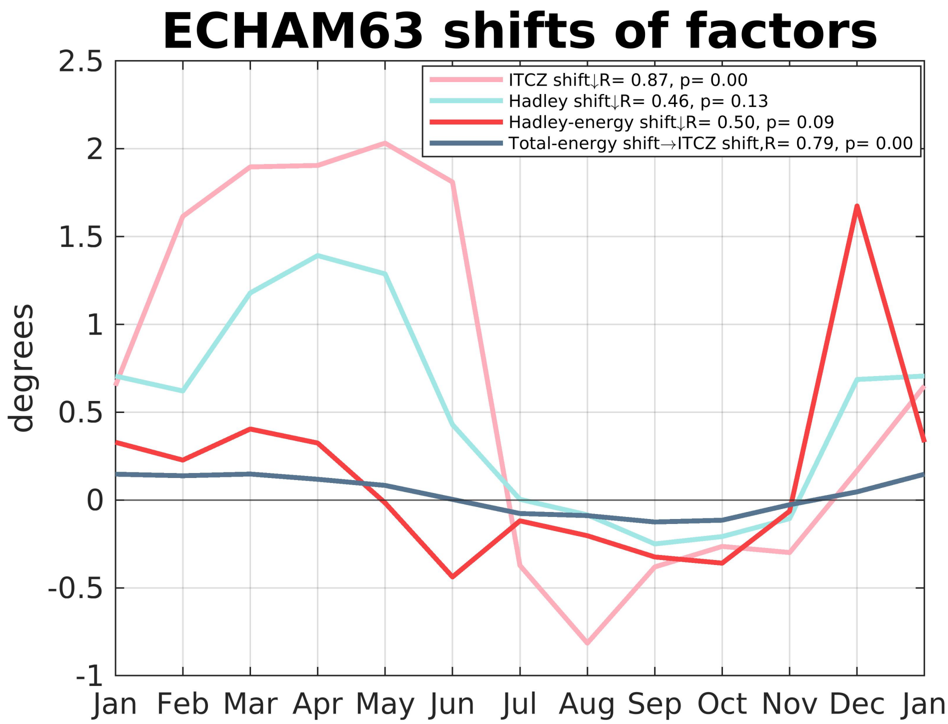

Figure 4.43: ECHAM63 simulated inner link factors' changes at each month. In legend, the factor name after the colored line indicates the curve's name. The down arrow indicates the r and p values are calculated between this factor and the factor below to save space.

LMDZ5A simulated a northward shift of ITCZ and mass transport for all months under a warming scenario (Fig. 4.44). AHT_{Hadley} and AHT_{total} shifts share the similar pattern, with a southward shift during the Northern Hemisphere tropical wet season and a northward shift during the Northern Hemisphere tropical dry season. Therefore, the correlations between ITCZ shift and mass transport changes, between AHT_{Hadley} and AHT_{total} changes are high. However, the relationships between mass transport changes and AHT_{Hadley} changes, between AHT_{total} changes and ITCZ shifts are not strong at all. Again, this model does not support the relationship between ITCZ shifts and AHT_{total} changes under climate change. This model simulated shift degrees are similar to CAM4's.

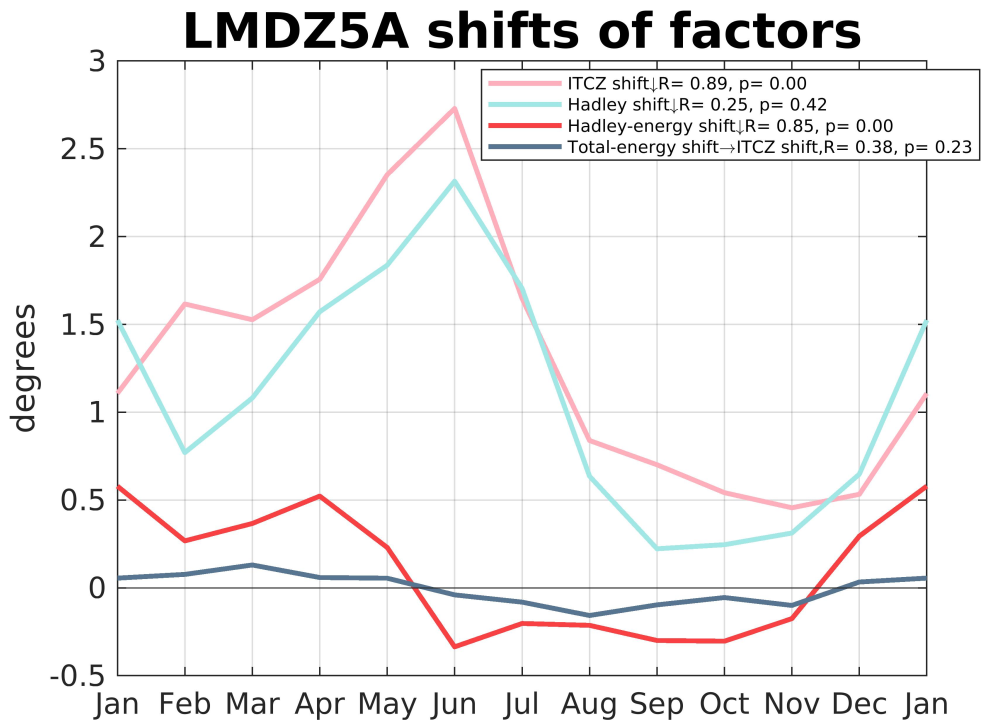

Figure 4.44: LMDZ5A simulated inner link factors' changes at each month. In legend, the factor name after the colored line indicates the curve's name. The down arrow indicates the r and p values are calculated between this factor and the factor below to save space.

MetUM_CTL simulated a northward shift of the ITCZ throughout the year and an in general northward shift of the mass transport except for April (Fig. 4.45). The relationship between ITCZ shift and mass transport changes is not as strong as the above models. AHT_{Hadley} and AHT_{total} changes are in general quite small and their relationship is relatively strong (r=0.68) with p value as 0.03. The changes of ITCZ and AHT_{total} are not well correlated. This model again does not support the energetic theory's expectation under a warming scenario.

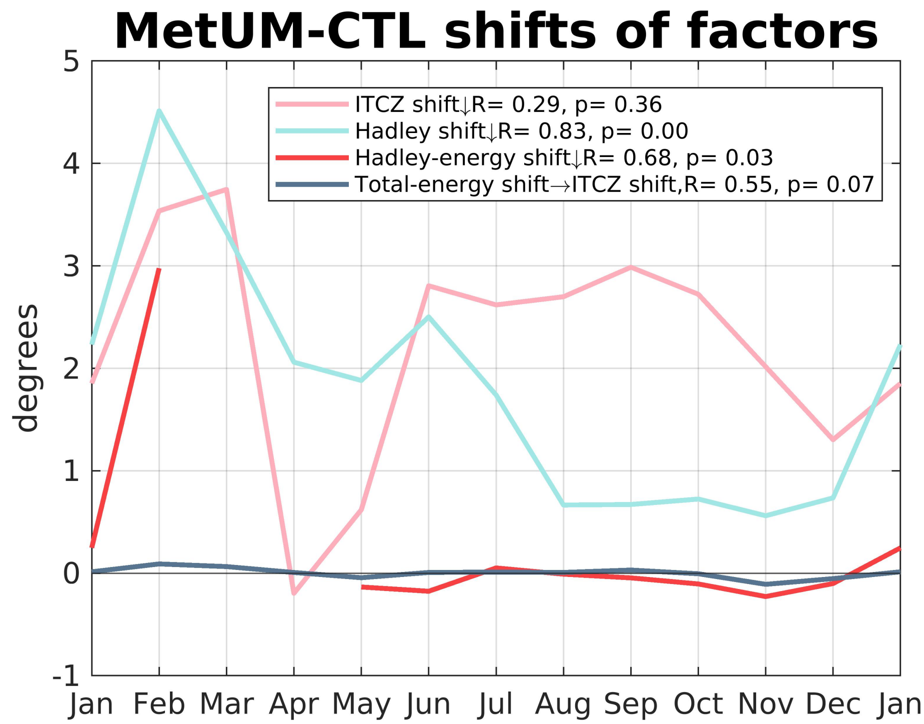

Figure 4.45: MetUM_CTL simulated inner link factors' changes at each month. In legend, the factor name after the colored line indicates the curve's name. The down arrow indicates the r and p values are calculated between this factor and the factor below to save space.

MetUM_ENT simulated northward shifts of ITCZ and mass transport, with larger shifts during the Northern Hemisphere tropical dry season. AHT_{Hadley} shifts to the north during Northern Hemisphere tropical dry season, and the shifts are subtle during Northern Hemisphere tropical wet season. AHT_{total} changes are very small throughout the year. The relationship between all factors' changes are relatively strong. This is the second model that supports the energetic theory's expectation of ITCZ shifts and AHT_{total} changes under climate change.

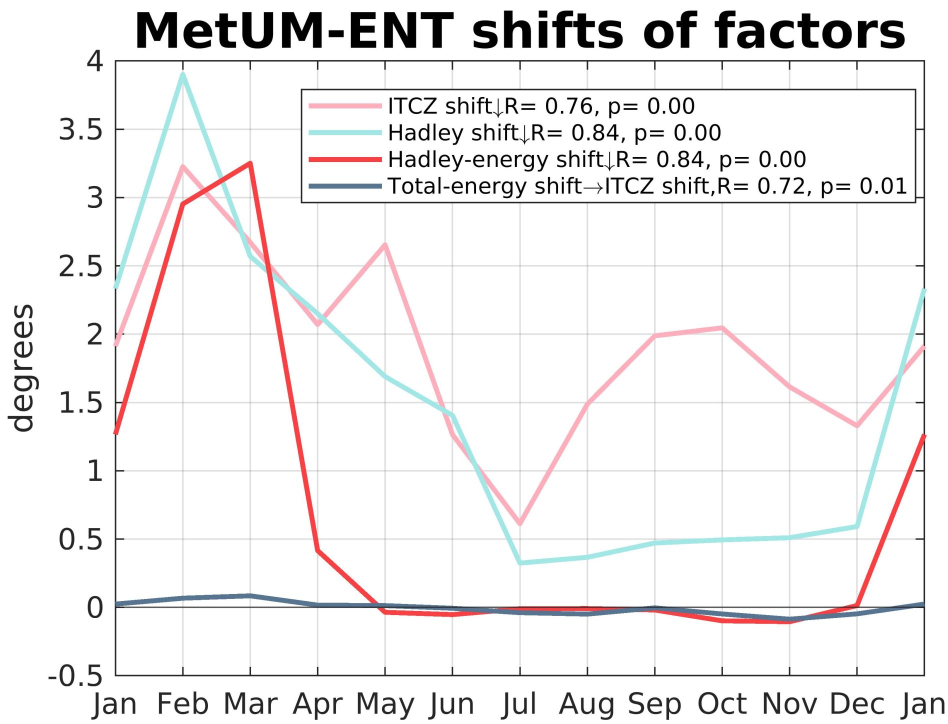

Figure 4.46: MetUM_ENT simulated inner link factors' changes at each month. In legend, the factor name after the colored line indicates the curve's name. The down arrow indicates the r and p values are calculated between this factor and the factor below to save space.

MIROC5 simulated shifts are relatively small (Fig. 4.47). MIROC5 and CAM3 are the only two models that simulated shifts under 1°. MIROC5 simulated a northward shift of the ITCZ except for September, October and November. Mass transport shifts to the north during Northern Hemisphere tropical dry season and shifts to the south during Northern Hemisphere tropical wet season. AHT_{Hadley} in general shifts to the north during Northern Hemisphere tropical wet season and shifts to the south during Northern Hemisphere tropical dry season. AHT_{total} shows the similar pattern of northward shift during Northern Hemisphere wet season and southward shift during Northern Hemisphere dry season. The correlation coefficient values between all factors are relatively small. The correlation between ITCZ shifts and AHT_{total} changes is even negative. Therefore, MIROC5 also disagrees with the expectation by the energetic theory under climate change. Considering the simple relationship between ITCZ position and AHT_{EQ} was initially strange simulated by MIROC5(Fig. 4.15), the shifts values simulated by MIROC5 are not outstandingly odd.

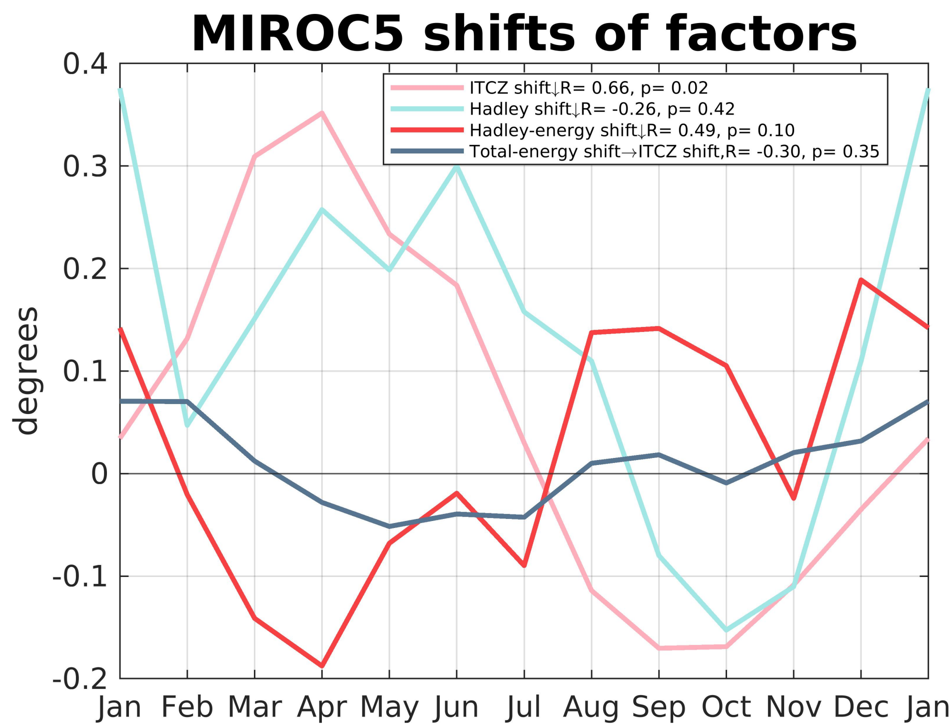

Figure 4.47: MIROC5 simulated inner link factors' changes at each month. In legend, the factor name after the colored line indicates the curve's name. The down arrow indicates the r and p values are calculated between this factor and the factor below to save space.

MPAS simulated relatively small shifts. In general, ITCZ and mass transport shifts are northward throughout the year. AHT_{Hadley} shifts to the north during Northern Hemisphere tropical dry season and to the south during Northern Hemisphere tropical wet season. The changes of the AHT_{total} is relatively small, with northward shift during Northern Hemisphere tropical dry season and southward shift during Northern Hemisphere tropical wet season. All factors' changes relationship are relatively well. This is the third model that supports the energetic theory under a warming scenario.

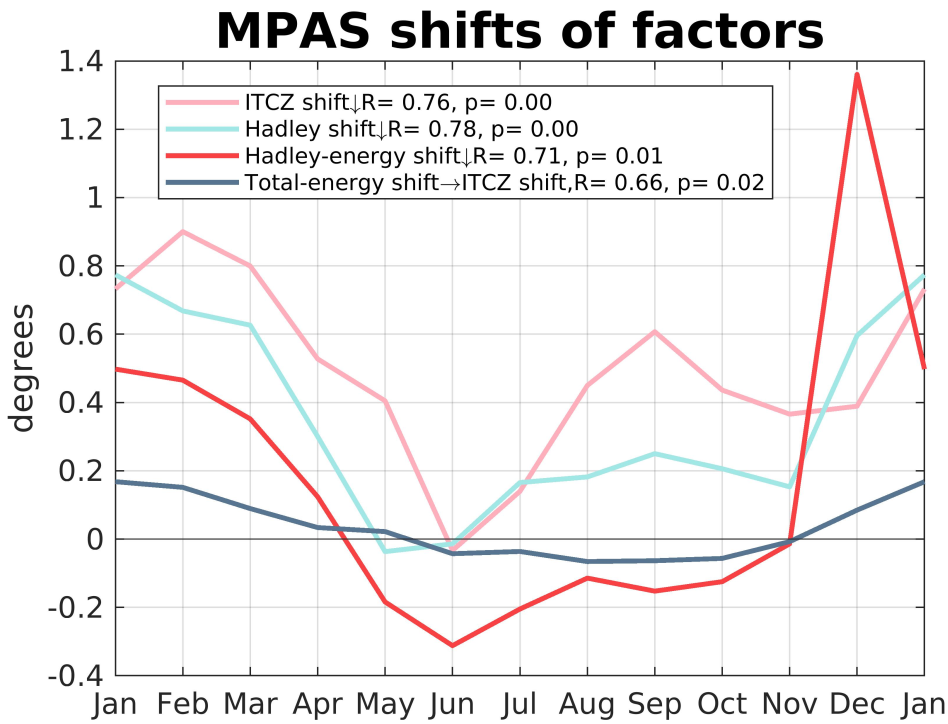

Figure 4.48: MPAS simulated inner link factors' changes at each month. In legend, the factor name after the colored line indicates the curve's name. The down arrow indicates the r and p values are calculated between this factor and the factor below to save space.

As a brief summary, almost all models simulated a northward shift of the ITCZ comparing 4xCO_2 to CTL. Mass transport changes in general agree with ITCZ shift. However, models disagree on how the AHT_{Hadley} and AHT_{total} will change under a warming scenario. Displaying the correlation coefficient values together on the same heatmap, we can get Fig. 4.49 and the p values (Fig. 4.50) corresponding with the r values.

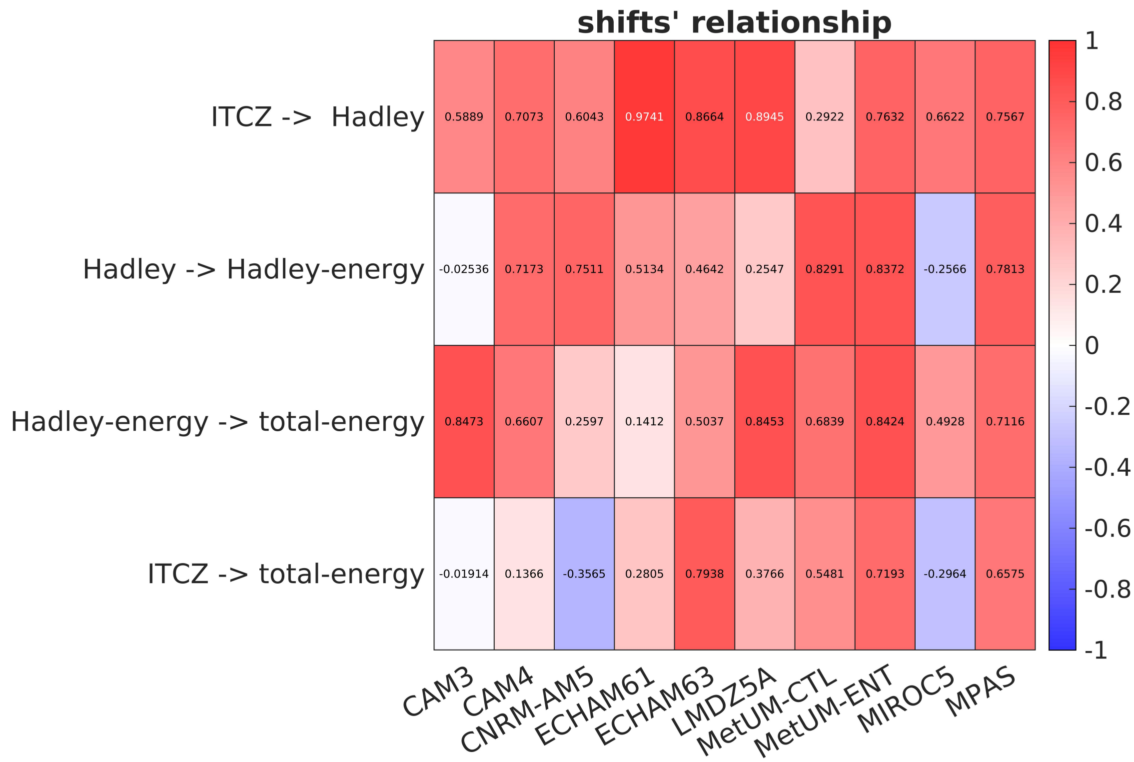

Figure 4.49: The correlation coefficient of the factors' shifts over seasonal cycle simulated by each model.

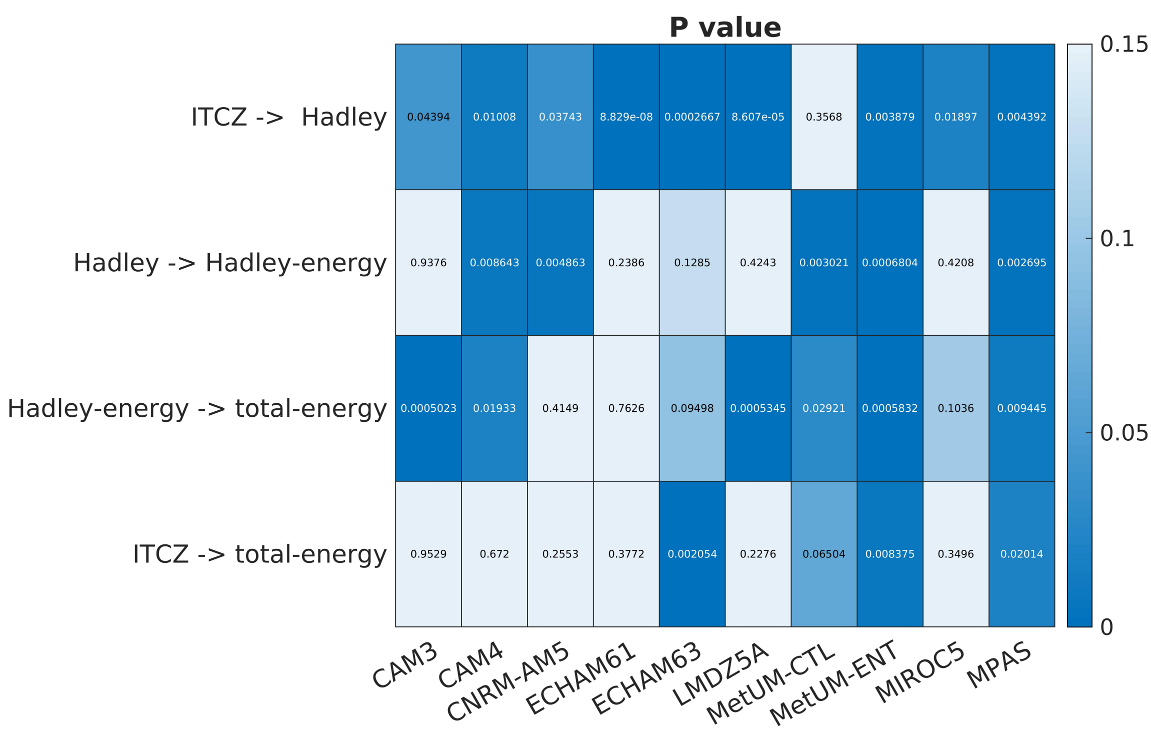

Figure 4.50: The p value corresponding to the correlation coefficient of the factors' shifts over seasonal cycle simulated by each model.

CHAPTER 5: DISCUSSION AND CONCLUSION

TRACMIP models simulated a reasonable precipitation distribution and ITCZ position in control runs. Under a 4xCO_2 scenario, our models all agree that the ITCZ shifts to the north. This result agrees with Merlis et al. (2013b) that found amplifying the hemispheric temperature asymmetry would move ITCZ to the north. Corresponding with the ITCZ shift, the Hadley Cells also shift to the north under a warming scenario. However, for the changes of energy transported by Hadley cells and the total energy transported by the atmosphere, models have different expectations. There is no clear sense that the ITCZ shifts are closely related to total energy transport changes at a monthly scale. Prior studies, like Donohoe et al. (2013), Kang et al. (2008, 2009), and Adam et al. (2016), would not suggest that zonal-mean energetic theory would break down at a seasonal scale.

Since the relationship between ITCZ shift and AHT_{EQ} changes was not as robust as the former studies would expect, we checked the monthly relationship between ITCZ position and AHT_{EQ}, and the annual relationship between ITCZ shifts and AHT_{EQ} changes. The relationships were still not as robust as the other studies'. We even used the same method as Donohoe et al. (2013) to calculate the annual relationship between ITCZ shifts and AHT_{EQ} changes but got a much smaller value than their paper. Therefore, we were convinced this was the TRACMIP models' behavior and wanted to figure out why the TRACMIP models in general disagree with zonal-mean energetic theory's expectations.

We divided the direct link between ITCZ shift and AHT_{total} changes into smaller links by adding more factors. They are mass transport changes and AHT_{Hadley} changes. The inner links led us to a clearer sense that the ITCZ shift and mass transport changes link was robust under most circumstances, while the links between mass transport changes and AHT_{Hadley} changes and/or between AHT_{Hadley} changes and AHT_{total} changes broke down for certain months of the year. The robust relationship between ITCZ shift and mass transport change supported Geen et al. (2020) that Hadley cells would respond to thermal forcing strongly once Hadley cells were angular momentum conserved.

Former studies, like Seo et al. (2017) and Kang et al. (2018), would suggest it was the unsteady GMS that caused the relationship between ITCZ shifts and AHT_{total} changes to break down. Our analysis showed that during some months in the Northern Hemisphere dry season, the GMS was relatively steady but the link between AHT_{Hadley} changes and AHT_{total} changes broke down. We also have months in the Northern Hemisphere tropical wet season, the link between mass transport changes and AHT_{Hadley} broke down the most, which supported Seo et al. (2017) and Kang et al. (2018). When the GMS was not steady anymore, Hadley cell energy transport efficiency was changed.

The AHT_{Hadley} and AHT_{total} changes link breakdown indicated that during the Northern Hemisphere tropical dry season, although the Hadley cells were efficiently transporting energy, there were other features that were transporting sufficient energy. These features, which can be Madden-Julian Oscillation (MJO), eddies, monsoons, and/or other systems, imply that Hadley transported energy was not the only large contributor to the total energy transported by the atmosphere in the tropics. TRACMIP models simulated clear African summer monsoon like patterns, which supported Bordoni and Schneider (2008) theory that monsoon can form as long as the thermal inertial is sufficiently low. The AHT_{Hadley} changes and AHT_{total} changes link breakdown was never noticed by previous studies, since we naturally tend to think that Hadley cells are the only large system in the tropics.

These changes of Hadley cells and other systems transporting energy under climate change require us to do more research on them. This also lead us to question if the TRACMIP settings are too complicated for the models to only focus on the ITCZ shifts under a warming scenario. We look forward to comparing to other model intercomparison projects that have similar settings. We are still hopeful that we would be able to combine the energetic theory and monsoon theory to generate a self-constrained model for the tropical precipitation.

Our methods of calculating ITCZ shifts and AHT_{total} changes overcame the shortcomings of focusing on fewer latitudes like AHT_{EQ} and EFE methods. However, this method calculated some unreasonable shifts especially when the curves' shapes were changed between CTL and $4xCO_2$. We look forward to finding a more optimal method to define the shifts of the curves. In addition, we only have monthly data to do our calculation. Many daily features cannot be shown in our analysis. What is more, when we were calculating mass transport and energy transported by Hadley cells, we only 1000 hPa as the bottom layer. So the mass and energy transported under 1000 hPa cannot be calculated. Since the relationship between mass transport and ITCZ is pretty well, the mass transport that cannot be calculated under 1000 hPa did not affect our calculations too much.

We examined TRACMIP simulations of a warming climate in this study. The analysis revealed that TRACMIP disagreed with energetic theory's expectations in a warming climate. We were able to explain if it was the mass transport changes to AHT_{Hadley} changes link, or AHT_{Hadley} changes to AHT_{total} changes link, that broke down the direct link between ITCZ shifts and total energy transport changes. We look forward to seeing more studies on improving the quantification methods of the changes, deepening the understandings of energetic theories, and developing a self-constrained model for the tropical precipitation.

REFERENCES

Adam, O., T. Bischoff, and T. Schneider, 2016: Seasonal and interannual variations of the energy flux equator and ITCZ. Part I: Zonally averaged itcz position. *Journal of Climate*, **29**, 3219–3230, doi:10.1175/JCLI-D-15-0512.1, https://doi.org/10.1175/JCLI-D-15-0512.1.

Biasutti, M., and A. Voigt, 2020: Seasonal and CO2-induced shifts of the ITCZ: Testing energetic controls in idealized simulations with comprehensive models. *Journal of Climate*, **33 (7)**, 2853–2870, doi:10.1175/JCLI-D-19-0602.1, https://doi.org/10.1175/JCLI-D-19-0602.1.

Biasutti, M., A. Voigt, and W. e. a. Boos, 2018: Global energetics and local physics as drivers of past, present and future monsoons. *Nature Geosci*, **11**, 392–400, doi:10.1038/s41561-018-0137-1, https://doi.org/10.1038/s41561-018-0137-1.

Bischoff, T., and T. Schneider, 2014: Energetic constraints on the position of the intertropical convergence zone. *Journal of Climate*, **27 (13)**, 4937–4951, doi:10.1175/jcli-d-13-00650.1, https://doi.org/10.1175/jcli-d-13-00650.1.

Bony, S., B. Stevens, I. M. Held, and et al., 2013: *Carbon Dioxide and Climate: Perspective on a Scientific assessment*. Springer, Dordrecht, doi:10.1007/978-94-007-6692-1_14, https://doi.org/10.1007/978-94-007-6692-1_14.

Boos, W., and R. Korty, 2016: Regional energy budget control of the intertropical convergence zone and application to mid-Holocene rainfall. *Nature Geosci*, **9**, 892–897, doi:10.1038/ngeo2833, https://doi.org/10.1038/ngeo2833.

Bordoni, S., 2020: Idealized simulations with zonally symmetric continents with different equatorward coastlines. *CaltechDATA Contact: K. Hui*, https://data.caltech.edu/records/1649.

Bordoni, S., and T. Schneider, 2008: Monsoons as eddy-mediated regime transitions of the tropical overturning circulation. *Nature Geosci*, **1**, 515–519, doi:10.1038/ngeo248, https://doi.org/10.1038/ngeo248.

Broccoli, A. J., K. A. Dahl, and S. R. J., 2006: Response of the ITCZ to northern hemisphere cooling. *Geophysical Researcher Letters*, **33 (1)**, L01 702, doi:10.1029/2005GL024546, https://doi.org/10.1029/2005GL024546.

Bryan, K., and M. D. Cox, 1968: A nonlinear model of an ocean driven by wind and differential heating: Part i. description of the three-dimensional velocity and density fields. *Journal of the Atmospheric Sciences*, **25**, 945–967.

Byrne, M. P., A. G. Pendergrass, A. D. Rapp, and K. R. Wodzicki, 2018: Response of the Intertropical Convergence zone to climate change: Location, Width, and Strength. *Current Climate Change Reports*, **4**, 355–370, doi:10.1007/s40641-018-0110-5, https://doi.org/10.1007/s40641-018-0110-5.

Chiang, J., and C. Bitz, 2005: Influence of high latitude ice cover on the marine Intertropical Convergence zone. *Climate Dynamics*, **25**, 477–496, doi:10.1007/s00382-005-0040-5, https://doi.org/10.1007/s00382-005-0040-5.

Chiang, J. C. H., M. Biasutti, and D. S. Battisti, 2003: Sensitivity of the atlantic intertropical convergence zone to Last Glacial Maximum boundary conditions. *Paleoceanography*, **18**, doi:10.1029/2003PA000916, http://doi.org/10.1029/2003PA000916.

Chiang, J. C. H., and A. R. Friedman, 2012: Extratropical cooling, interhemispheric thermal gradients, and tropical climate change. *Annual Review of Earth and Planetary Sciences*, **40**, 383–412, doi:10.1146/annurev-earth-042711-105545, https://doi.org/10.1146/annurev-earth-042711-105545.

Codron, F., 2012: Ekman heat transport for slab oceans. *Clim Dyn*, **38**, 379–389, doi:10.1007/s00382-011-1031-3, https://doi.org/10.1007/s00382-011-1031-3.

Dima, I. M., and J. M. Wallace, 2003: On the seasonality of the hadley cell. *Journal of the Atmospheric Sciences*, **60**, 1522–1527, doi: 10.1175/1520-0469(2003)060<1522:OTSOTH>2.0.CO;2, https://doi.org/10.1175/1520-0469(2003)060<1522:OTSOTH>2.0.CO;2.

Donohoe, A., and D. S. Battisti, 2013: The seasonal cycle of atmospheric heating and temperature. *Journal of Climate*, **26 (14)**, 4962–4980, doi:10.1175/JCLI-D-12-00713.1, https://doi.org/10.1175/JCLI-D-12-00713.1.

Donohoe, A., J. Marshall, D. Ferreira, and et al., 2013: The relationship between ITCZ location and cross-equatorial atmospheric heat transport: From the seasonal cycle to the last glacial maximum. *Journal of Climate*, **26**, 3597–3618, doi:10.1175/JCLI-D-12-00467.1, https://doi.org/10.1175/JCLI-D-12-00467.1.

Friedman, A. R., Y.-T. Hwang, J. C. H. Chiang, and D. M. W. Frierson, 2013: Interhemispheric temperature asymmetry over the twentieth century and in future projections. *Journal of Climate*, **26 (15)**, 5419–5433, doi:10.1175/JCLI-D-12-00525.1, https://doi.org/10.1175/JCLI-D-12-00525.1.

Frierson, D., Y. Hwang, N. Fučkar, and et al., 2013: Contribution of ocean overturning circulation to tropical rainfall peak in the Northern Hemisphere. *Nature Geosci*, **6**, 940–944, doi:10.1038/ngeo1987, https://doi.org/10.1038/ngeo1987.

Frierson, D. M. W., and Y.-T. Hwang, 2012: Extratropical influence on ITCZ shifts in slab ocean simulations of global warming. *Journal of Climate*, **25 (2)**, 720–733, doi:10.1175/JCLI-D-11-00116.1, https://doi.org/10.1175/JCLI-D-11-00116.1.

Fučkar, N. S., S.-P. Xie, R. Farneti, E. A. Maroon, , and D. M. W. Frierson, 2013: "influence of the extratropical ocean circulation on the Intertropical Convergence Zone in an idealized coupled general circulation model. *Journal of Climate*, **26**, 4612–4629, doi:10.1175/JCLI-D-12-00294.1, https://doi.org/10.1175/JCLI-D-12-00294.1.

Geen, R., S. Bordoni, D. S. Battisti, and K. Hui, 2020: Monsoons, ITCZs, and the concept of the global monsoon. *Reviews of Geophysics*, **58**, e2020RG000 700, doi:10.1029/2020RG000700, https://doi.org/10.1029/2020RG000700.

Geen, R., F. H. Lambert, and G. K. Vallis, 2019: Processes and timescales in onset and withdrawal of "aquaplanet monsoons". *Journal of the Atmospheric Sciences*, **76**, doi:10.1175/JAS-D-18-0214.1, https://doi.org/10.1175/JAS-D-18-0214.1.

Harrop, B. E., J. Lu, F. Liu, O. A. Garuba, and L. Ruby Leung, 2018: Sensitivity of the ITCZ location to ocean forcing via q-flux green's function experiments. *Geophysical Research Letters*, **45**, 13,116–13,123, doi:10.1029/2018GL080772, https://doi.org/10.1029/2018GL080772.

Hartmann, D. L., 2016: Chapter 6 - Atmospheric General Circulation and Climate. *Global Physical Climatology (Second Edition)*, D. L. Hartmann, Ed., second edition ed., Elsevier, Boston, 159–193, doi:10.1016/B978-0-12-328531-7.00006-2, https://www.sciencedirect.com/science/article/pii/B9780123285317000062.

Held, I. M., 2001: The partitioning of the poleward energy transport between the tropical ocean and atmosphere. *Journal of the Atmospheric Sciences*, **58**, 943–948, doi:10.1175/1520-0469(2001)058\%3C0943:TPOTPE\%3E2.0.CO;2, https://doi.org/10.1175/1520-0469(2001)058%3C0943:TPOTPE%3E2.0.CO;2.

Held, I. M., 2005: The gap between simulation and understanding in climate modeling. *American Meteorology Society*, 1609–1614, doi:10.1175/BAMS-86-11-1609, https://doi.org/10.1175/BAMS-86-11-1609.

Horel, J. D., and J. M. Wallace, 1981: Planetary-scale atmospheric phenomena associated with the southern oscillation. *Monthly Weather Review*, **109**, 813–829, doi:10.1175/1520-0493(1981)109<0813:PSAPAW>2.0.CO;2, https://doi.org/10.1175/1520-0493(1981)109<0813:PSAPAW>2.0.CO;2.

Hoskins, B. J., and D. J. Karoly, 1981: The steady linear response of a spherical atmosphere to thermal and orographic forcing. *Journal of Atmospheric Sciences*, **38**, 1179–1196, doi:10.1175/1520-0469(1981)038<1179:TSLROA>2.0.CO;2, https://doi.org/10.1175/1520-0469(1981)038<1179:TSLROA>2.0.CO;2.

Huffman, G. J., R. F. Adler, D. T. Bolvin, and G. Gu, 2009: Improving the global precipitation record: GPCP version 2.1. *Geophys. Res. Lett.*, **36**, L17 808, doi:10.1029/2009GL040000, https://doi.org/10.1029/2009GL040000.

Hwang, Y.-T., and D. M. W. Frierson, 2013: Link between the double-intertropical convergence zone problem and cloud biases over the southern ocean. *Proceedings of the National Academy of Sciences*, **110**, 4935–4940, doi:10.1073/pnas.1213302110, https://www.pnas.org/content/110/13/4935.

Hwang, Y.-T., D. M. W. Frierson, and S. M. Kang, 2013: Anthropogenic sulfate aerosol and the southward shift of tropical precipitation in the late 20th century. *Geophys. Res. Lett.*, **40**, 2845– 2850, doi:10.1002/grl.50502, https://doi.org/10.1002/grl.50502.

Jeevanjee, N., P. Hassanzadeh, S. Hill, and A. Sheshadri, 2017: A perspectiveon climate model hierarchies. *J. Adv.Model. Earth Syst.*, **9**, 1760–1771, doi:10.1002/2017MS001038, https://doi.org/10.1002/2017MS001038.

Kang, S., 2020: Extratropical influence on the tropical rainfall distribution. *Curr Clim Change Rep*, **6**, 24–36, doi:10.1007/s40641-020-00154-y, https://doi.org/10.1007/s40641-020-00154-y.

Kang, S., and I. Held, 2012: Tropical precipitation, SSTs and the surface energy budget: a zonally symmetric perspective. *Climate Dynamics*, **38**, 1917–1924, doi: s00382-011-1048-7, https://doi.org/10.1007/s00382-011-1048-7.

Kang, S., I. Held, and S. Xie, 2013: Contrasting the tropical responses to zonally asymmetric extratropical and tropical thermal forcing. *Climate Dynamics*, **42**, 2033–2043, doi:10.1007/s00382-013-1863-0, https://doi.org/10.1007/s00382-013-1863-0.

Kang, S. M., D. M. W. Frierson, and I. M. Held, 2009: The tropical response to extratropical thermal forcing in an idealized GCM: The importance of radiative feedbacks and convective parameterization. *Journal of the Atmospheric Sciences*, **66 (9)**, 2812–2827, doi:10.1175/2009JAS2924.1, https://doi.org/10.1175/2009JAS2924.1.

Kang, S. M., I. M. Held, D. M. W. Frierson, and et al., 2008: The response of the ITCZ to extratropical thermal forcing: idealized slab-ocean experiments with a GCM. *Journal of Climate*, **21**, 3521–3532, doi:10.1175/2007JCLI2146.1, https://doi.org/10.1175/2007JCLI2146.1.

Kang, S. M., Y. Shin, and S. Xie, 2018: Extratropical forcing and tropical rainfall distribution: energetics framework and ocean ekman advection. *npj Clim Atmos Sci*, **1**, 20 172, doi:10.1038/s41612-017-0004-6, https://doi.org/10.1038/s41612-017-0004-6.

Lee, M.-I., M. J. Suarez, and I.-S. e. a. Kang, 2008: A moist benchmark calculation for atmospheric general circulation models. *Journal of Climate*, **21**, 4934–4954, doi:10.1175/2008JCLI1891.1, https://doi.org/10.1175/2008JCLI1891.1.

Lindzen, R. S., and A. V. Hou, 1988: Hadley circulations for zonally averaged heating centered off the equator. *Journal of Atmospheric Sciences*, **45**, 2416–2427, doi:

10.1175/1520-0469(1988)045<2416:HCFZAH>2.0.CO;2, https://doi.org/10.1175/1520-0469(1988)045<2416:HCFZAH>2.0.CO;2.

Manabe, S., and K. Bryan, 1969: Climate calculations with a combined ocean-atmosphere model. *Journal of the Atmospheric Sciences*, **26**, 786–789.

Manabe, S., R. J. Stouffer, M. J. Spelman, and K. Bryan, 1991: Transient responses of a coupled ocean-atmosphere model to gradual changes of atmospheric co2. *Journal of Climate*, **4**, 785–818.

Marshall, J., A. Donohoe, D. Ferreira, and D. McGee, 2014: The ocean's role in setting the mean position of the Inter-Tropical Convergence Zone. *Climate Dynamics*, **42**, 1967–1979, doi:10.1007/s00382-013-1767-z, https://doi.org/10.1007/s00382-013-1767-z.

McGuffie, K., and A. Henderson-Sellers, Eds., 2014: *The climate modelling primer*. Wiley Blackwell, Chichester, West Sussex, https://www.wiley.com/en-us/The+Climate+Modelling+Primer%2C+4th+Edition-p-9781119943372.

Merlis, T. M., T. Schneider, S. Bordoni, and I. Eisenman, 2013a: Hadley circulation response to Orbital Precession. part I: Aquaplanets. *Journal of Climate*, **26**, 740–753, doi:10.1175/JCLI-D-11-00716.1, https://doi.org/10.1175/JCLI-D-11-00716.1.

Merlis, T. M., M. Zhao, and I. M. Held, 2013b: The sensitivity of hurricane frequency to itcz changes and radiatively forced warming in aquaplanet simulations. *Geophysical Research Letters*, **40**, 4109–4114.

Murphy, J. M., 1995: Transient response of the hadley centre coupled ocean-atmosphere model to increasing carbon dioxide. part 1: Control climate and flux adjustment. *Journal of Climate*, **8**, 36–56, doi:10.1175/1520-0442(1995)008<0036:TROTHC>2.0.CO;2, https://doi.org/10.1175/1520-0442(1995)008<0036:TROTHC>2.0.CO;2.

Neelin, J. D., and I. M. Held, 1987: Modeling tropical convergence based on the moist static energy budget. *Monthly Weather Review*, **115**, 3–12, https://doi.org/10.1175/1520-0493(1987)115<0003:MTCBOT>2.0.CO;2.

Plumb, R. A., and A. Y. Hou, 1992: The response of a zonally symmetric atmosphere to subtropical thermal forcing: Threshold behavior. *Journal of Atmospheric Sciences*, **49**, 1790–1799, doi:10.1175/1520-0469(1992)049<1790:TROAZS>2.0.CO;2, https://doi.org/10.1175/1520-0469(1992)049<1790:TROAZS>2.0.CO;2.

Raymond, D. J., S. L. Sessions, A. H. Sobel, and B. Fuchs, 2009: The mechanics of gross moist stability. *J. of Adv. Model. Earth Syst.*, **1**, doi:10.3894/JAMES.2009.1.9., https://agupubs.onlinelibrary.wiley.com/doi/abs/10.3894/JAMES.2009.1.9.

Rencurrel, M. C., and B. E. J. Rose, 2018: The efficiency of the hadley cell response to wide variations in ocean heat transport. *Journal of Climate*, **33**, 1643–1658, https://doi.org/10.1175/JCLI-D-19-0334.1.

Roberts, C., C. Gordon, and C. Cooper, 1997: The origin of flux adjustments in a coupled model. *Monthly Weather Review*, **125**, 909–925.

Schneider, S. H., and R. E. Dickinson, 1974: Climate modeling. *Rev. Geophys.*, **12**, 447–493, doi:10.1029/RG012i003p00447, https://doi.org/10.1029/RG012i003p00447.

Schneider, T., 2006: The general circulation of the atmosphere. *Annual Review of Earth and Planetary Sciences*, **34 (1)**, 655–688, doi:10.1146/annurev.earth.34.031405.125144, https://doi.org/10.1146/annurev.earth.34.031405.125144.

Schneider, T., T. Bischoff, and G. H. Haug, 2014: Migrations and dynamics of the intertropical convergence zone. *Nature*, **513**, 45–53, doi:10.1038/nature13636, https://doi.org/10.1038/nature13636.

Seo, J., S. M. Kang, and T. M. Merlis, 2017: A model intercomparison of the tropical precipitation response to a CO2 doubling in aquaplanet simulations. *Geophys. Res. Lett.*, **44**, 993 – 1000, doi:10.1002/2016GL072347, https://doi.org/10.1002/2016GL072347.

Trenberth, K., and A. Solomon, 1994: The global heat balance: heat transports in the atmosphere and ocean. *Climate Dynamics*, **10**, 107–134, doi:10.1007/BF00210625, https://doi.org/10.1007/BF00210625.

Voigt, A., B. M., and e. a. Scheff, J., 2016: The tropical rain belts with an annual cycle and a continent model intercomparison project: TRACMIP. *Journal of Advances in Modeling Earth Systems*, **8**, doi:10.1002/2016MS000748, https://doi.org/10.1002/2016MS000748.

Waliser, D., and X. Jiang, 2014: *Tropical Meteorology and Climate: Intertropical Convergence Zone*, 121–131. Elsevier, doi:10.1016/B978-0-12-382225-3.00417-5, https://doi.org/10.1016/B978-0-12-382225-3.00417-5.

Wang, Y. J., H. Cheng, R. L. Edwards, Z. S. An, J. Y. Wu, C.-C. Shen, and J. A. Dorale, 2001: A high-resolution absolute-dated late pleistocene monsoon record from hulu cave, china. *Science*, **294 (5550)**, 2345–2348, doi:10.1126/science.1064618, https://www.science.org/doi/abs/10.1126/science.1064618, https://www.science.org/doi/pdf/10.1126/science.1064618.

Wei, H.-H., and S. Bordoni, 2018: Energetic constraints on the ITCZ position in idealized simulations with a seasonal cycle. *Journal of Advances in Modeling Earth Systems*, **10**, 1708–1725, doi:10.1029/2018MS001313, https://doi.org/10.1029/2018MS001313.

Yoshimori, M., and A. J. Broccoli, 2009: On the link between Hadley circulation changes and radiative feedback processes. *Geophys. Res. Lett.*, **36**, L20 703, doi: 10.1029/2009GL040488, https://doi.org/10.1029/2009GL040488.

APPENDIX A: Regional summer surface configuration

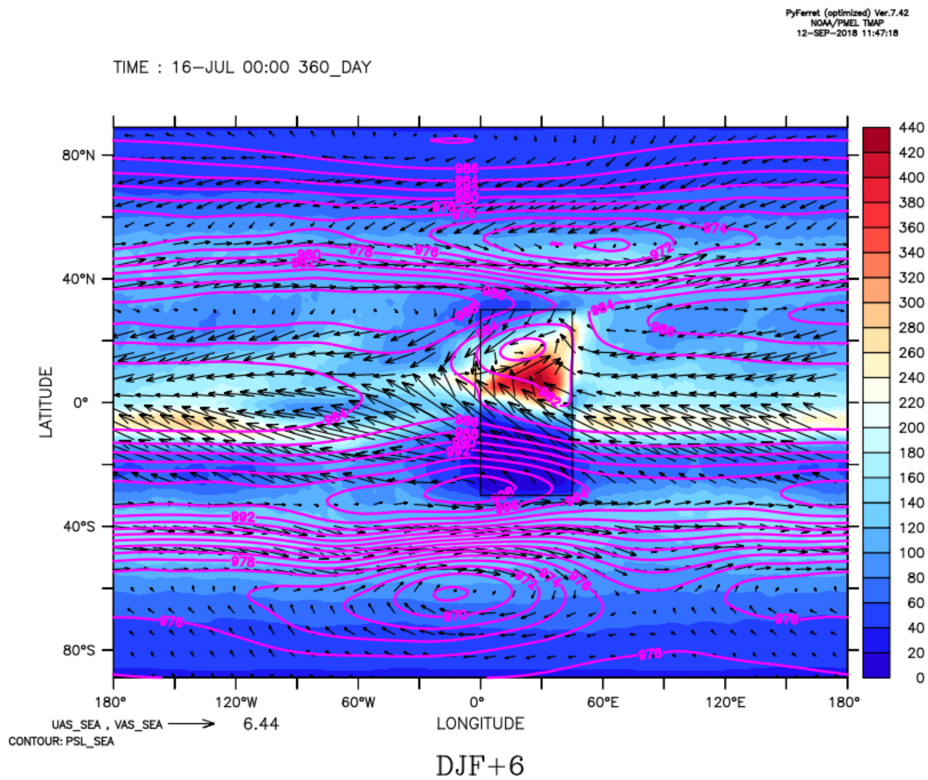

Figure A.1: MIROC5 JJA precipitation (mm/month, shading), pressure (hPa, contour) and wind (m/s, vector) simulations. The box indicates where the idealized continent is. Content of the left corner (Time) means the average is calculated from one month before July to one month after July.

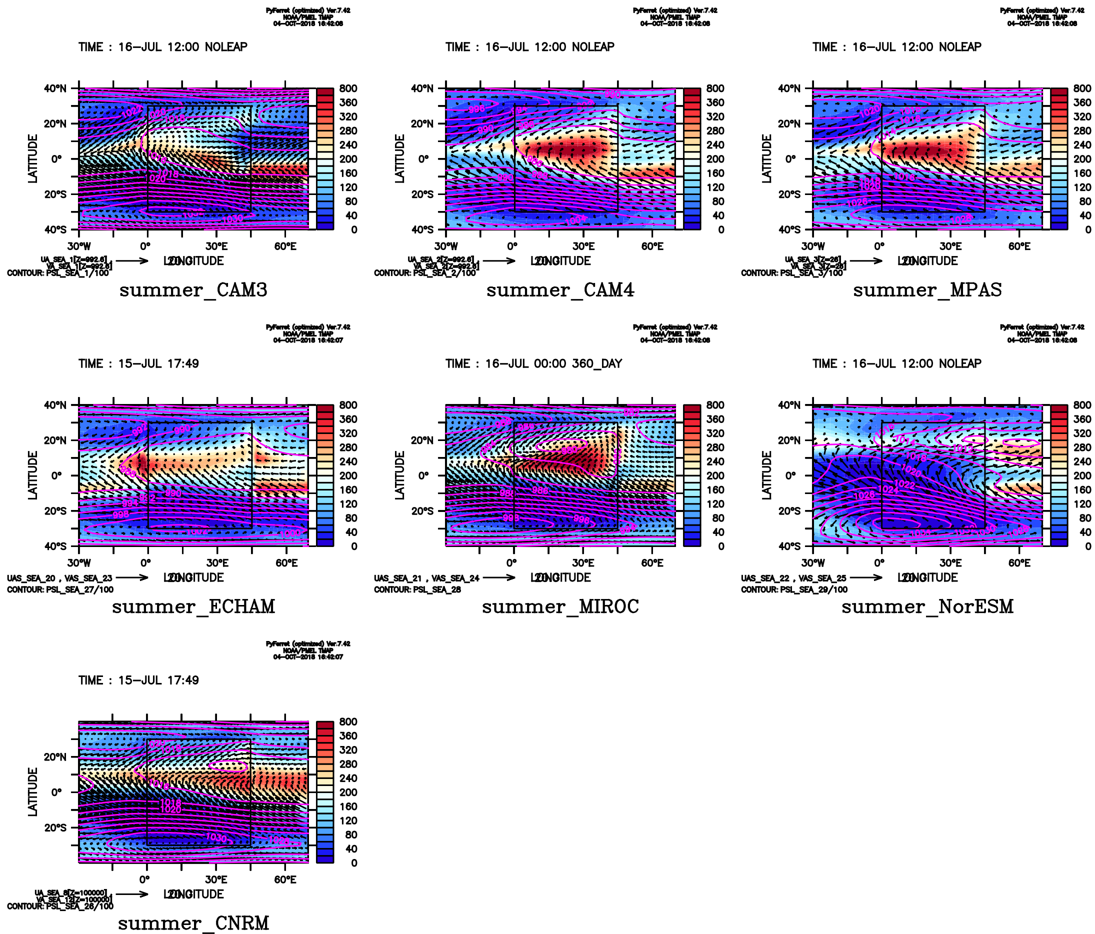

Figure A.2: Regional summer surface patterns of JJA precipitation (mm/month, shading), pressure (hPa, contour) and wind (m/s, vector) simulations. The box indicates where the idealized continent is. Content of the left corner (Time) means the average is calculated from one month before July to one month after July.

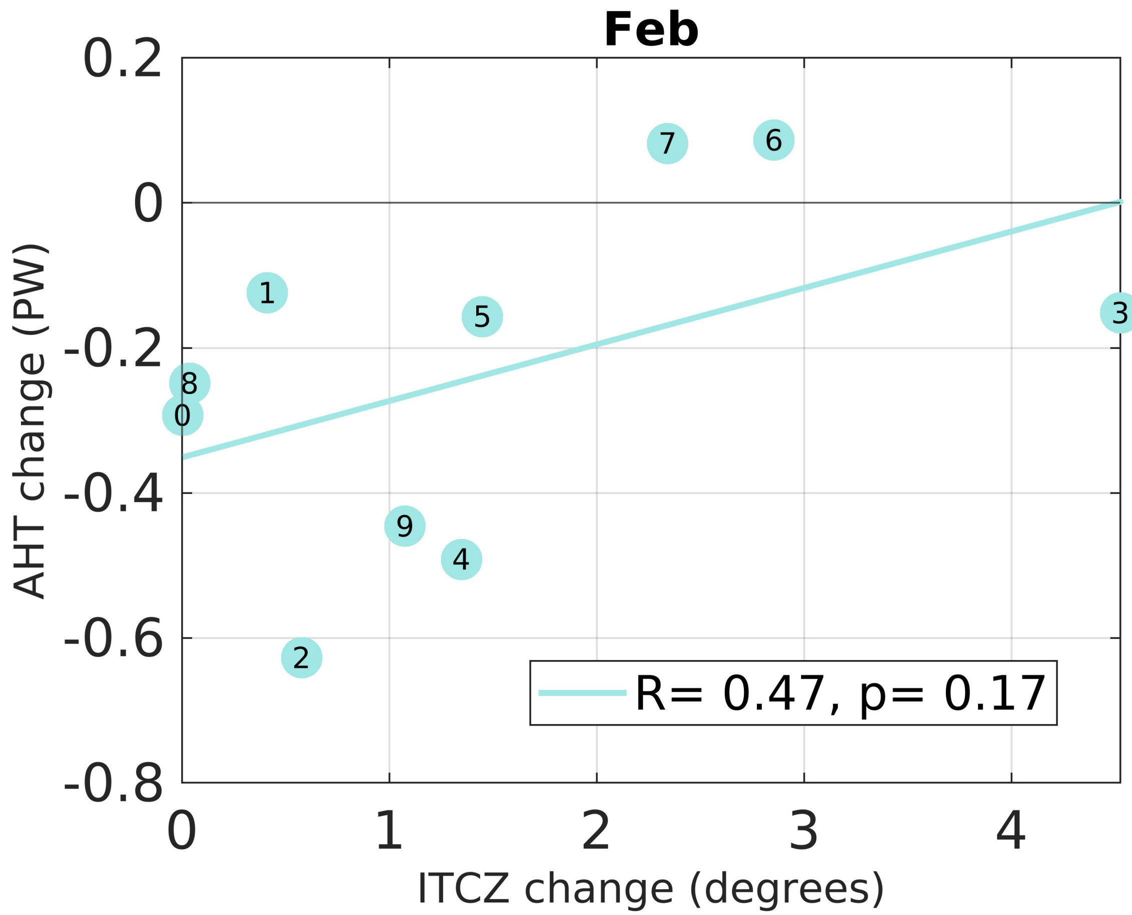

Figure B.1: As Fig. 4.8 but for February.

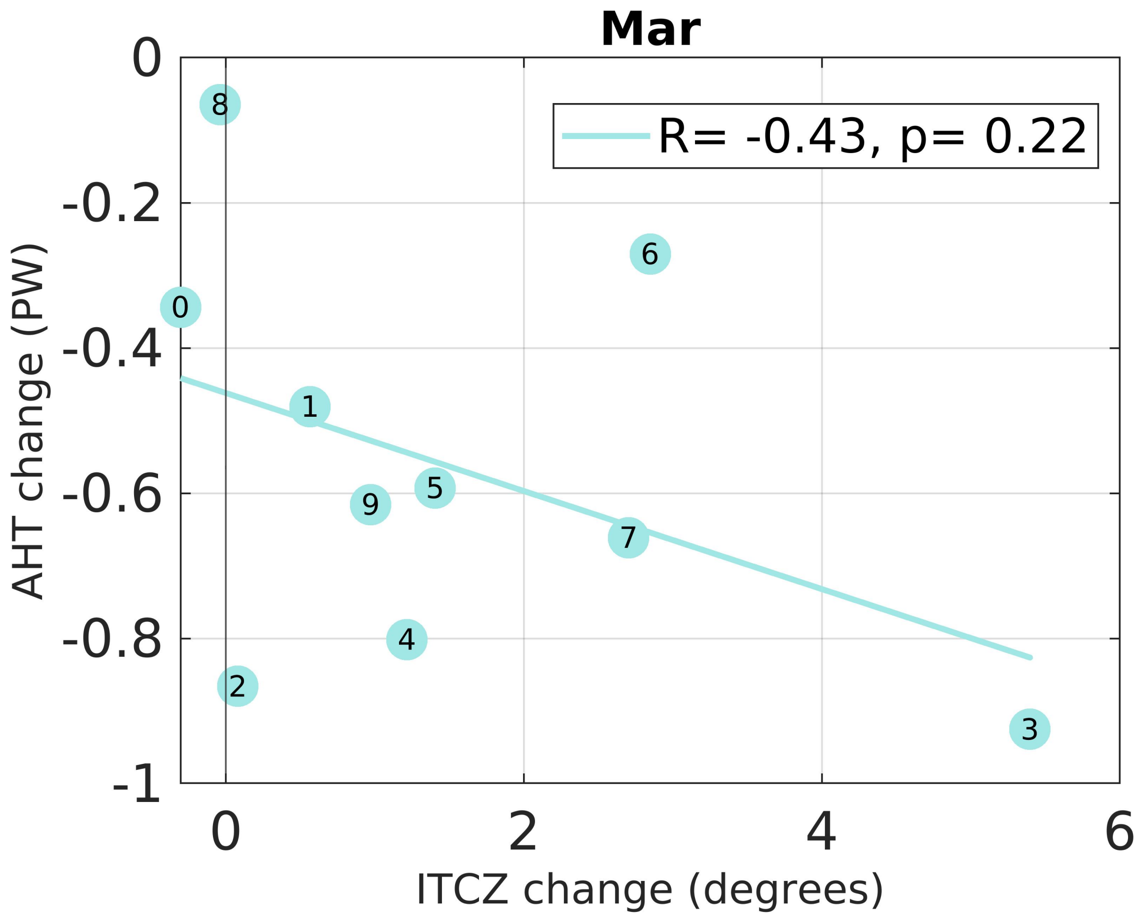

Figure B.2: As Fig. 4.8 but for March.

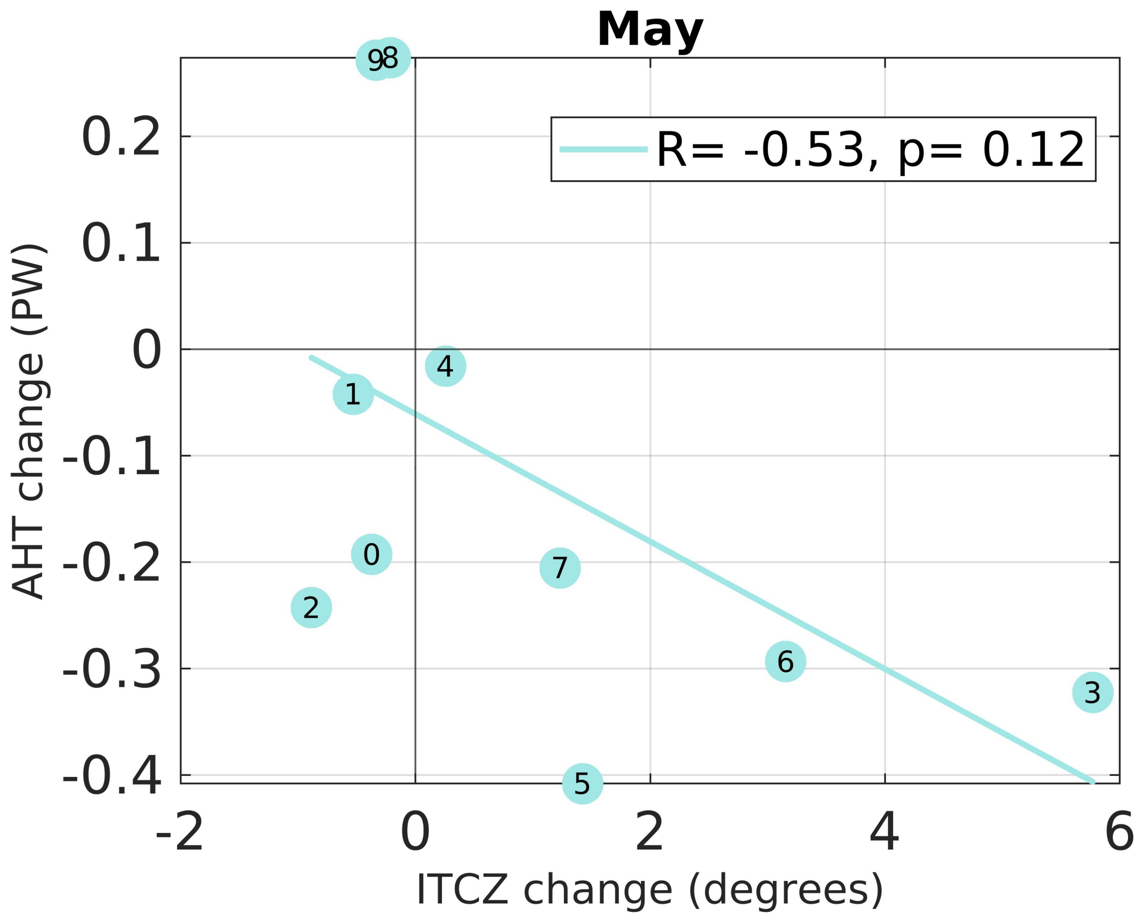

Figure B.3: As Fig. 4.8 but for May.

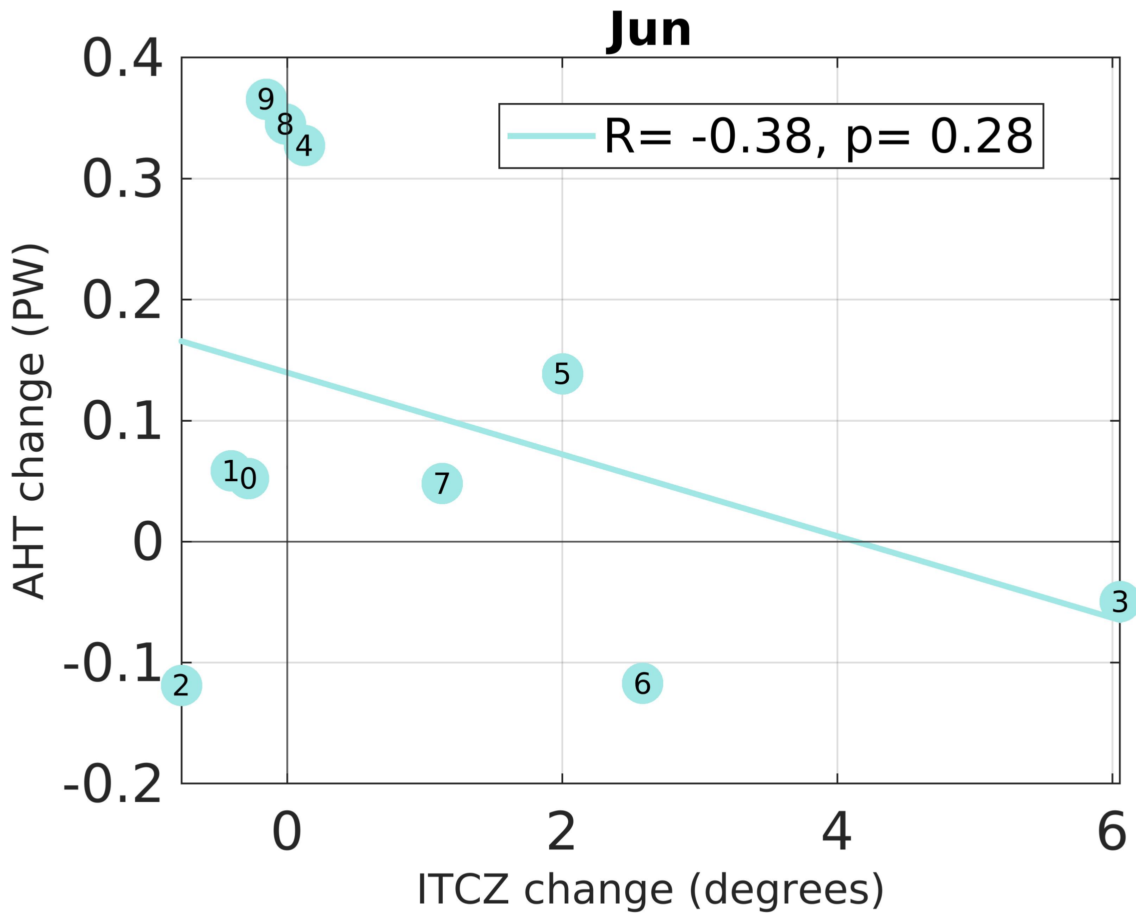

Figure B.4: As Fig. 4.8 but for June.

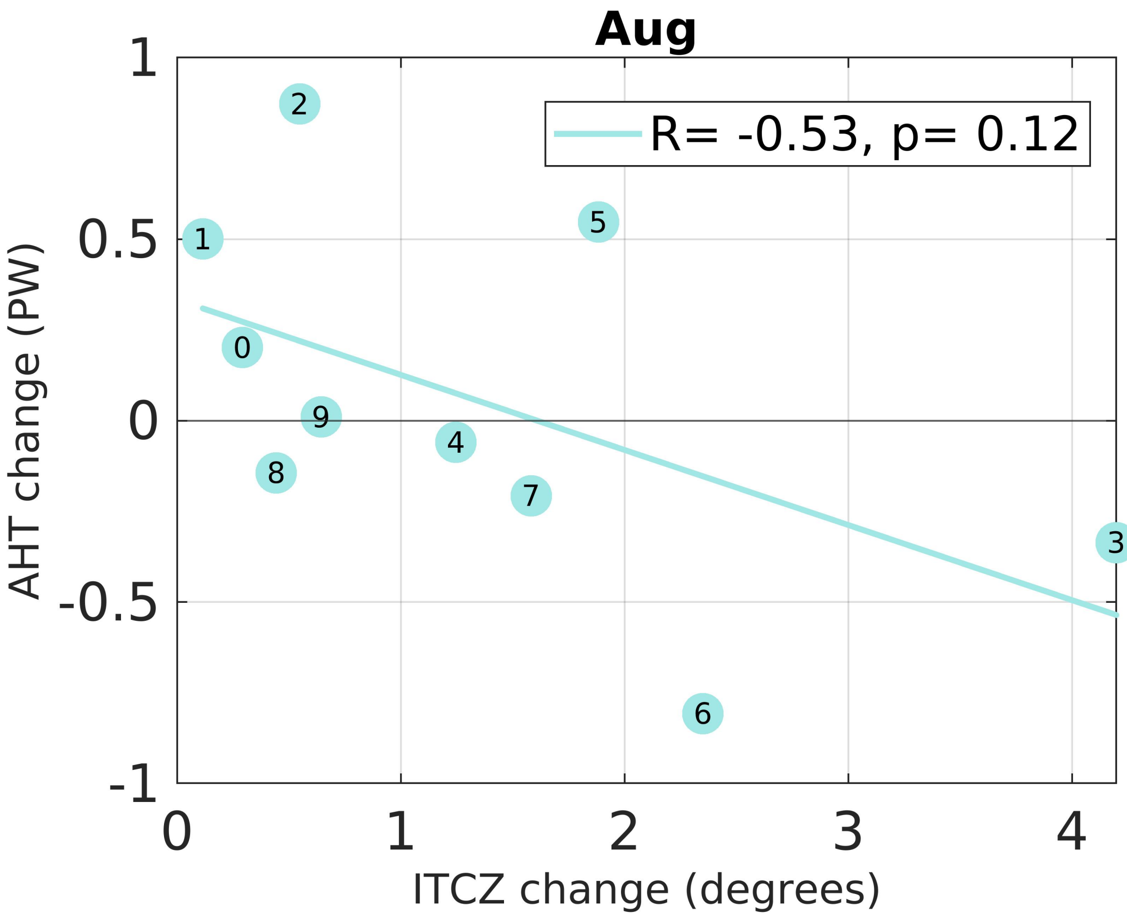

Figure B.5: As Fig. 4.8 but for August.

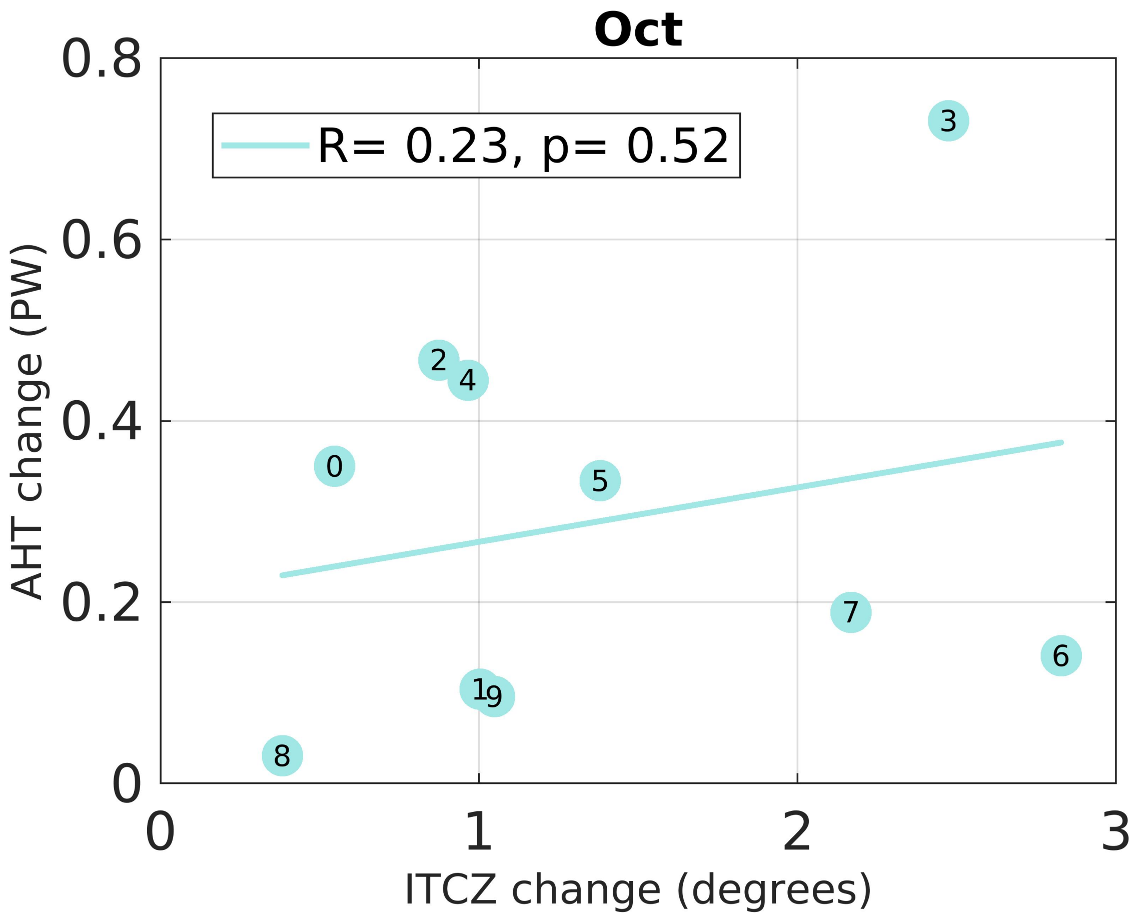

Figure B.6: As Fig. 4.8 but for October.

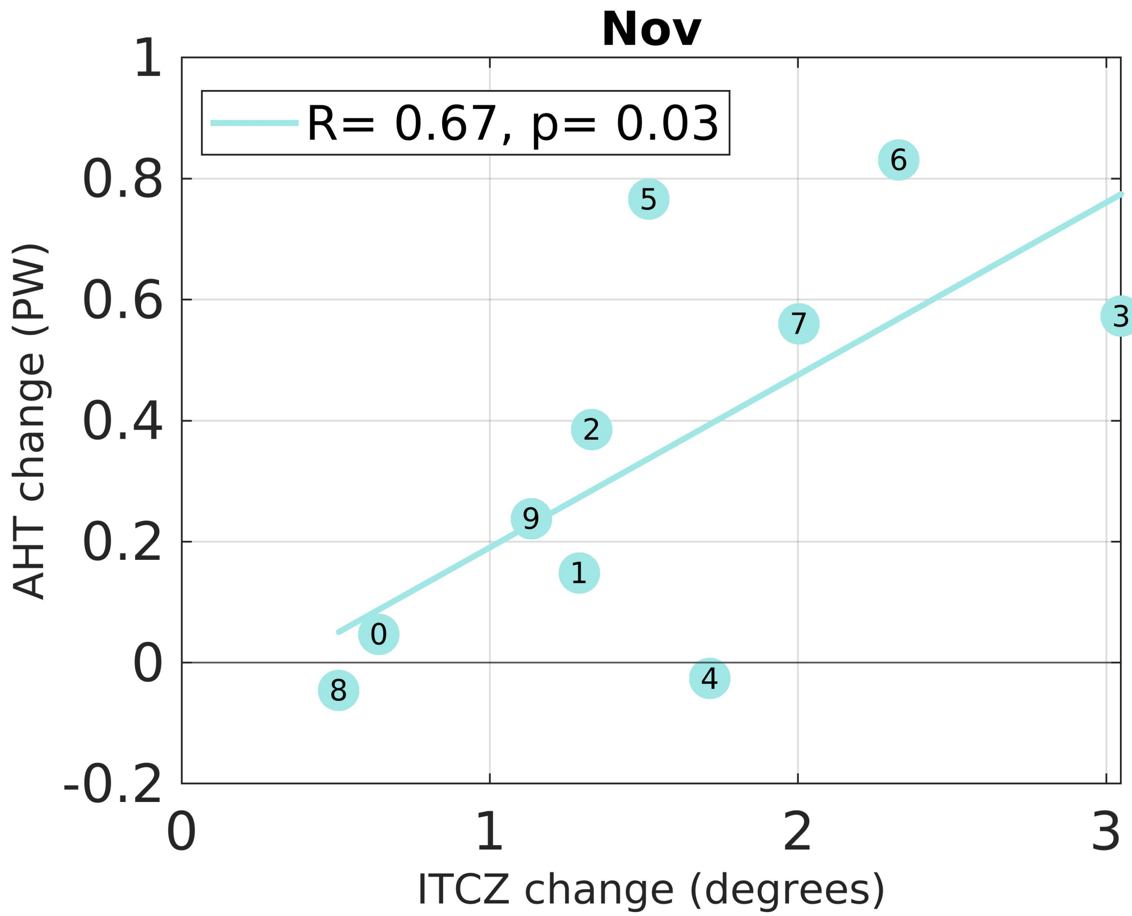

Figure B.7: As Fig. 4.8 but for November.

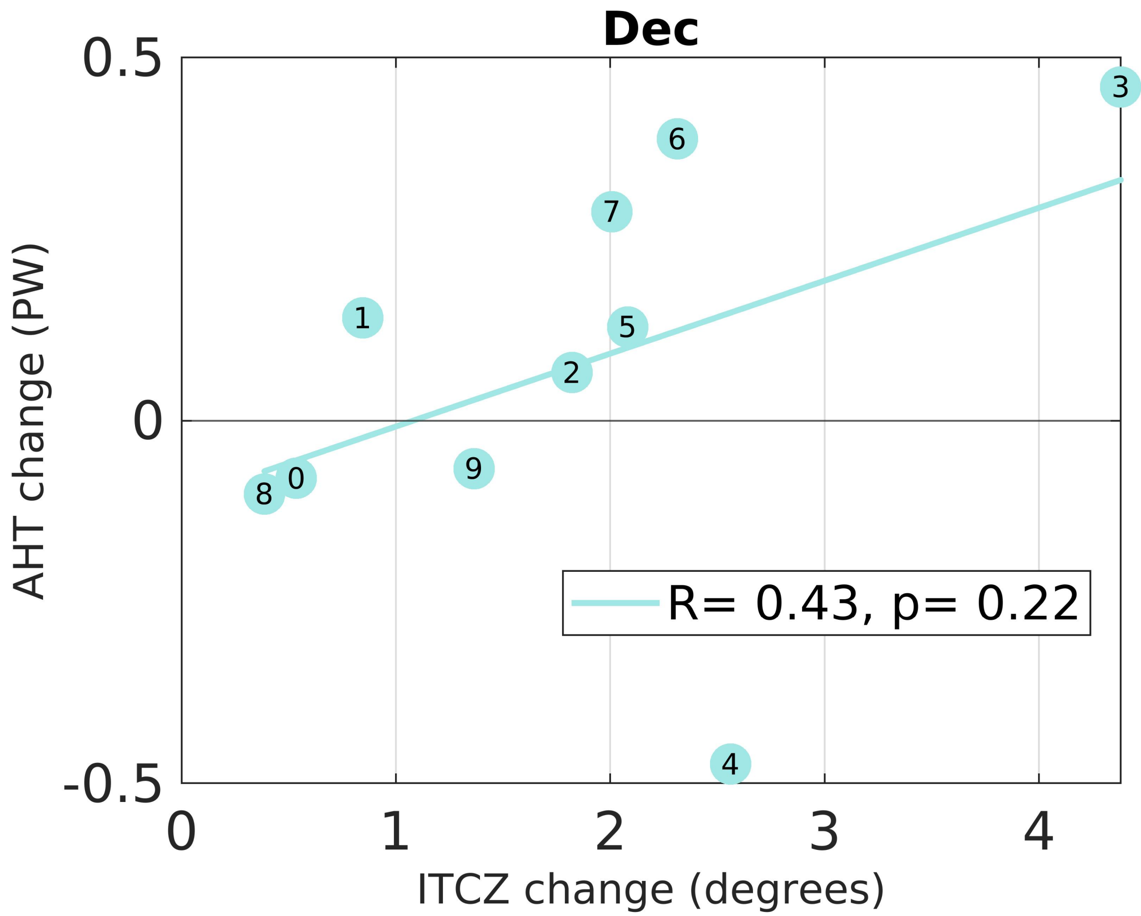

Figure B.8: As Fig. 4.8 but for December.

APPENDIX C: Seasonal relationship between ITCZ position and cross-equatorial AHT for each model

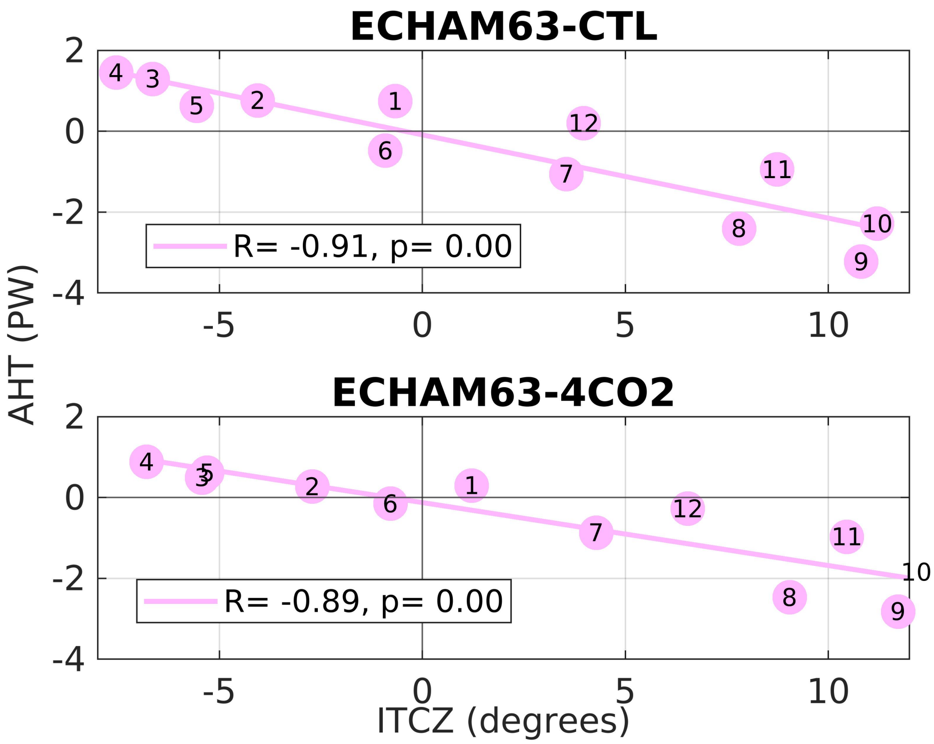

Figure C.1: As Fig. 4.13 but for ECHAM63.

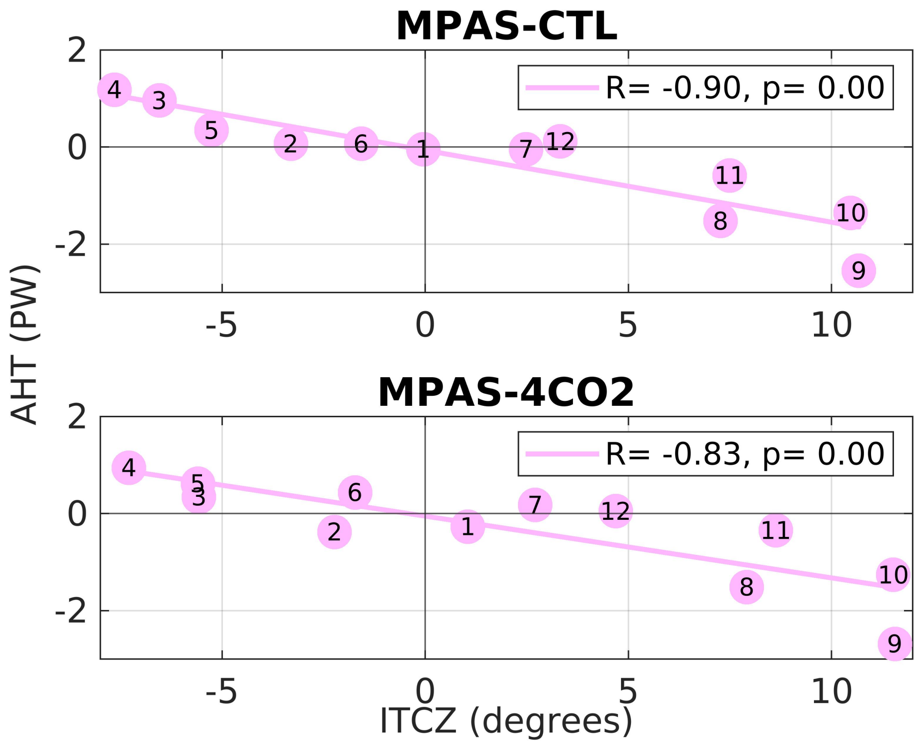

Figure C.2: As Fig. 4.13 but for MPAS.

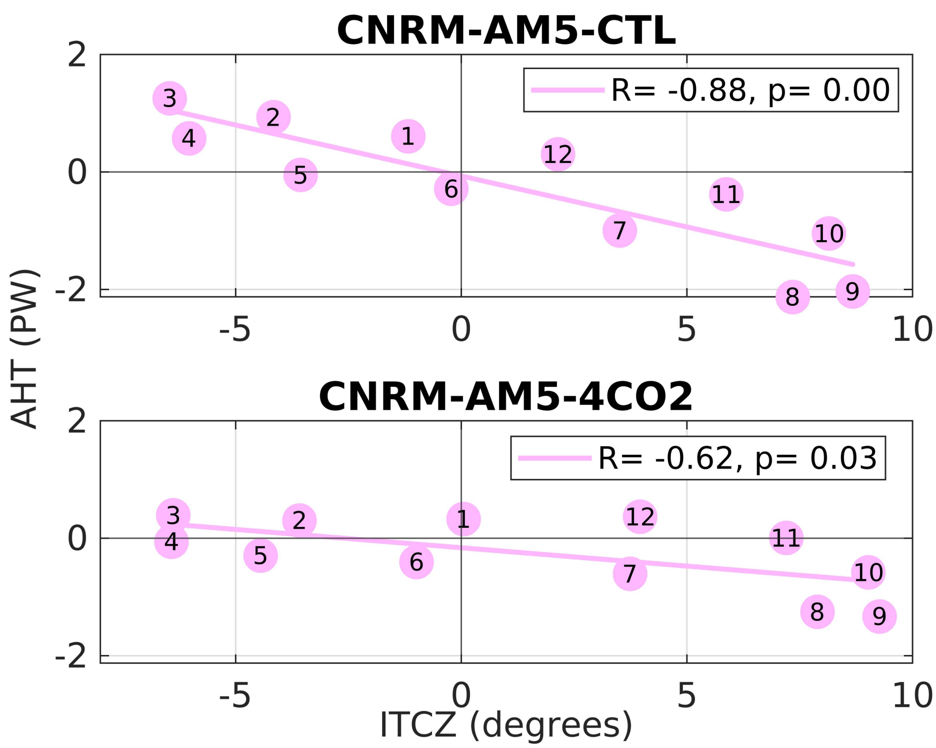

Figure C.3: As Fig. 4.13 but for CNRM_AM5.

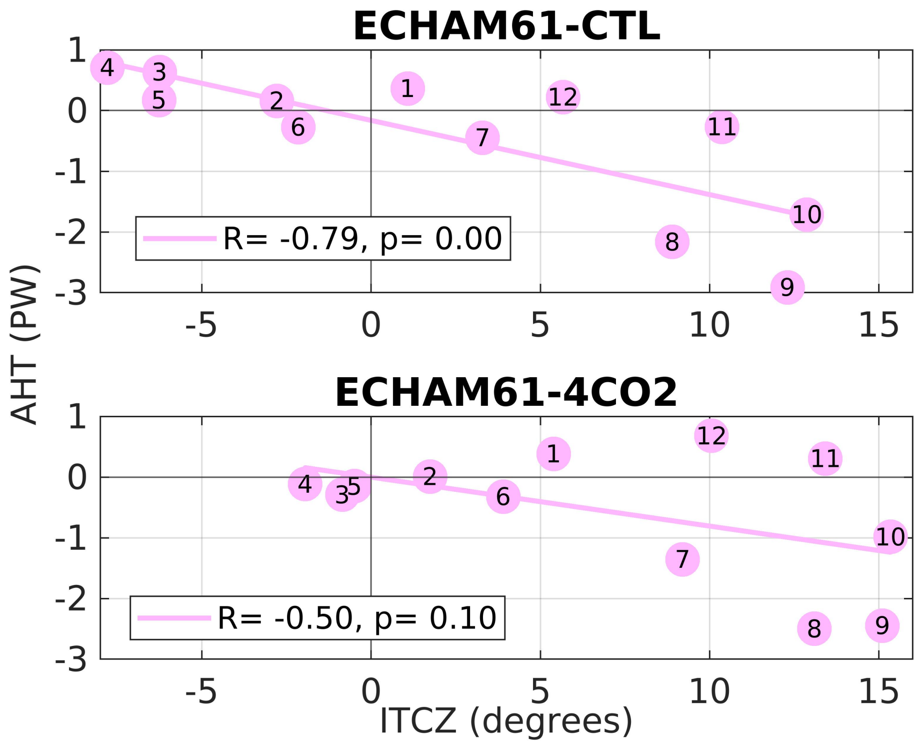

Figure C.4: As Fig. 4.13 but for ECHAM61.

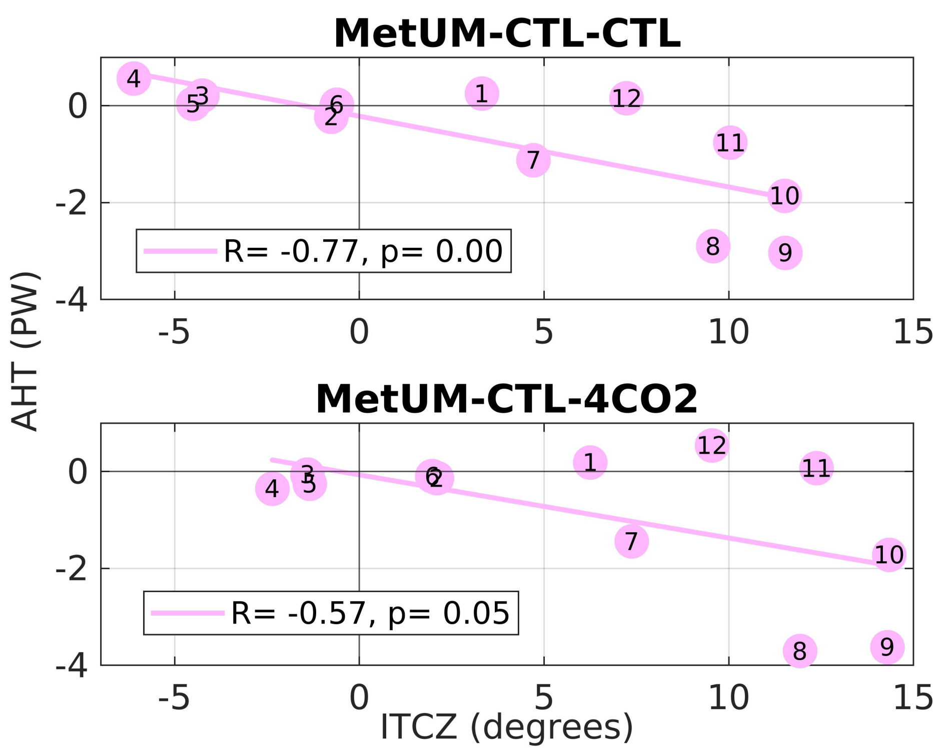

Figure C.5: As Fig. 4.13 but for MetUM_CTL.

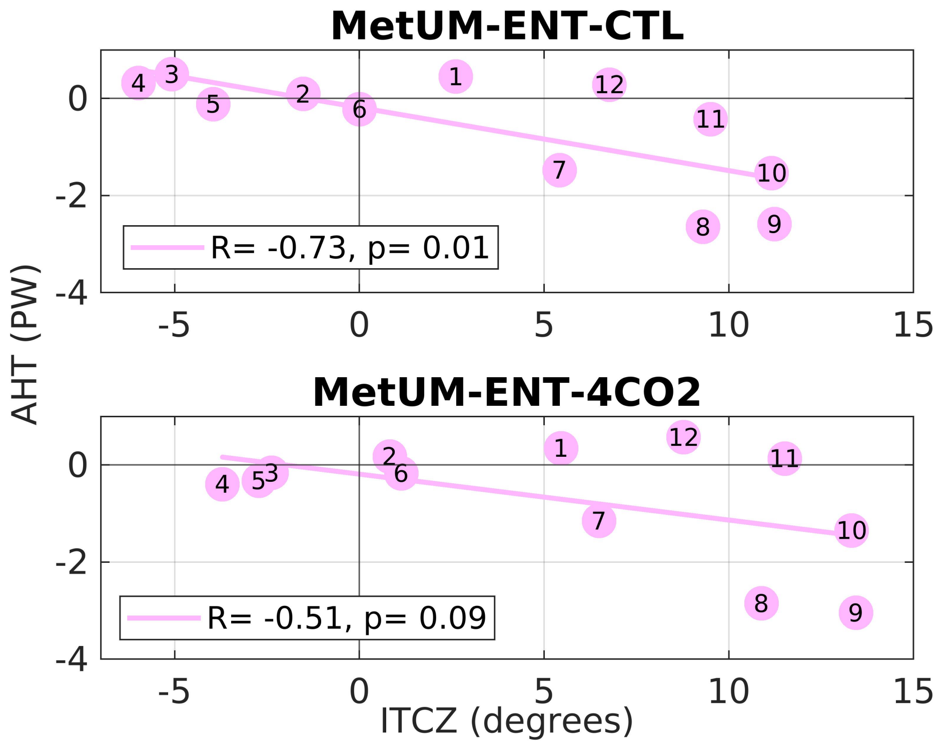

Figure C.6: As Fig. 4.13 but for MetUM_ENT.

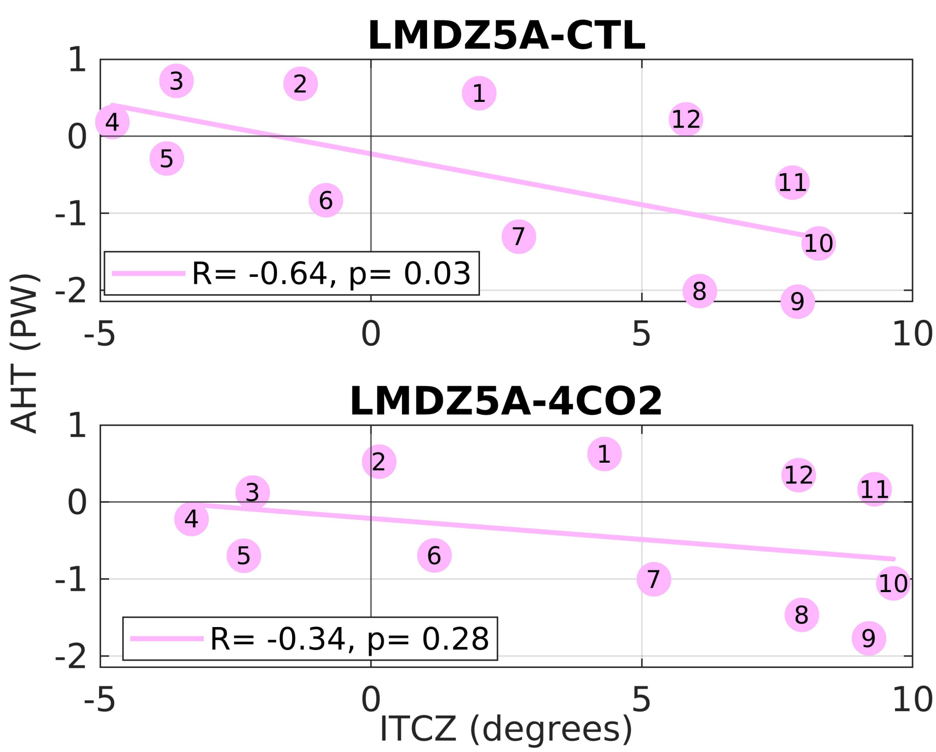

Figure C.7: As Fig. 4.13 but for LMDZ5A.

APPENDIX D: No robust ITCZ and total AHT changes relationship

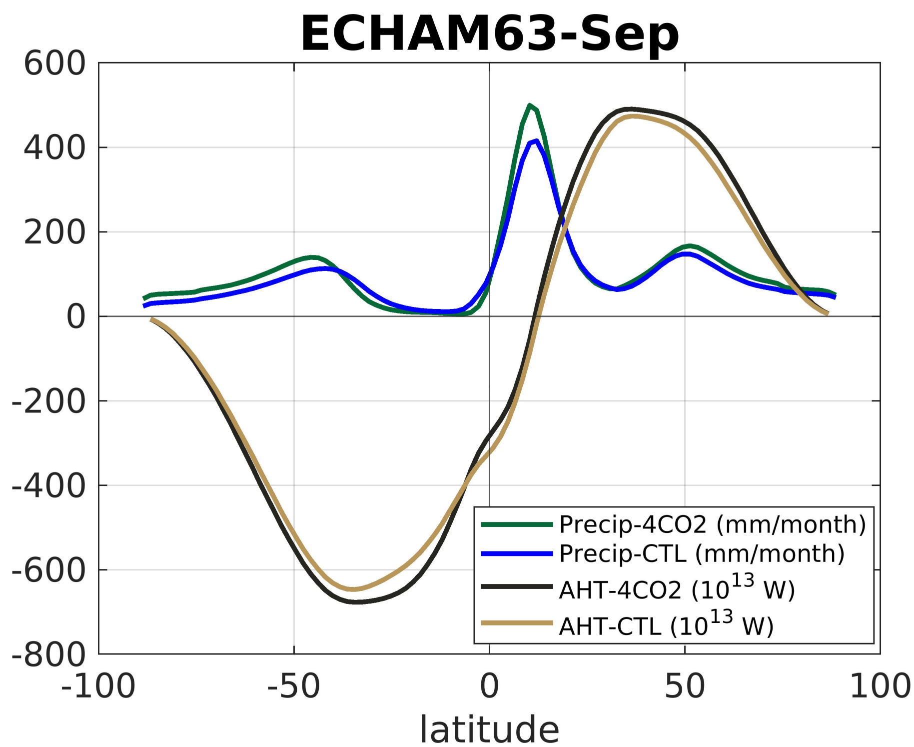

Figure D.1: As Fig. 4.16 but for ECHAM63.

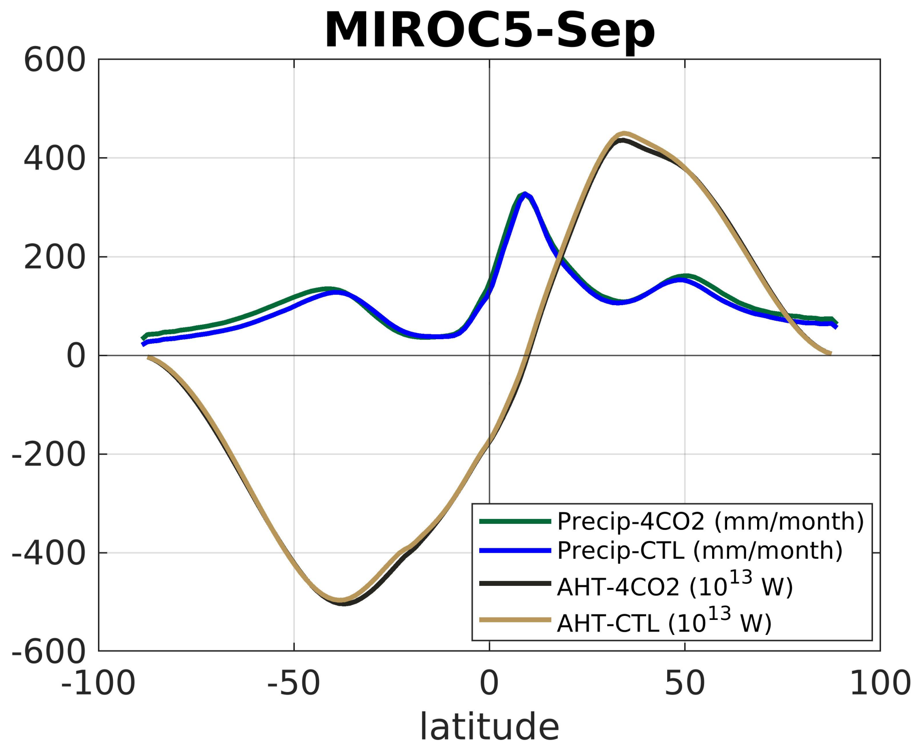

Figure D.2: As Fig. 4.16 but for MIROC5.

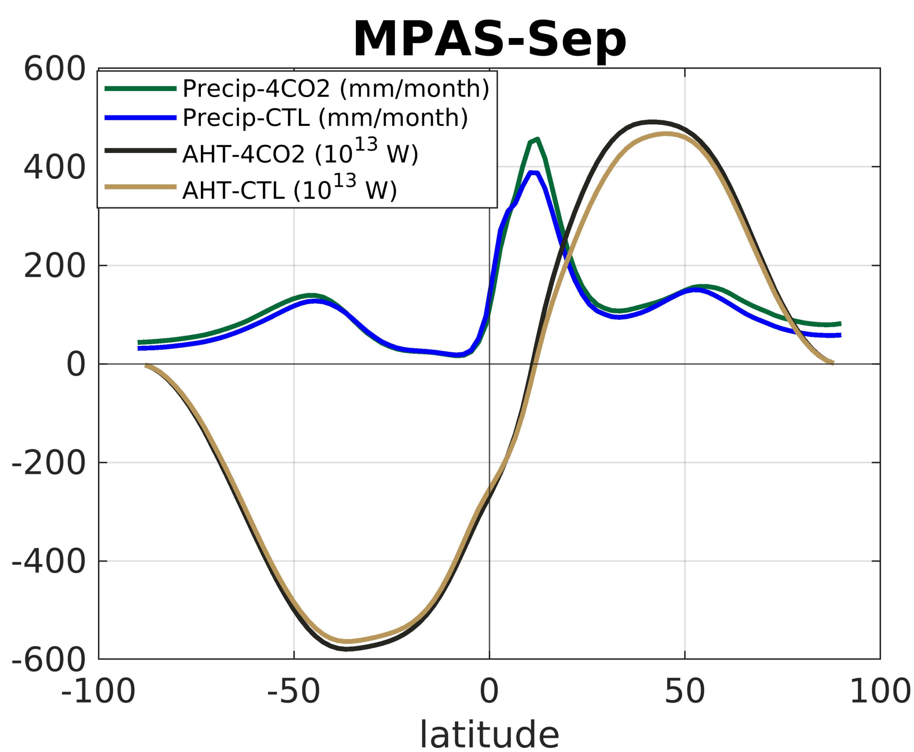

Figure D.3: As Fig. 4.16 but for MPAS.

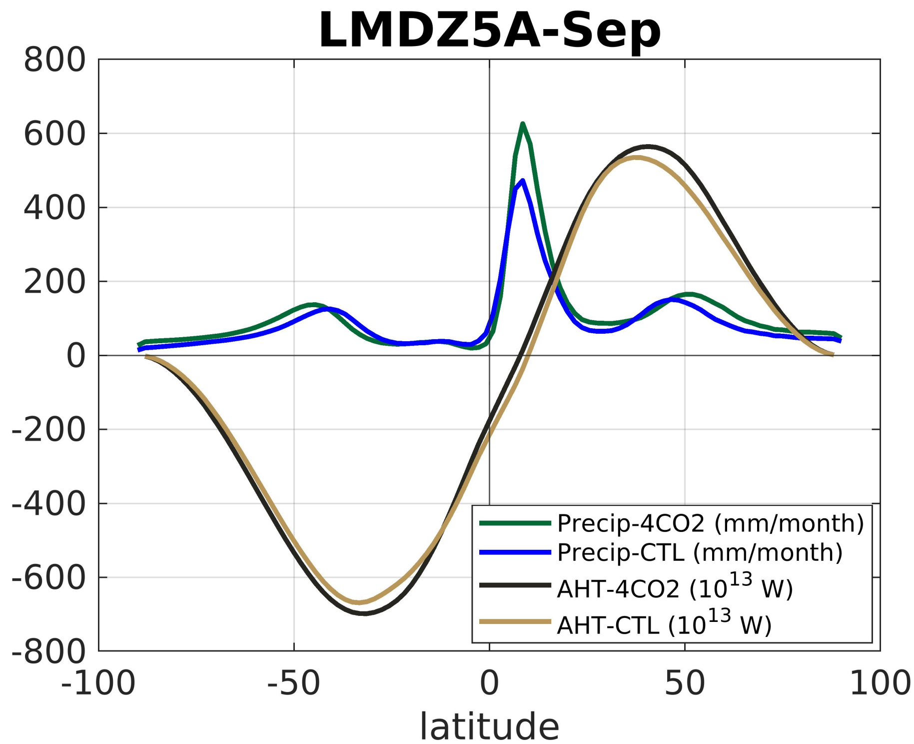

Figure D.4: As Fig. 4.16 but for LMDZ5A.

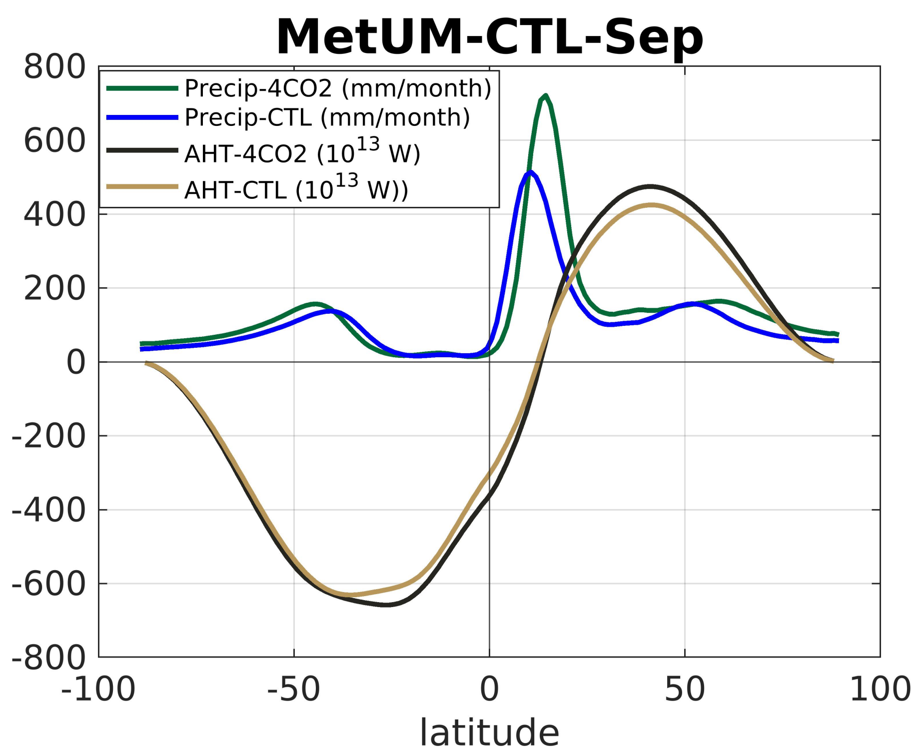

Figure D.5: As Fig. 4.16 but for MetUM_CTL.

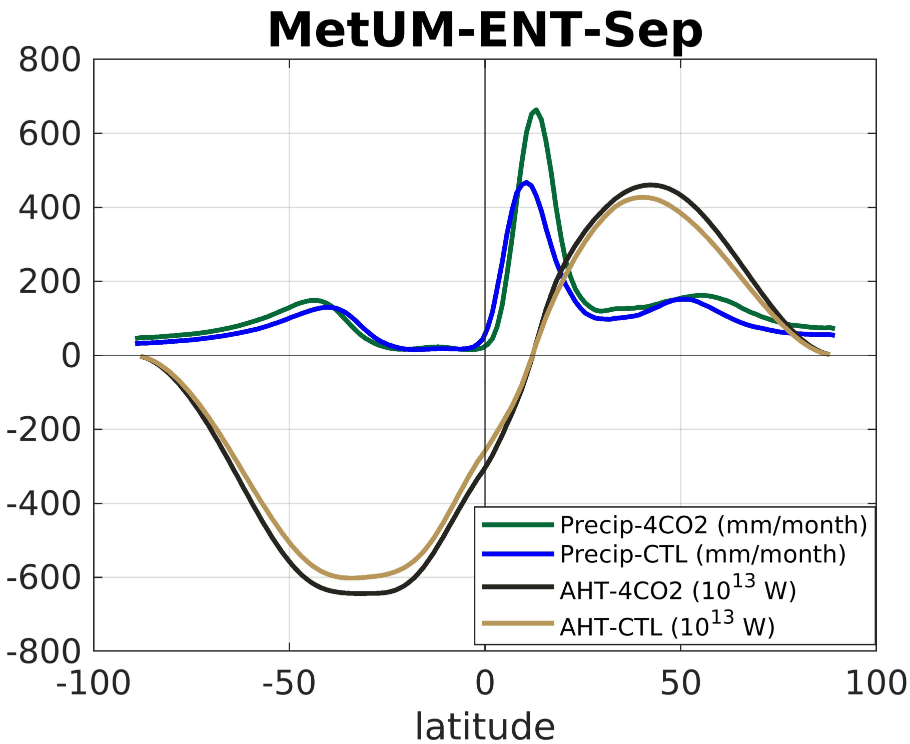

Figure D.6: As Fig. 4.16 but for MetUM_ENT.

APPENDIX E: September factors' curves

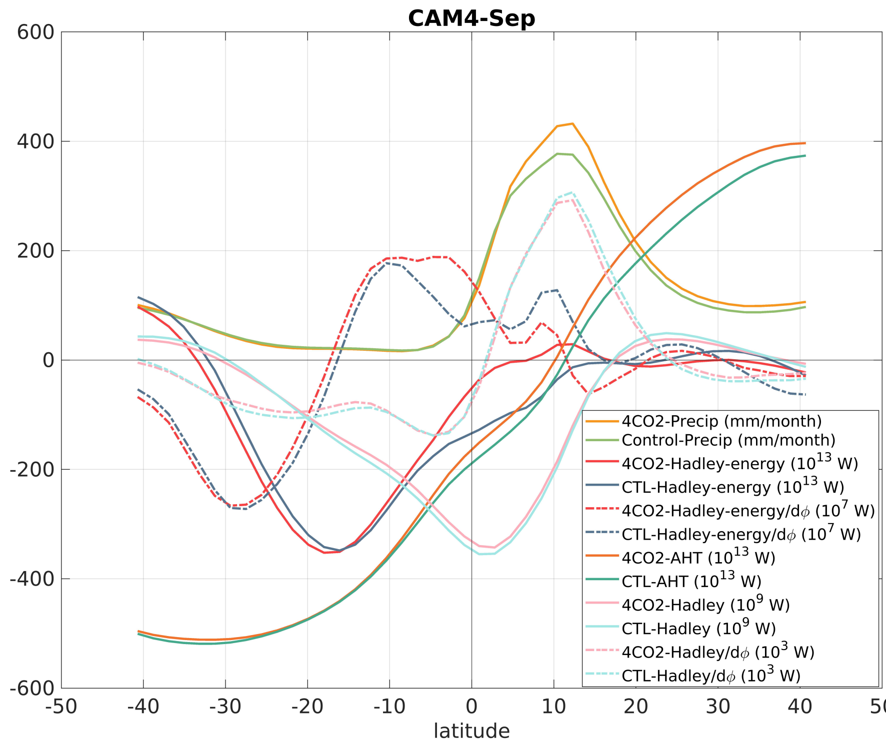

Figure E.1: As Fig. 4.21 but for CAM4.

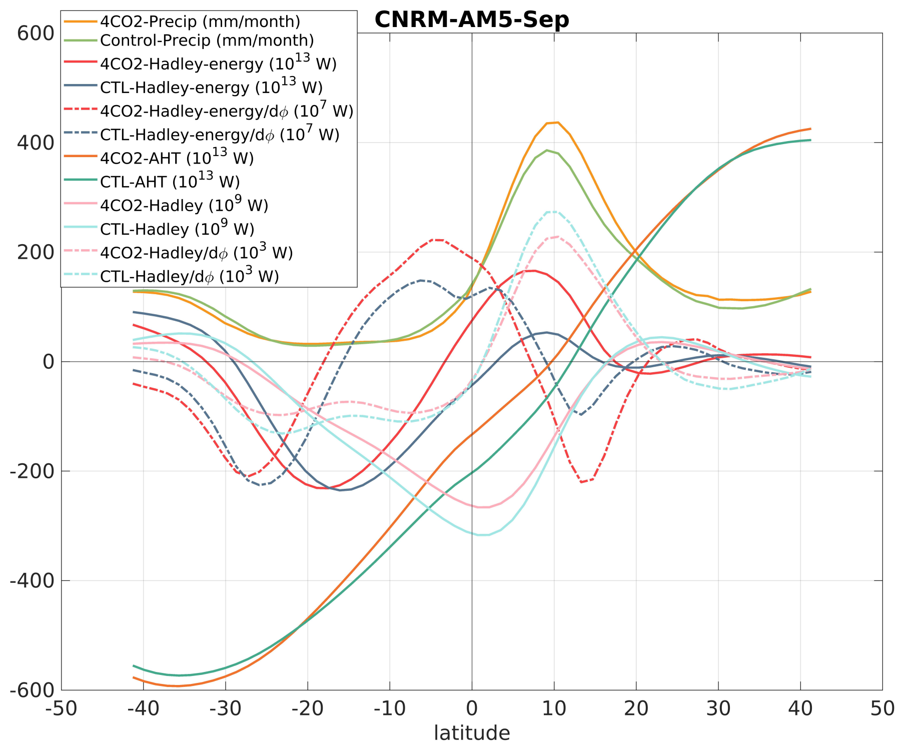

Figure E.2: As Fig. 4.21 but for CNRM_AM5.

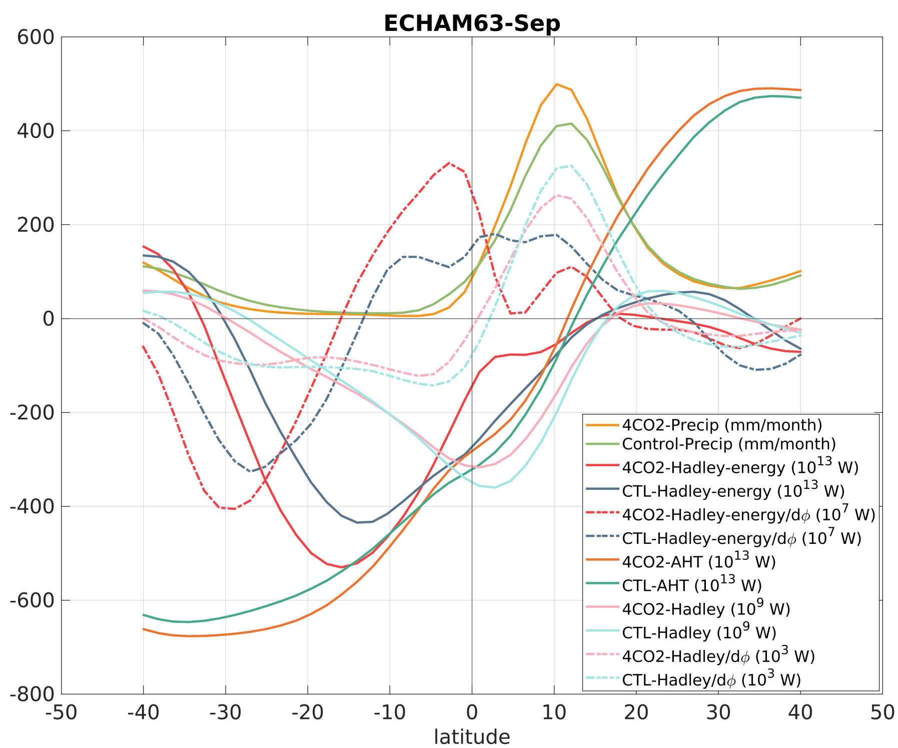

Figure E.3: As Fig. 4.21 but for ECHAM61.

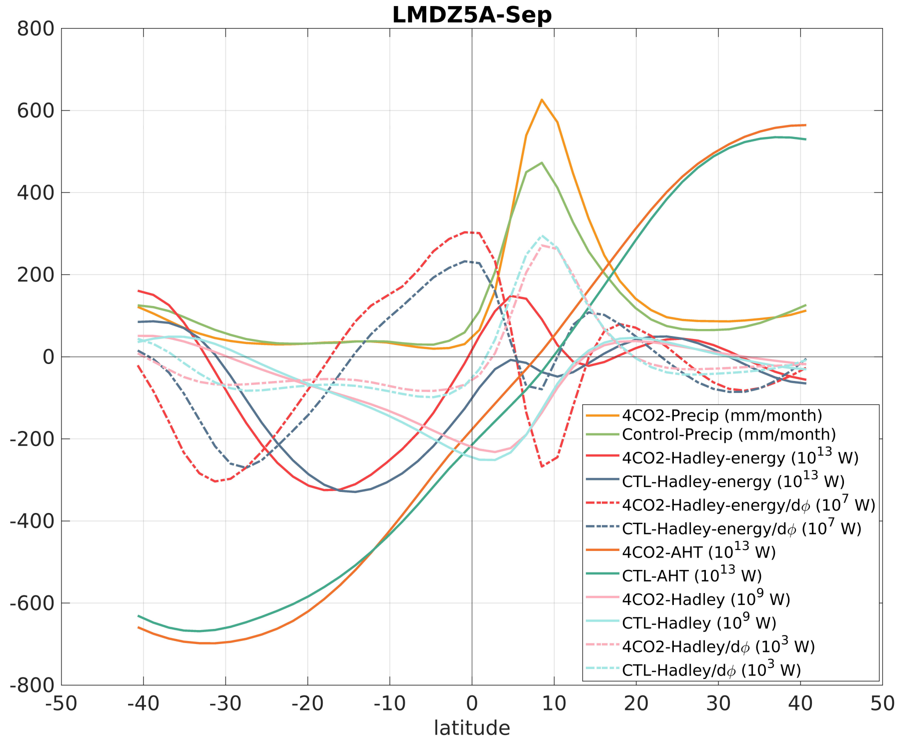

Figure E.4: As Fig. 4.21 but for LMDZ5A.

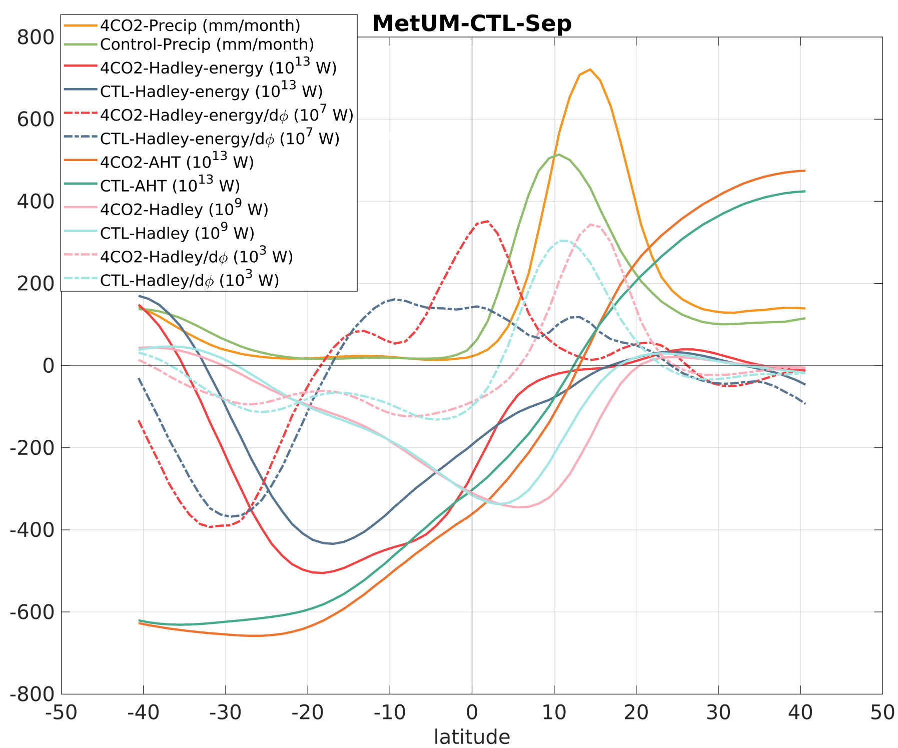

Figure E.5: As Fig. 4.21 but for MetUM_CTL.

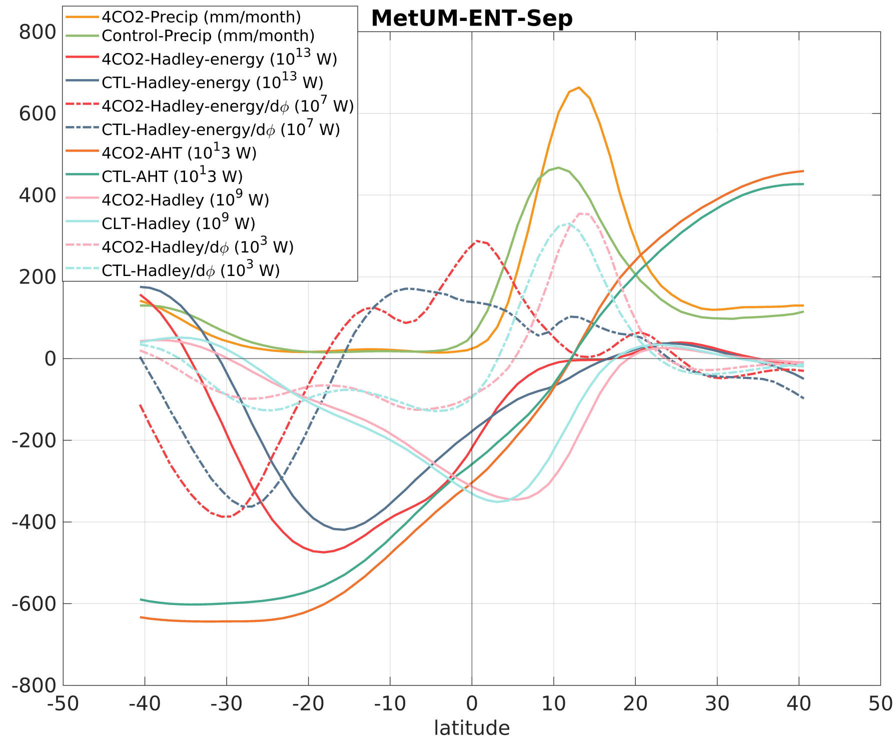

Figure E.6: As Fig. 4.21 but for MetUM_ENT.

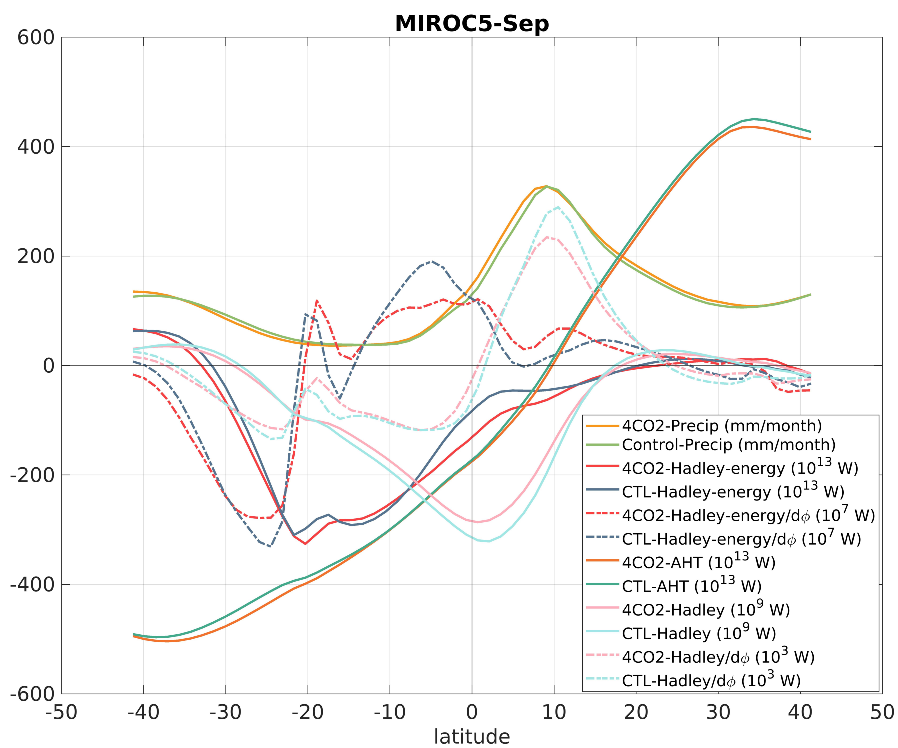

Figure E.7: As Fig. 4.21 but for MIROC5.

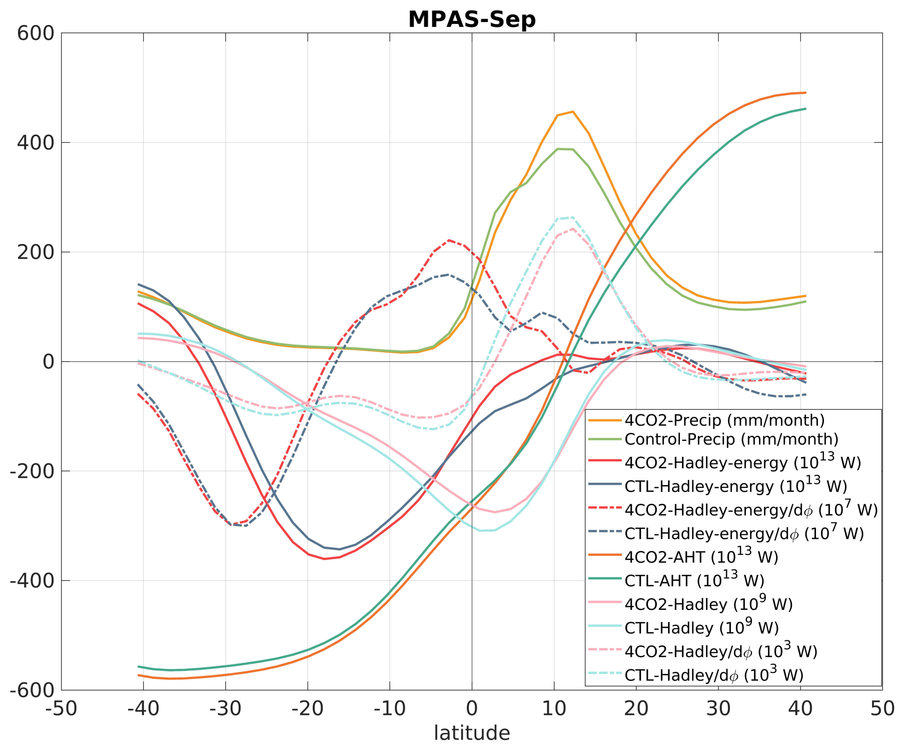

Figure E.8: As Fig. 4.21 but for MPAS.

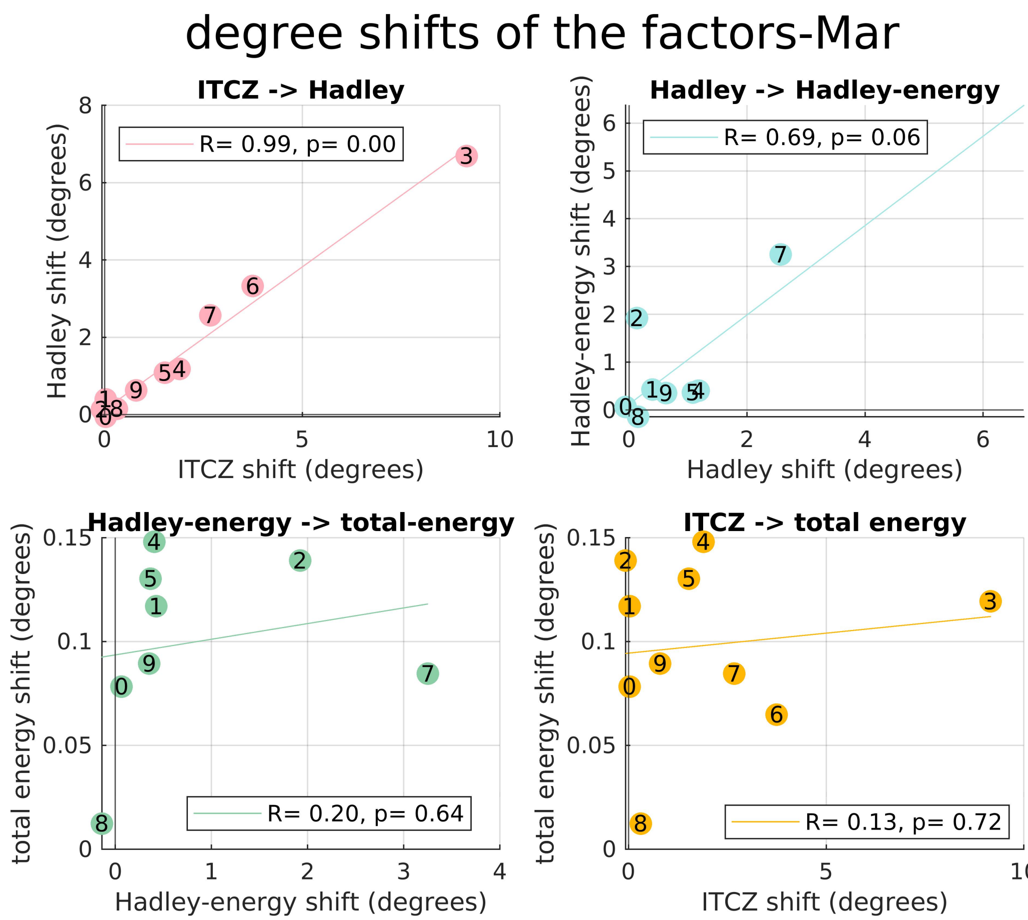

Figure F.1: March inner links simulated by the models.

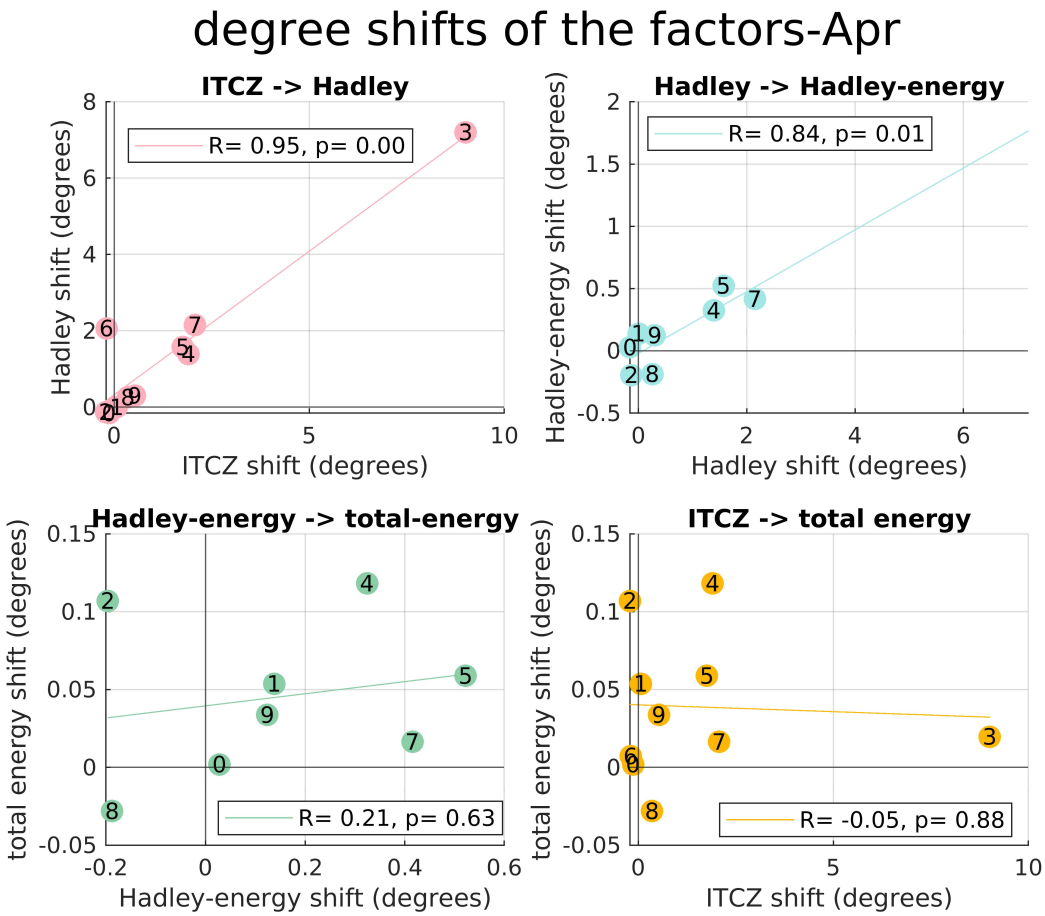

Figure F.2: April inner links simulated by the models.

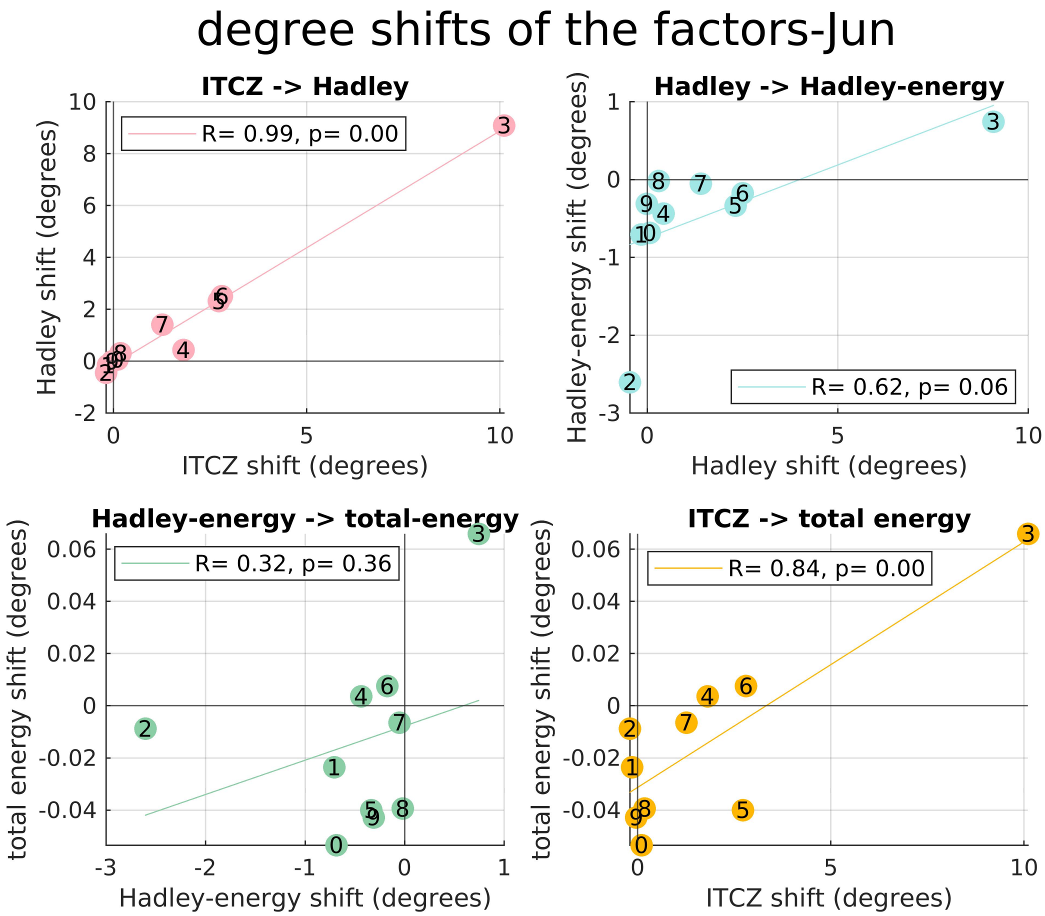

Figure F.3: June inner links simulated by the models.

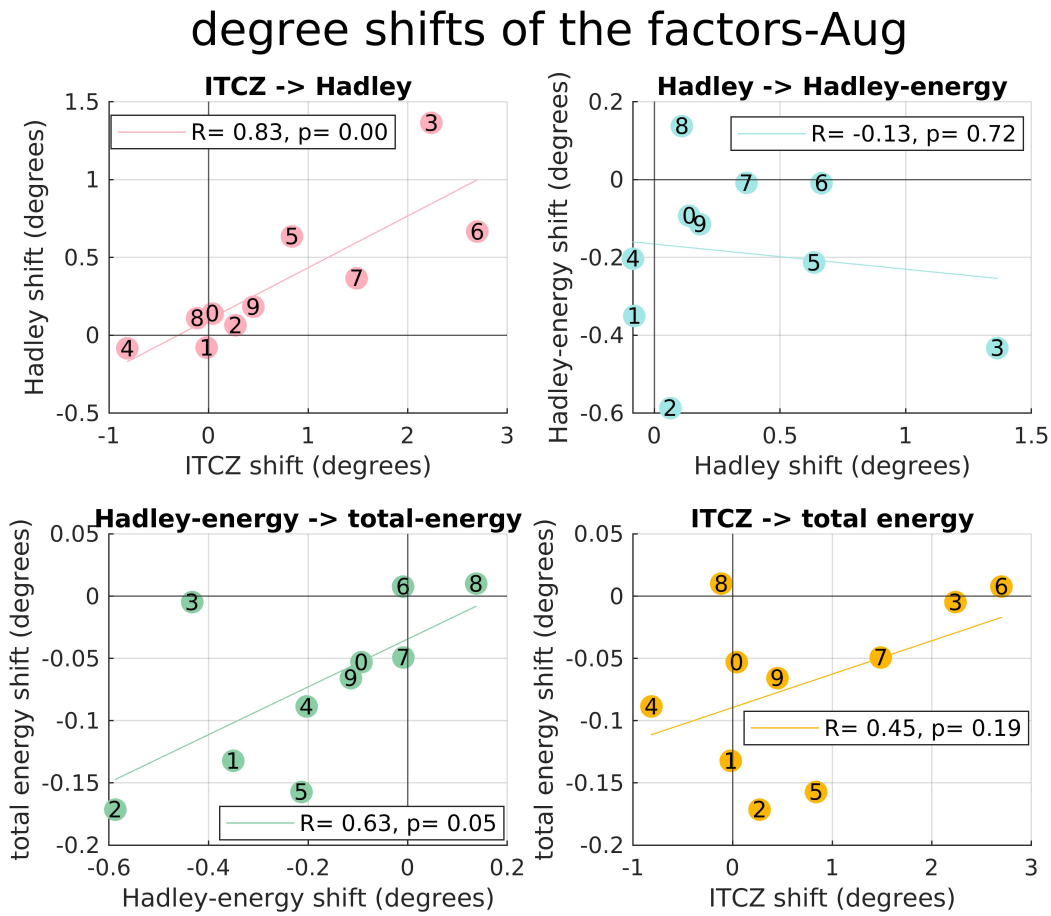

Figure F.4: August inner links simulated by the models.

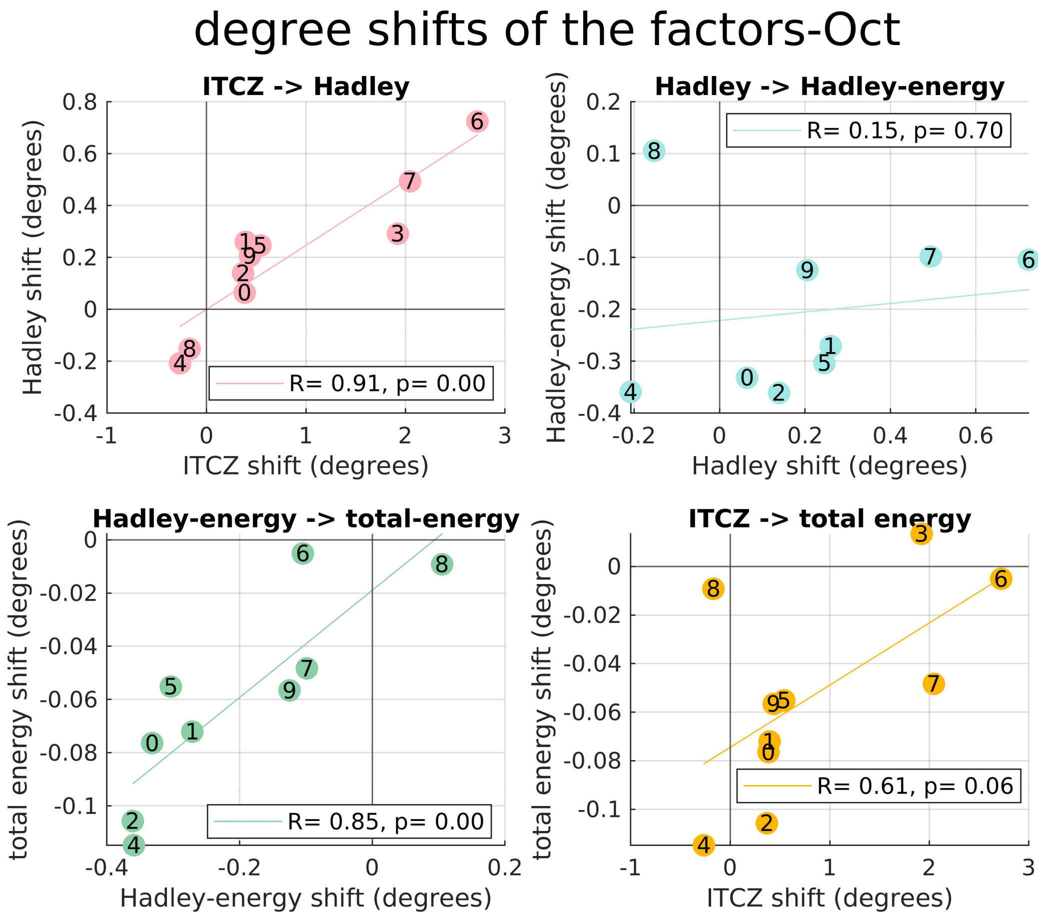

Figure F.5: October inner links simulated by the models.

APPENDIX G: Inner links between d/dϕ quantities

The inner links between d/dϕ quantities showed a similar pattern, with well correlated ITCZ and $d\Psi_{M,Hadley}/d\phi$ and a decreased $d\Psi_{M,Hadley}/d\phi$ and $dAHT_{Hadley}/d\phi$ relationship from the Northern Hemisphere tropical dry season to the wet season (Fig. G.1). The $dAHT_{Hadley}/d\phi$ to $dAHT_{Hadley}/d\phi$ link behaves differently from the AHT$_{Hadley}$ and AHT$_{total}$ link. The $dAHT_{Hadley}/d\phi$ to $dAHT_{total}/d\phi$ link suggests that except for the first three months (January, February, and March), the correlation coefficients are relatively low. In other words, the second set of link may indicate that the link between $dAHT_{Hadley}/d\phi$ to $dAHT_{total}/d\phi$ broke the most for many of the months. This link breakdown means that the rate of Hadley transported energy changes along latitudes acts differently from the rate of AHT$_{total}$ changes along latitudes. The p value corresponding to the r value heatmap can be found in Fig. G.2. The scatter plots are as follows.

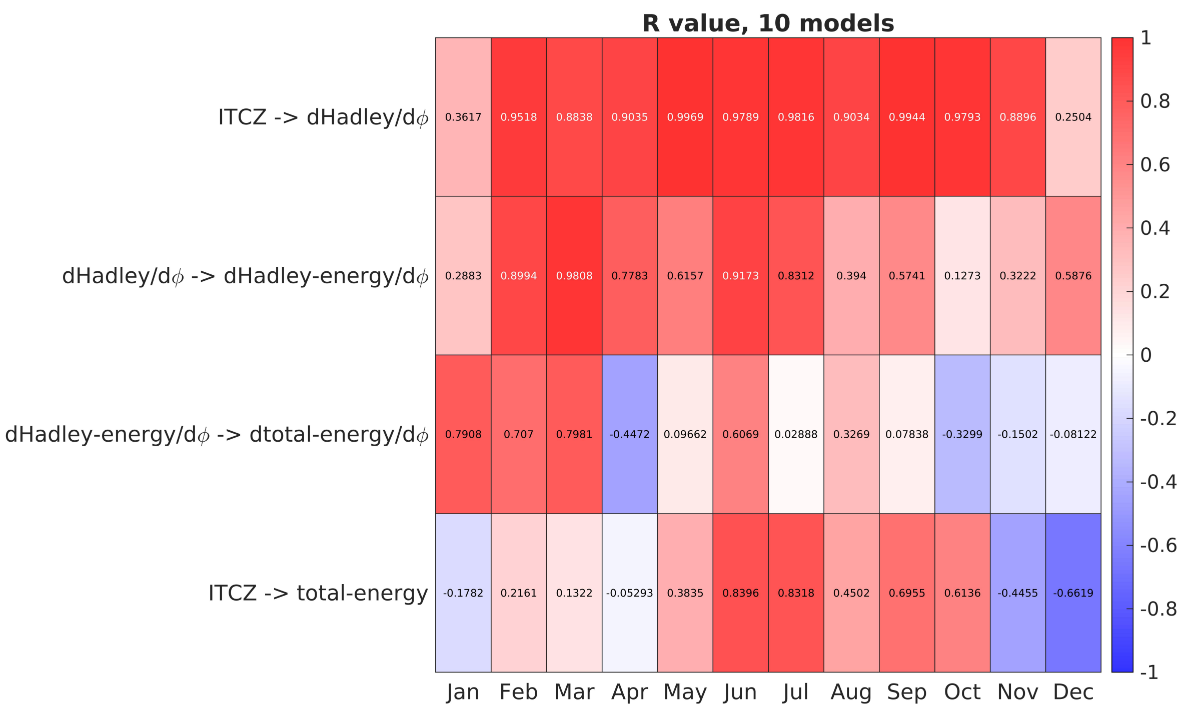

Figure G.1: Heatmap of the d/dϕ inner links' correlation coefficient at each month.

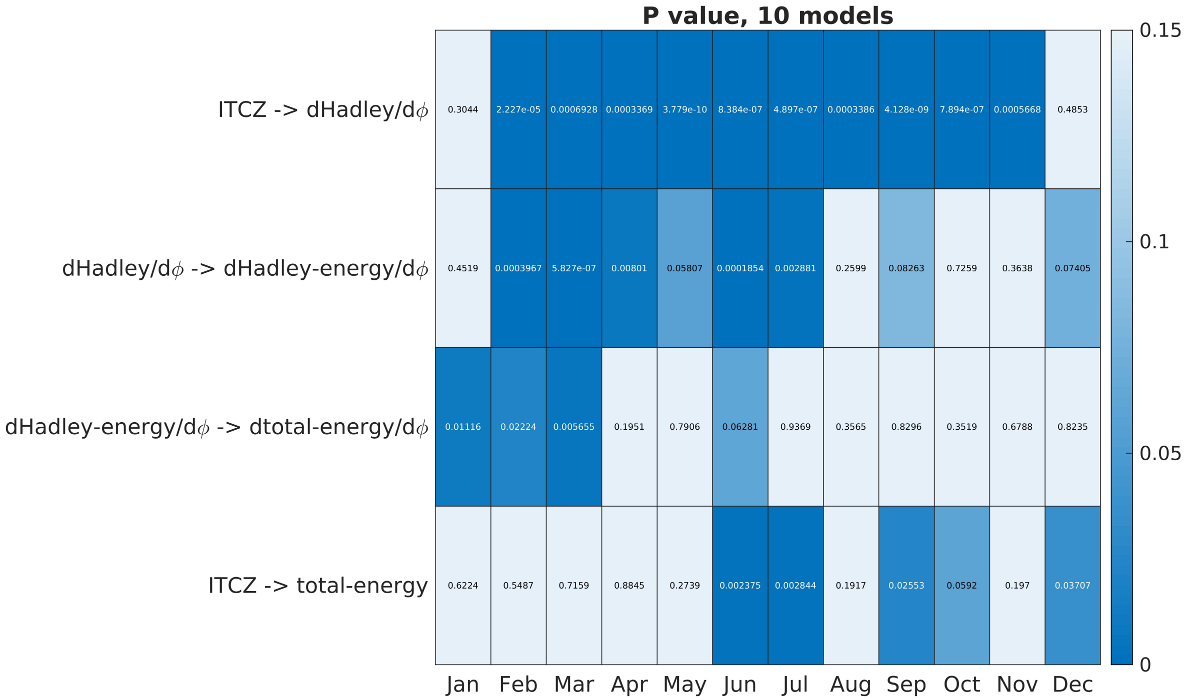

Figure G.2: Heatmap of the inner links' p values corresponding with the correlation coefficient at each month.

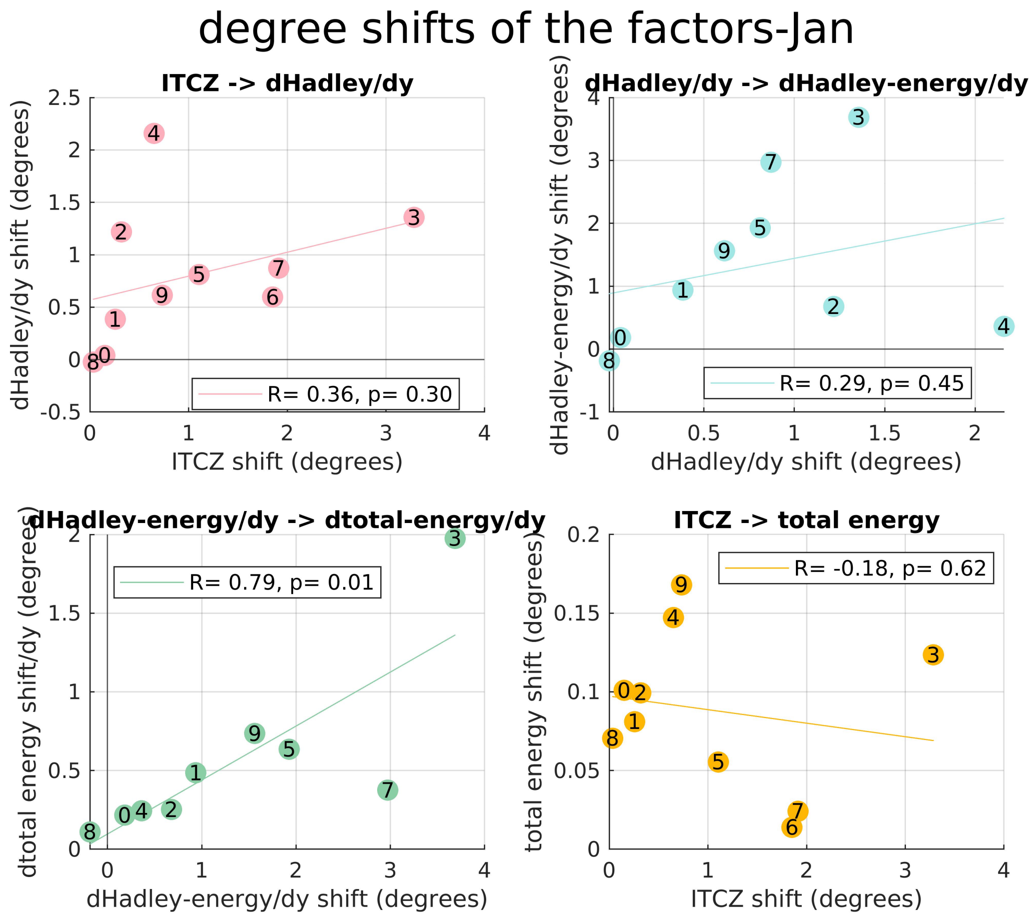

Figure G.3: January inner links (dϕ terms) simulated by the models.

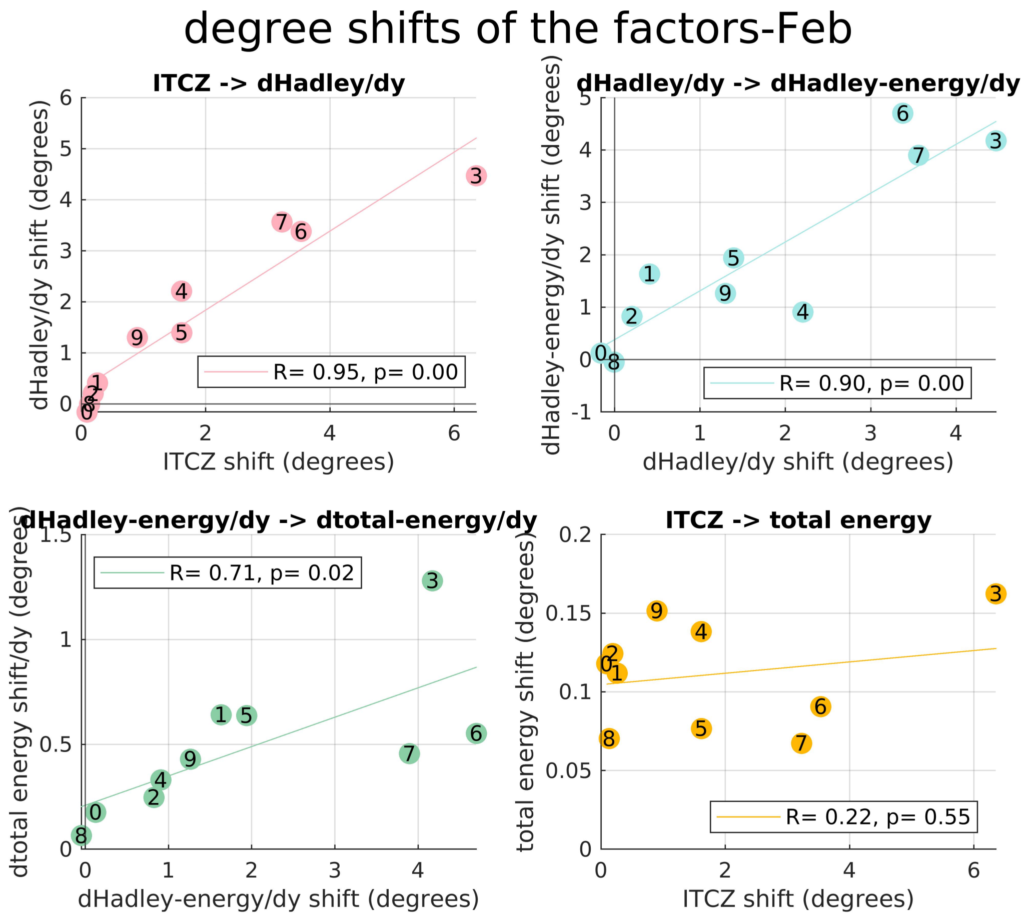

Figure G.4: February inner links (dϕ terms) simulated by the models.

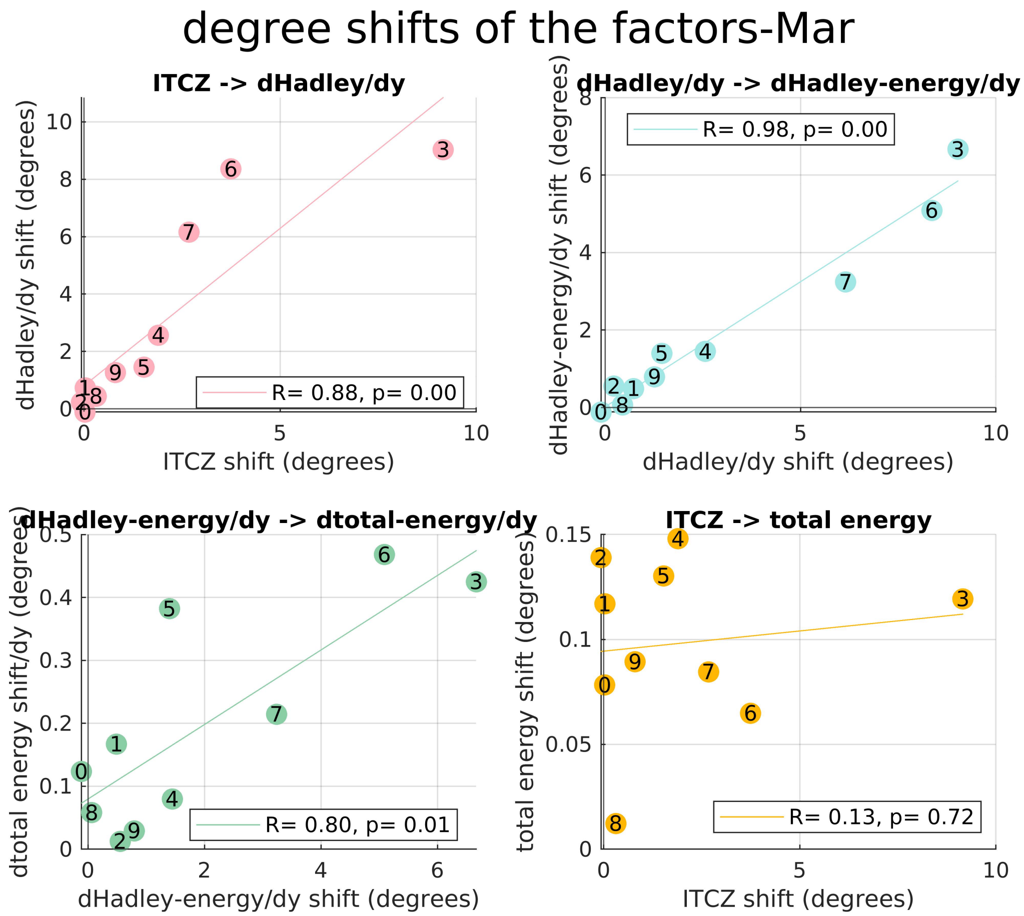

Figure G.5: March inner links (dϕ terms) simulated by the models.

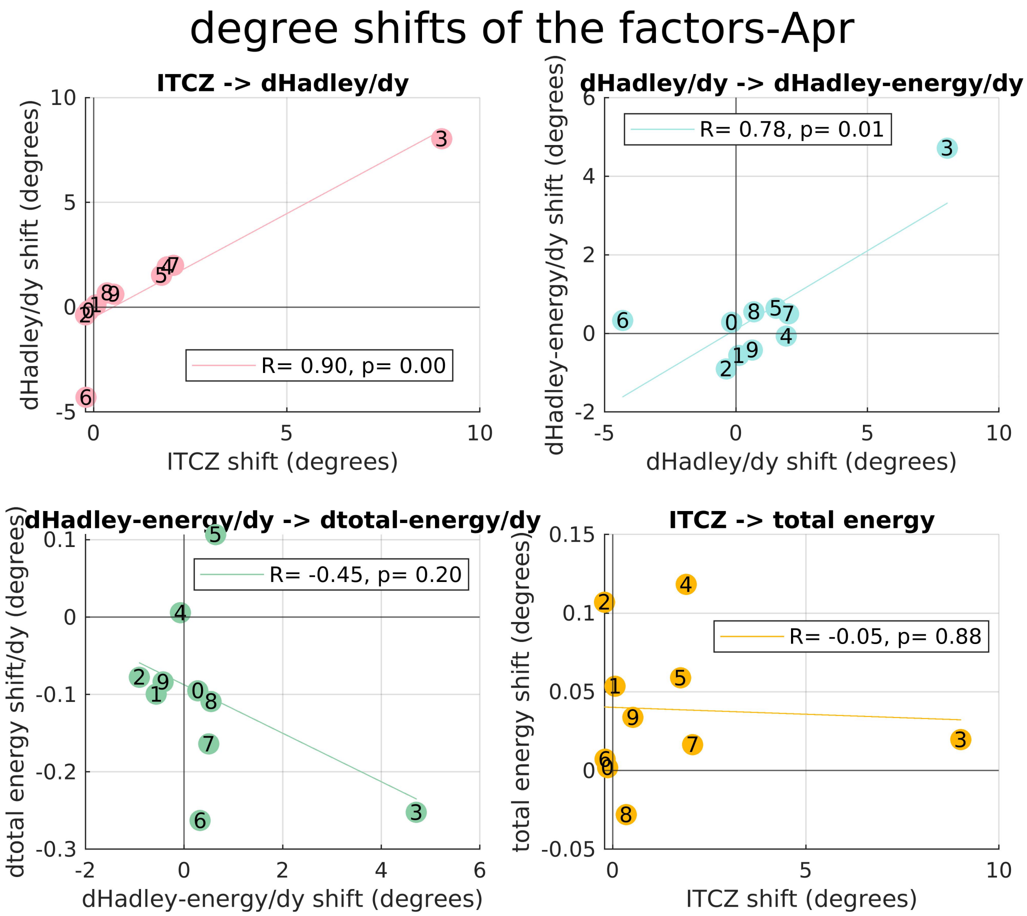

Figure G.6: April inner links (dϕ terms) simulated by the models.

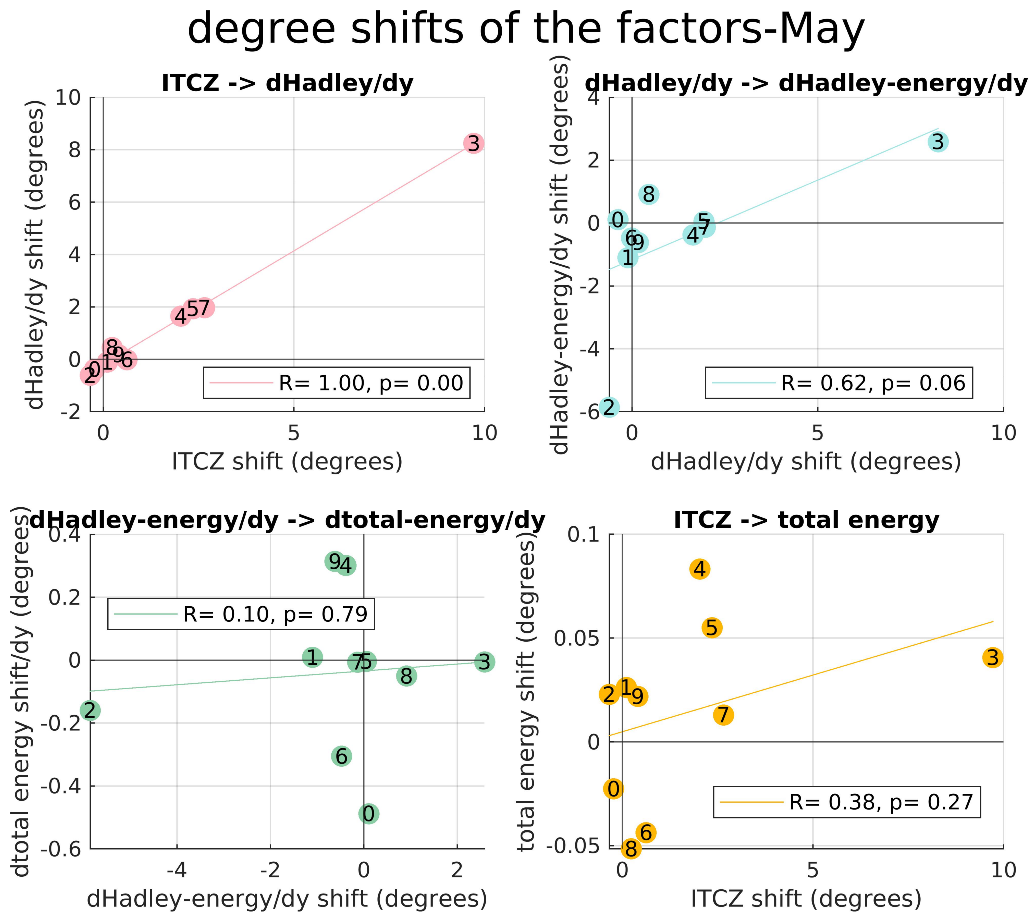

Figure G.7: May inner links ($d\phi$ terms) simulated by the models.

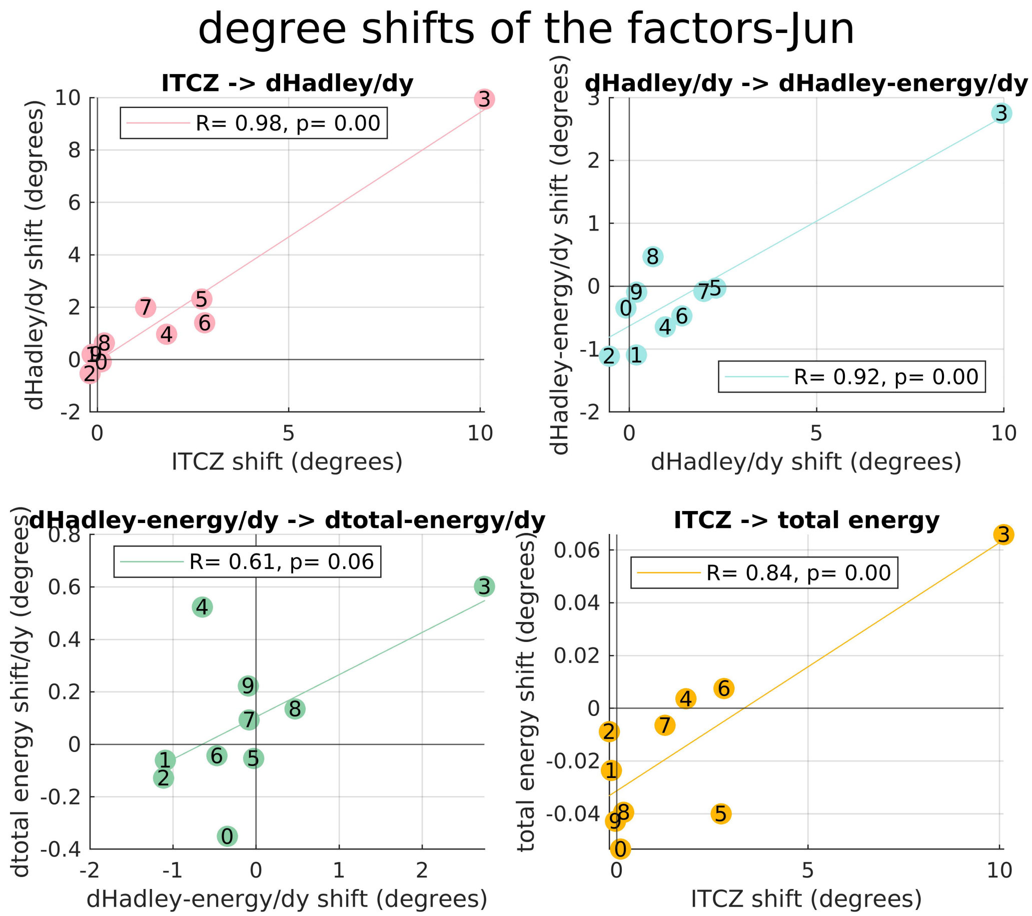

Figure G.8: June inner links (dϕ terms) simulated by the models.

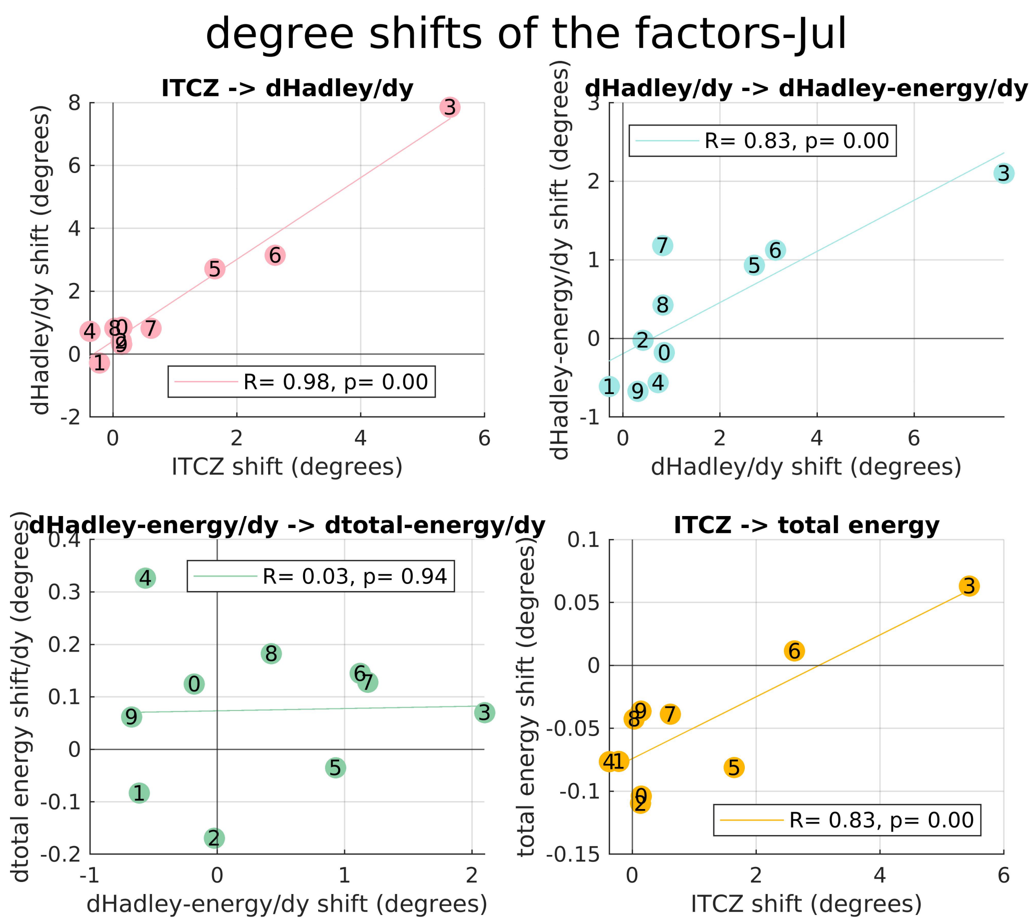

Figure G.9: July inner links (dϕ terms) simulated by the models.

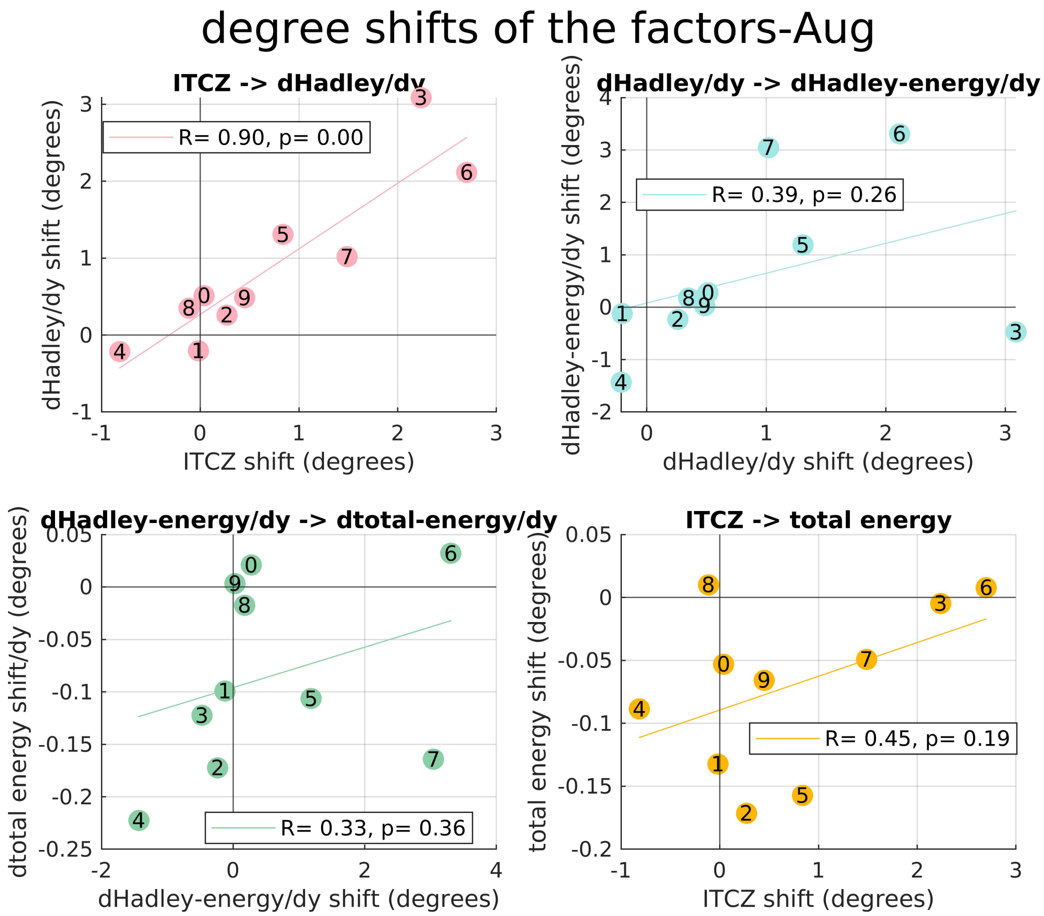

Figure G.10: August inner links (dϕ terms) simulated by the models.

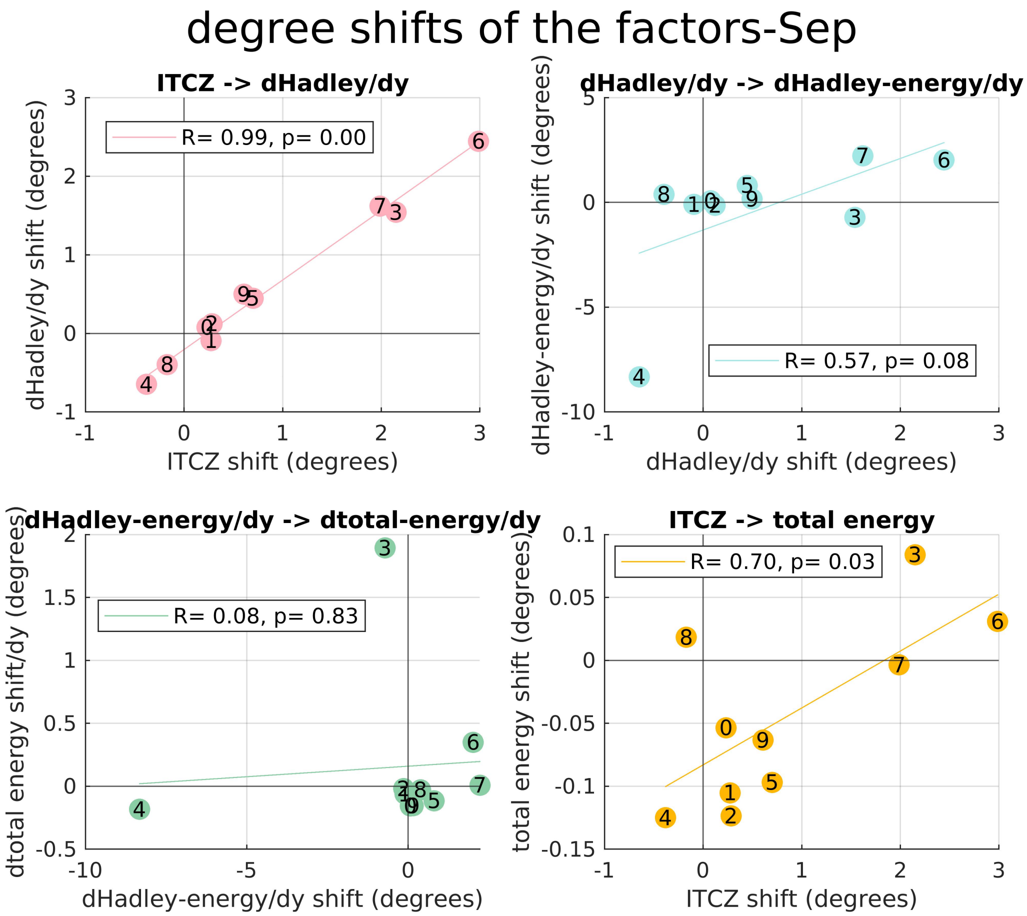

Figure G.11: September inner links (dϕ terms) simulated by the models.

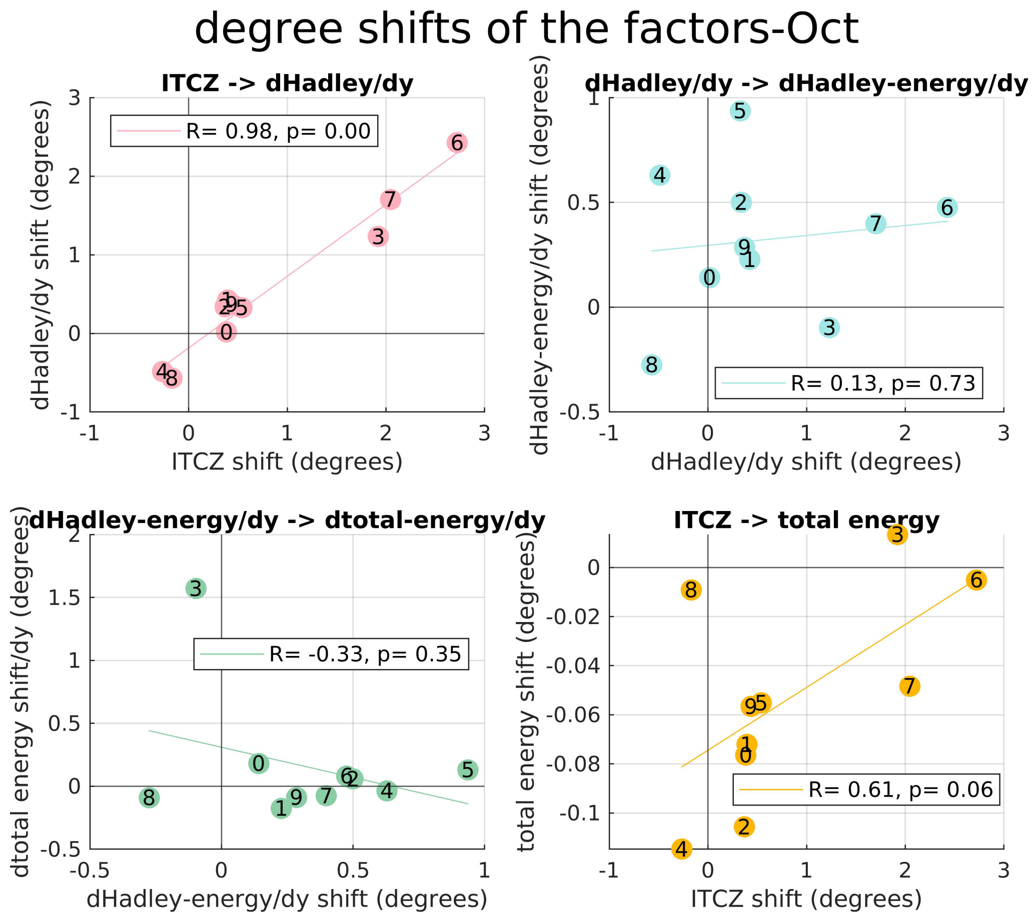

Figure G.12: October inner links ($d\phi$ terms) simulated by the models.

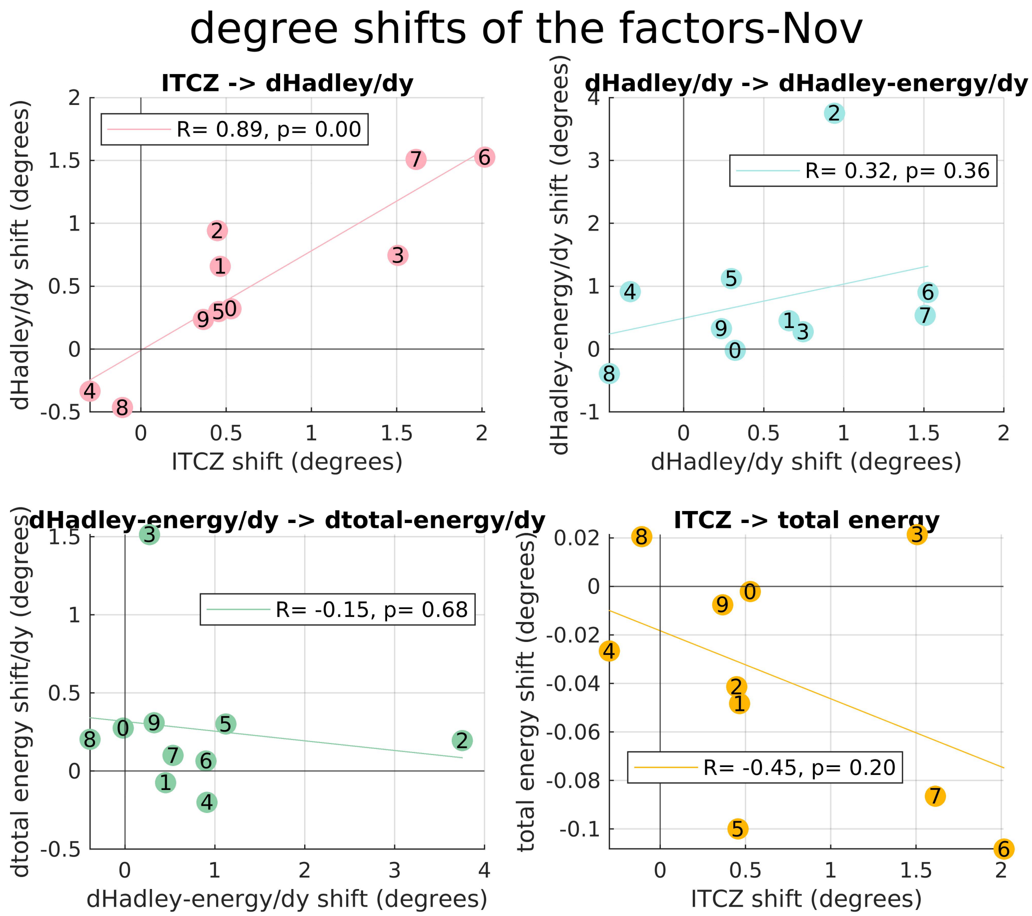

Figure G.13: November inner links (dϕ terms) simulated by the models.

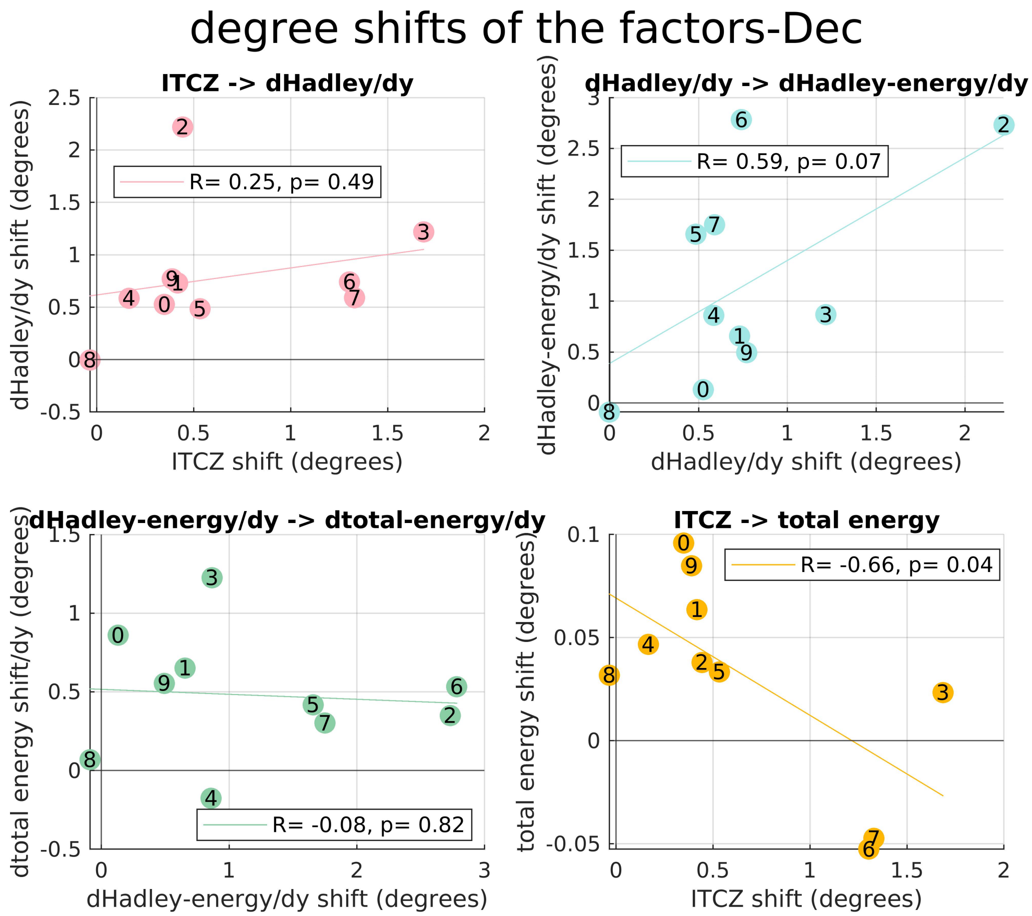

Figure G.14: December inner links (dϕ terms) simulated by the models.

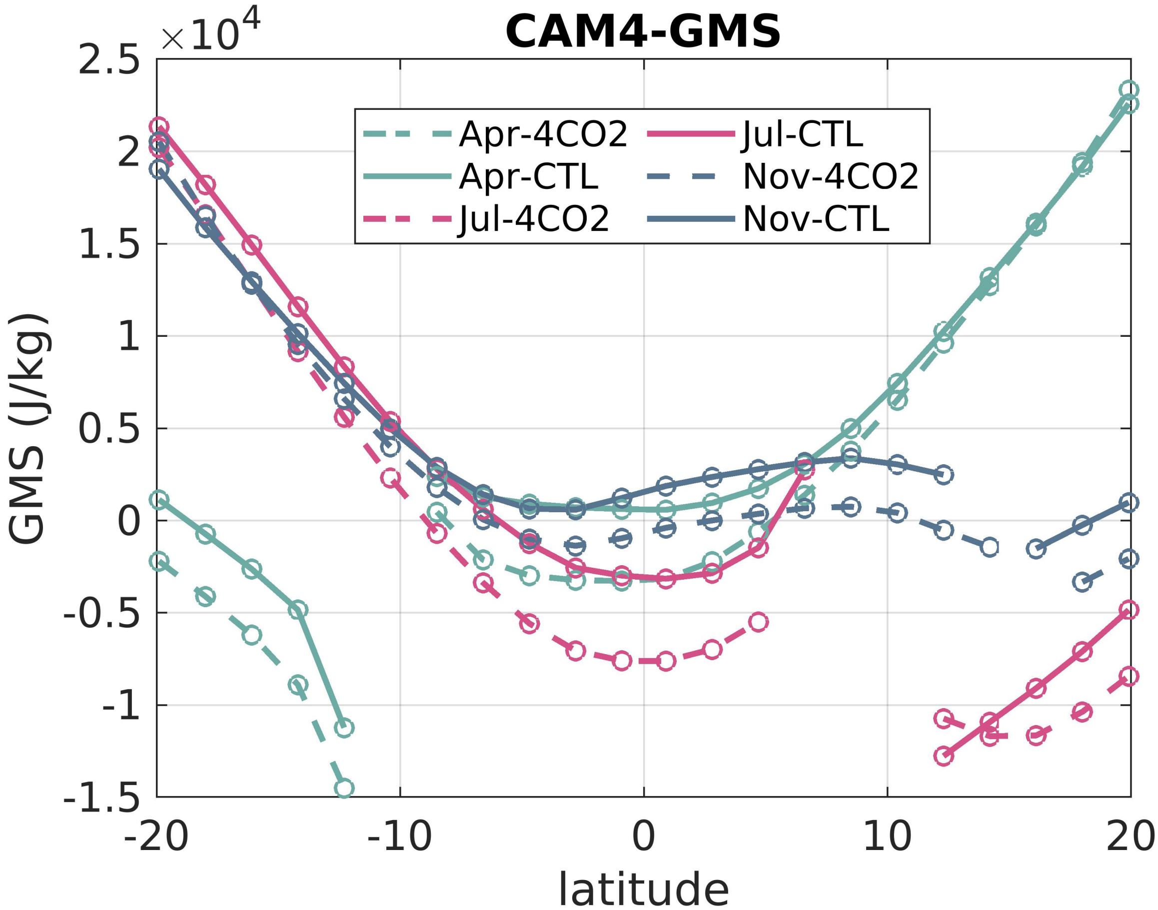

Figure H.1: CAM4 simulated GMS in April, July and November.

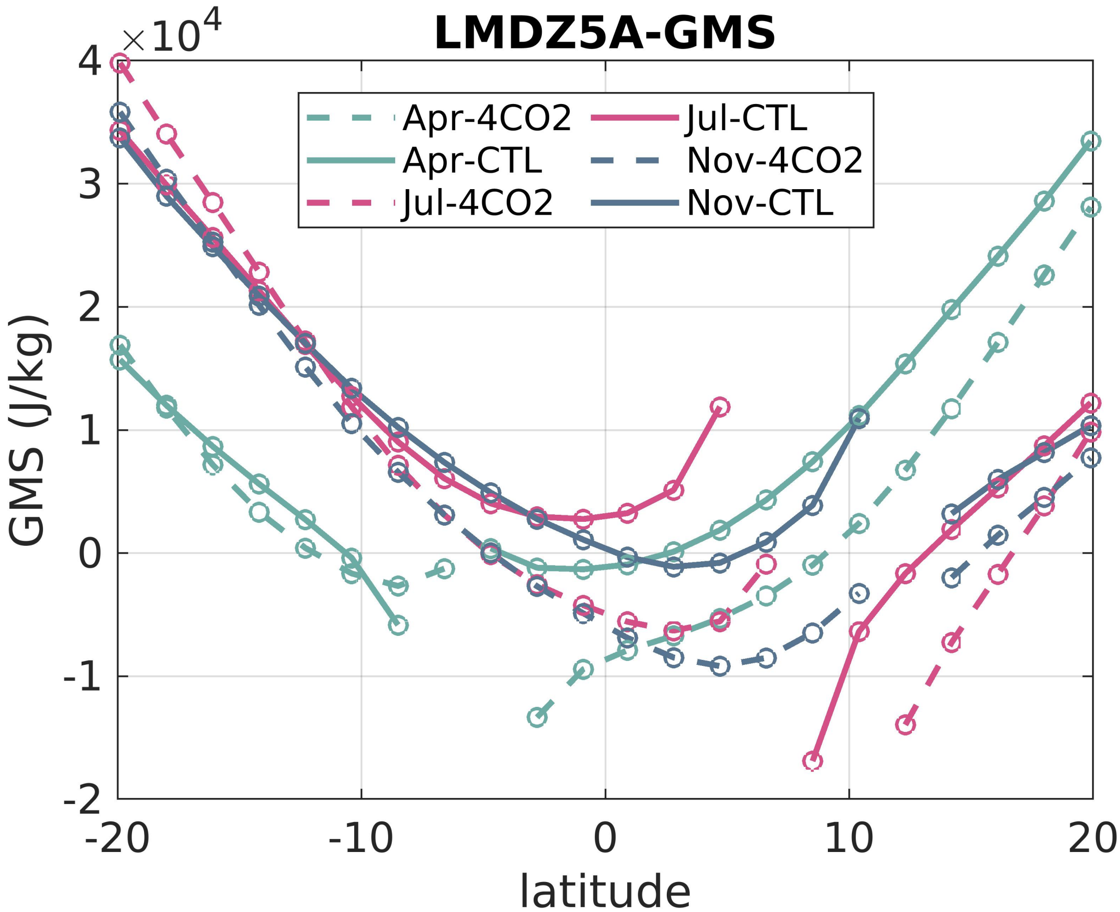

Figure H.2: LMDZ5A simulated GMS in April, July and November.

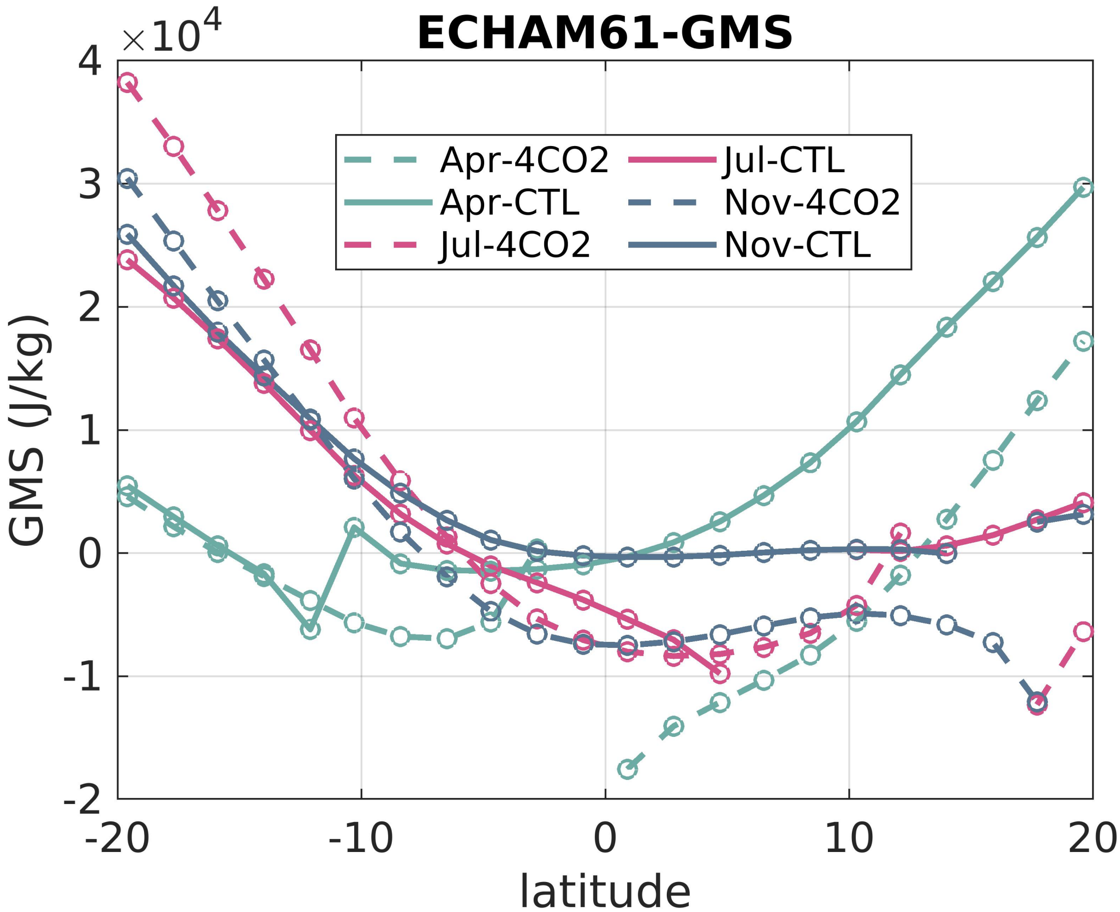

Figure H.3: ECHAM61 simulated GMS in April, July and November.

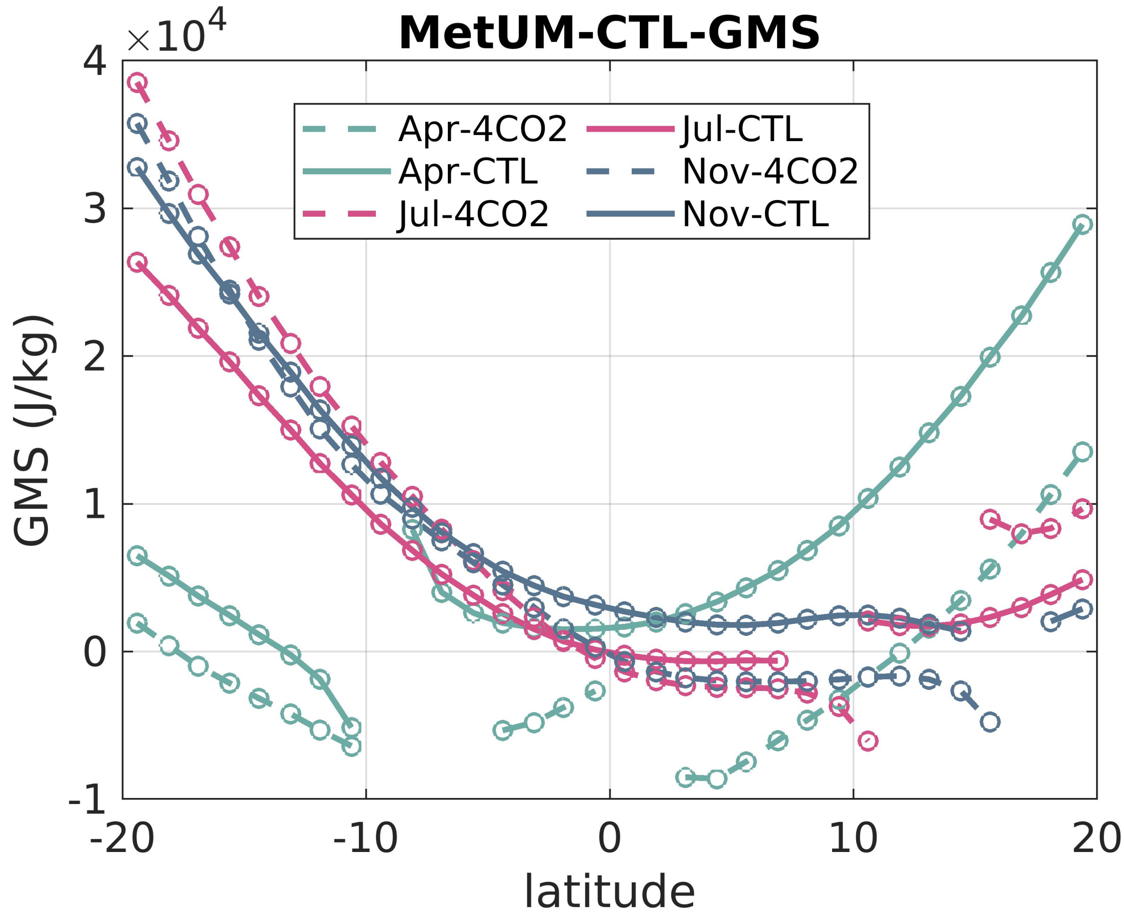

Figure H.4: MetUM_CTL simulated GMS in April, July and November.

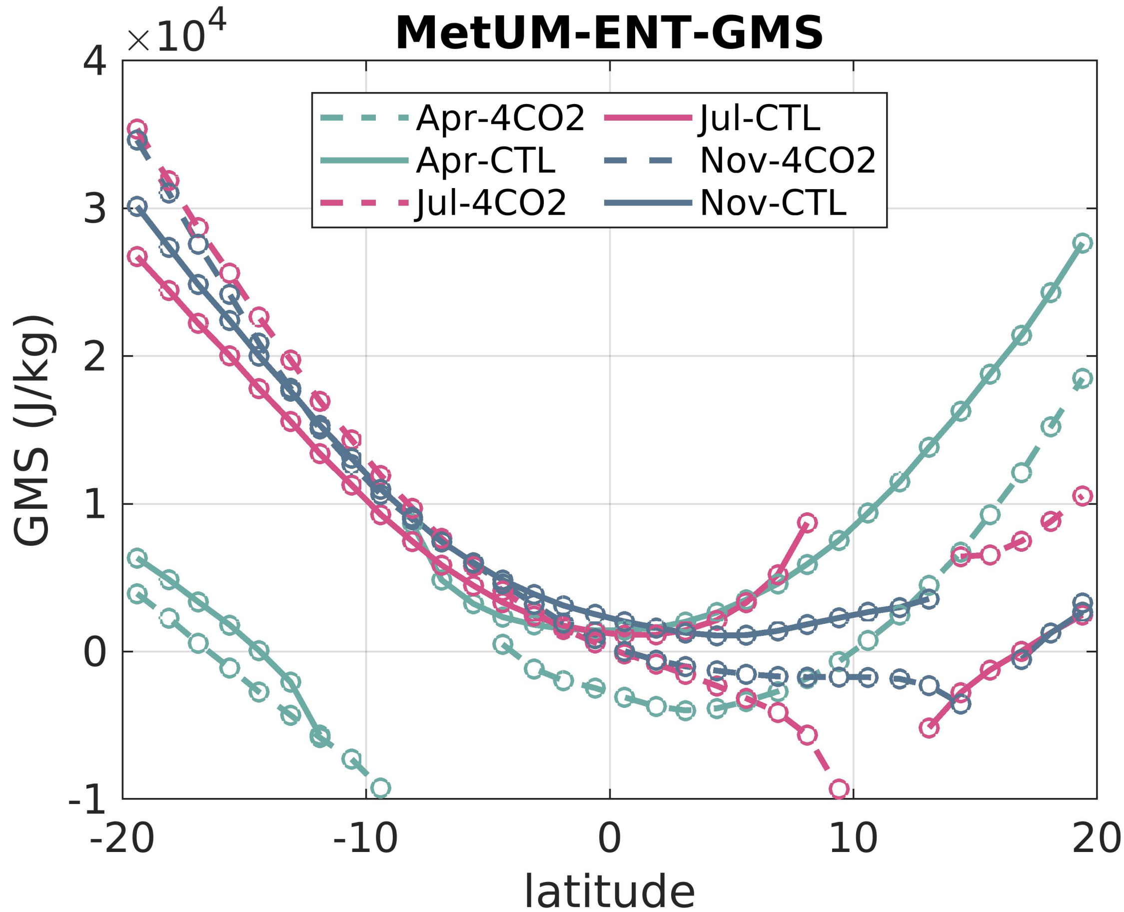

Figure H.5: MetUM_ENT simulated GMS in April, July and November.

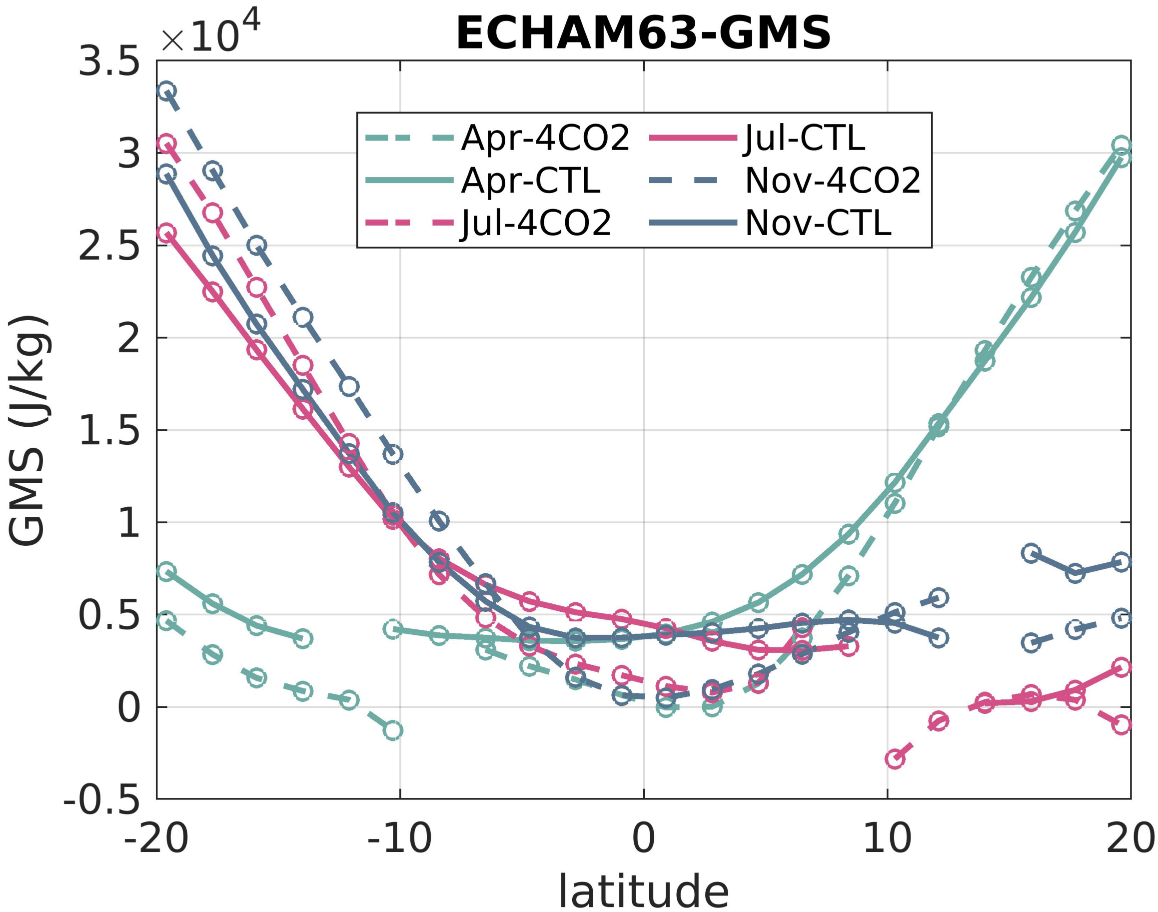

Figure H.6: ECHAM63 simulated GMS in April, July and November.

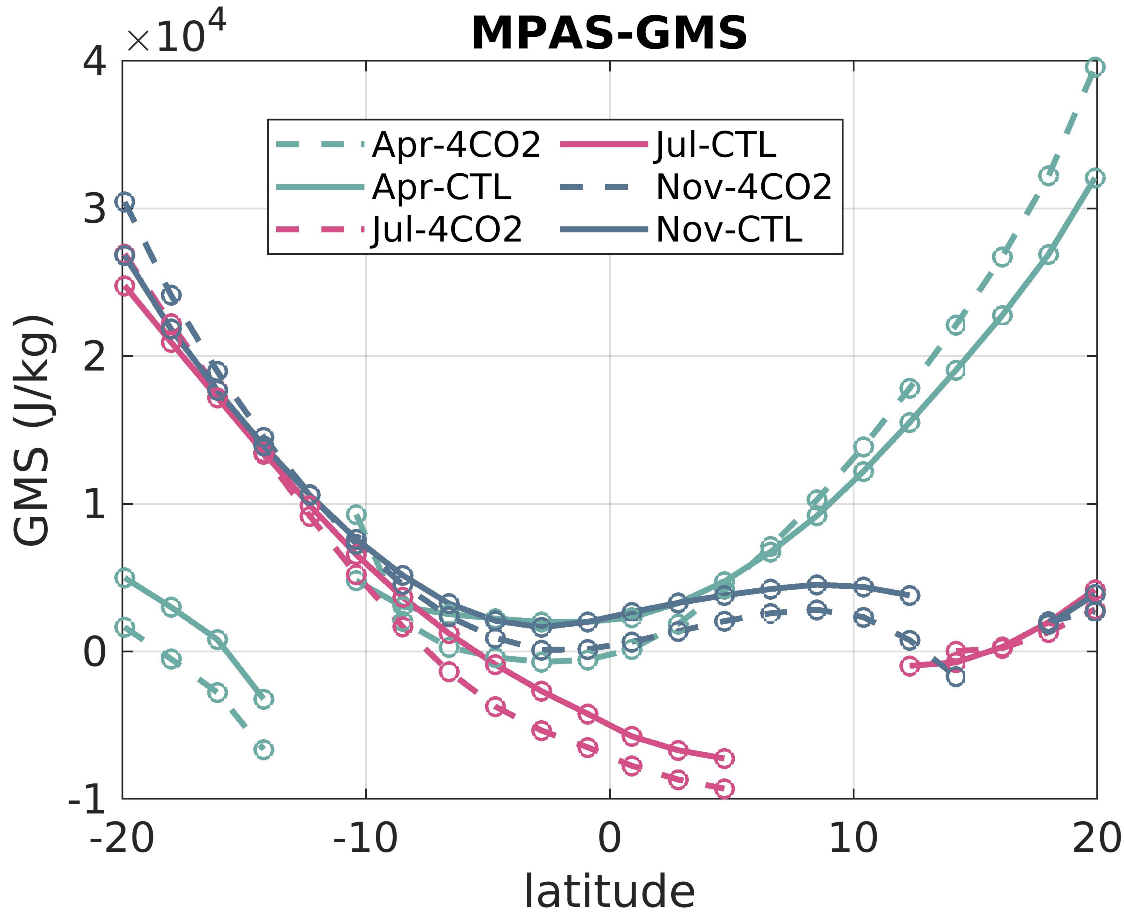

Figure H.7: MPAS simulated GMS in April, July and November.